UNIVERSIDAD CARLOS III DE MADRID

Escuela Politécnica Superior

EXPERIMENTAL AND ANALYTICAL STUDY OF THE INTERACTION BETWEEN SHORT ACOUSTIC PULSES AND SMALL CLOUDS OF MICROBUBBLES

Tesis Doctoral

Autor
Ana Medina

Director
Javier Rodríguez Rodríguez

DEPARTAMENTO DE INGENIERÍA TÉRMICA Y DE FLUIDOS

Leganés, Junio 2015

DEPARTAMENTO DE INGENIERÍA TÉRMICA Y DE FLUIDOS
Escuela Politécnica Superior

EXPERIMENTAL AND ANALYTICAL STUDY OF THE INTERACTION BETWEEN SHORT ACOUSTIC PULSES AND SMALL CLOUDS OF MICROBUBBLES

Autor
Ana Medina

Director de Tesis
Javier Rodríguez Rodríguez

Leganés, Junio 2015

To my parents, my sister, and to Wil

TESIS DOCTORAL

EXPERIMENTAL AND ANALYTICAL STUDY OF THE INTERACTION BETWEEN SHORT ACOUSTIC PULSES AND SMALL CLOUDS OF MICROBUBBLES

Autor: Ana Medina

Director de Tesis: Javier Rodríguez Rodríguez

Firma del Tribunal Calificador:

Firma

Presidente: D. Norman Riley

Vocal: D. Amable Liñán

Secretario: D. José Manuel Gordillo Arias de Saavedra

Suplente: D. Carlos Martínez Bazán

Calificación:

Leganés, de Junio de 2015

. . . In physics, you don't have to go
around making trouble for yourself,
-nature does for you . . .

Frank Wilczek

. . . If we knew what it was we were doing,
it would not be called research, would it?. . .

Albert Einstein

Abstract

Bubbles appear in many technological and industrial applications, in the fields of medicine, pharmacology, material science and in the chemical industry. In medicine, microbubbles are used as contrast agents in combination with ultrasound waves, since they enhance the backscatterd signal, improving the quality of the images. They are also applied in novel therapeutical techniques oriented to the elimination of thrombi or to tumor ablation, since they can be selectively driven towards precise targets. These important applications emphasize the relevance of knowing the physical behavior of bubbles under ultrasound waves.

One of the most important properties of bubbles is that they behave as oscillators when they are excited with a pressure wave, and they can act as nonlinear resonators. The resonance frequency of a bubble is strongly related to its size, but also to the properties of the surrounding medium, being the ambient pressure one of the most relevant ones. In theory, analyzing the acoustical spectrum of a bubble and determining the resonance frequency, we can determine the pressure of the medium. This is precisely the main goal of this thesis: to study the accuracy with which the pressure can be determined.

It is well known that an isolated bubble subjected to ultrasound behaves differently than a group of bubbles forming a cloud and interacting among them. Consequently, their acoustic responses are totally different. This means that the knowledge acquired when studying a single bubble cannot directly be applied to a cloud. Nevertheless, under some conditions multiple interactions among neighboring bubbles can be neglected, and the collective response can be approximated as the addition of the individual response of each of the bubbles forming the cloud. But even in this case, the response will be different depending on the properties of the cloud. In this thesis, we study the influence of the properties of the bubble cloud on the acoustical response and on the resonance frequency.

In the first part of the thesis, we explain the different equations used to model the oscillatory motion of bubbles under the influence of ultrasound waves. We then focus on collective effects present in clouds of bubbles in order to determine under which conditions these effects can be neglected, concluding that if the cloud is very diluted, multiple interactions do not significantly affect its properties. We also examine the importance of the thermal effects in the acoustic response of bubbles, concluding that these cannot be ignored since they play a fundamental role in the damping of

the bubble oscillations and consequently in the acoustic response.

In the second part, we study numerically the acoustic spectra of different polydisperse bubble clouds. We examine how the parameters of the size distribution affect the spectra and consequently the accuracy in the determination of the resonance frequency. We are also interested in selecting the acoustic excitation parameters that maximize the response of the bubbles. We conclude that bubble populations with a small polydispersion have a stronger acoustic response than highly polydisperse clouds. Moreover, we found that to use a frequency chirp is the best option to excite the resonance behavior of the bubbles. In order to find a less expensive method—from the computational point of view—to study the acoustic spectrum of bubble clouds, we developed an analytic formulation for the pressure radiated by a cloud, based on a linear analysis of the equations.

In the third part of the thesis, hydrogen microbubbles are generated using water electrolysis. We show how mini clusters of bubbles with a size of a few tens of microns can be produced in an easy and inexpensive manner. The technique consists of using a train of short intensity pulses to produce the electrolysis, instead of using a continuous voltage. In this way, only a few bubbles are produced. Moreover, they are sufficiently distant from each other to be considered as isolated.

The bubbles produced by electrolysis are used to study experimentally the displacement suffered by the bubble as a consequence of the radiation force produced by an ultrasound wave. In chapter 6, we study the displacement achieved by bubbles of different sizes, as well as the maximum velocities that they attain. The most relevant result is that a same bubble, subjected to two consecutive and identical pulses, can reach different maximum velocities and consequently can experience different displacements. Through a numerical study of the Bjerknes force, we show that the initial condition of the velocity of the bubble has a significant effect on the experienced radiation force, and therefore on the maximum velocity.

Finally, monodisperse microbubbles produced using flow-focusing techniques are excited with an ultrasound wave. Their backscatterd signal is analyzed in order to detect their resonance frequency. Although we are able to detect a peak around the expected resonance frequency in some cases, unfortunately no conclusive results are obtained, as shown in chapter 4.

Resumen

Las burbujas aparecen en numerosas aplicaciones tecnológicas e industriales, en el campo de la medicina, farmacología, ciencia de los materiales o en la industria química. En medicina, las microburbujas son usadas como agentes de contraste en combinación con ultrasonidos, puesto que aumentan el eco de la señal recibida, mejorando así la calidad de las imágenes ecográficas. Actualmente además se están aplicando a nuevas técnicas terapéuticas orientadas a la eliminación de trombos, puesto que estos agentes de contraste pueden ser dirigidos selectivamente hacia zonas específicas. Estas importantes aplicaciones ponen de manifiesto la relevancia de conocer como se comportan las burbujas ante los ultrasonidos.

Una de las propiedades más importantes de las burbujas es que se comportan como osciladores cuando son sometidas a una onda de presión, pudiendo actuar como resonadores no lineales. La frecuencia de resonancia de una burbuja está muy relacionada con su tamaño, pero también a las propiedades del medio que la rodea, especialmente a la presión del ambiente. En teoría, analizando el espectro acústico de una burbuja y detectando su frecuencia de resonancia en él, la presión ambiente podría ser determinada. Este es precisamente el principal objetivo de esta tesis: determinar con cuánta precisión la presión ambiente podría ser determinada.

Una burbuja aislada que está sometida a ultrasonidos se comporta de manera muy diferente que un grupo o nube de burbujas que interactúan entre ellas. Como consecuencia, sus respuestas acústicas serán totalmenteamen diferentes. Esto lamentablemente implica que el conocimiento adquirido al estudiar una única burbuja no puede ser extrapolado directamente a una nube de burbujas. Sin embargo, en algunas circunstancias las interacciones múltiples entre burbujas de un grupo pueden despreciarse, y calcular la respuesta colectiva como la suma de las respuestas individuales de cada una de las burbujas de la nube. Incluso en este caso, las propiedades de la nube afectarán mucho a la respuesta colectiva. En esta tesis, estudiaremos la influencia de las propiedades de la nube de burbujas en la respuesta acústica y por ende, en la frecuencia de resonancia.

En la primera parte de la tesis, explicamos las diferentes ecuaciones usadas para modelar el movimiento oscilatorio de las burbujas sometidas a campos de ultrasonidos. Posteriormente evaluamos los efectos colectivos presentes en nubes de burbujas para determinar bajo que condiciones estos efectos pueden ser despreciados, concluyendo que para nubes de burbujas muy diluídas las interacciones múltiples

entre burbujas son insignificantes y pueden obviarse. Además, examinamos la importancia de los efectos térmicos en la respuesta acústica de las burbujas, llegando a la conclusión de que estos no pueden ignorarse puesto que desempeñan un papel fundamental en el amortiguamiento de las burbujas y por tanto en su respuesta acústica.

En la segunda parte de la tesis, estudiamos numéricamente los espectros acústicos de distintas poblaciones de burbujas. Examinamos la influencia de los parámetros de la distribución de tamaños de la población sobre el espectro acústico y consecuentemente, sobre la frecuencia de resonancia. Además nos interesa seleccionar los parámetros de la excitación acústica que son más idóneos para maximizar la respuesta de la nube de burbujas. Se concluye que las poblaciones de burbujas que tienen una pequeña dispersión en tamaños tienen una respuesta acústica más fuerte que las poblaciones muy polidispersas. Además, afirmamos que el uso de un chirp en frecuencia es la mejor opción para excitar una nube de burbujas. Por último, realizamos una formulación analítica y lineal para poder calcular de una forma sencilla, desde el punto de vista computacional, el espectro acústico de una nube de burbujas.

En la tercera parte de la tesis, generamos microburbujas de hidrógenos por medio de electrólisis del agua. Mostramos como producir pequeñas nubes de burbujas, con diámetros comprendidos en las decenas de micras, de una foma sencilla y económica. La técnica consiste en usar pulsos eléctricos muy cortos para producir la electrólisis, en vez de aplicar un voltaje continuo. De esta forma, sólo unas pocas burbujas son producidas en cada pulso. Además, están lo suficientemente alejadas unas de otras para considerarse como burbujas aisladas.

Las burbujas generadas por electrólisis se usan para estudiar experimentalmente el desplazamiento sufrido por una burbuja como consecuencia de la fuerza de radiación primaria que induce el ultrasonido. En el capítulo 6, estudiamos tanto el desplazamiento como la velocidad máxima alcanzada por burbujas de distinto tamaño. El resultado más relevante es, sin duda, que una misma burbuja sometida a pulsos consecutivos e iguales, alcanza distintas velocidades máximas y desplazamientos en cada pulso. Mediante un estudio numérico de la fuerza de Bjerknes, demostramos cómo las condiciones iniciales en la velocidad y aceleración de la burbuja tienen un efecto muy significativo en la fuerza de Bjerknes experimentada, y por tanto, en la maxima velocidad alcanzada.

Finalmente, microburbujas monodispersas producidas usando técnicas de flow-focusing son excitadas con ultrasonidos. La señal dispersada por éstas es anlizada con el objetivo de detectar su frecuencia de resonancia. Aunque en algunos casos somos capaces de detectar un pico en el espectro alrededor de la frecuencia de resonancia, lamentablemente no obtuvimos resultados concluyentes con eta técnica, como se explica en el capítulo 4.

Contents

CHAPTER

ONE

Introduction and theoretical background

1.1 Motivation

Gas bubbles behave as oscillators when they are excited with a pressure wave. They can either oscillate at the driving frequency of the acoustic wave, or they can oscillate at their resonance frequency, which is strongly related with their size and with the pressure of the liquid medium in which they are suspended. Without regard to technical difficulties, in principle, the resonance frequency can be determined by analyzing the acoustic signal scattered by a cloud of bubbles. This turns the bubbles into a suitable tool for noninvasive pressure measurement. In the field of medicine, the intended application of this technique is the noninvasive measurement of the pressure inside the heart or at any other point in the vascular system. Currently, these pressure measurements are performed invasively by means of a pressure catheter.

The use of ultrasound is widespread in the field of medicine. Echographies are employed to detect possible illnesses or pathological conditions, or to check the correct functioning of organs. To improve the quality of the images, ultrasound contrast agents (UCA's) are used, being Gramiak & Shah (1968) the first one who reported this possibility. These UCA's are microbubbles with diameters smaller than 10 μm filled with an innocuous gas and coated with a shell, normally made of phospholipids. The large difference in acoustic impedance between the gas bubbles and their surrounding medium produces large backscattered ultrasound signals. This enhances echoes from the bloodstream in which the microbubbles flow, and improves the quality of the obtained images.

Another medical application ultrasound and UCA's is sonothrombolysis, which consists in dissolving and eliminating blood clots formed in arteries. When microbubbles are excited with a high-intensity ultrasound wave, they cavitate, helping the dissolution and elimination of the thrombus. This application was first proposed in 1975 by Roberts (1975) and was put in practice in 1976 by Trubestein (1976).

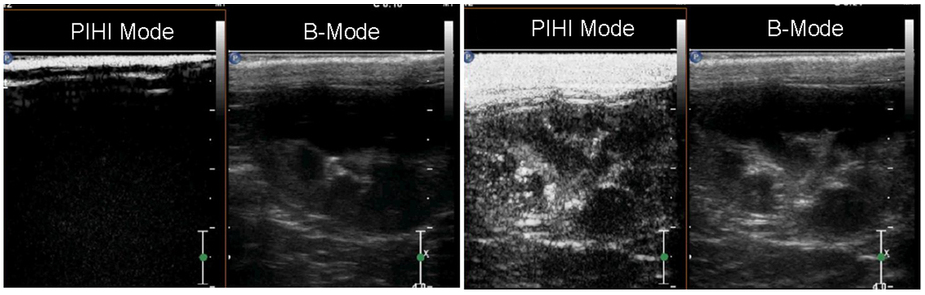

Figure 1.1: In vivo ultrasonograms of a rabbit's right kidney, (left) before and (right) after administration of polypyrrole hollow microspheres. Figure from Zha *et al.* (2013)

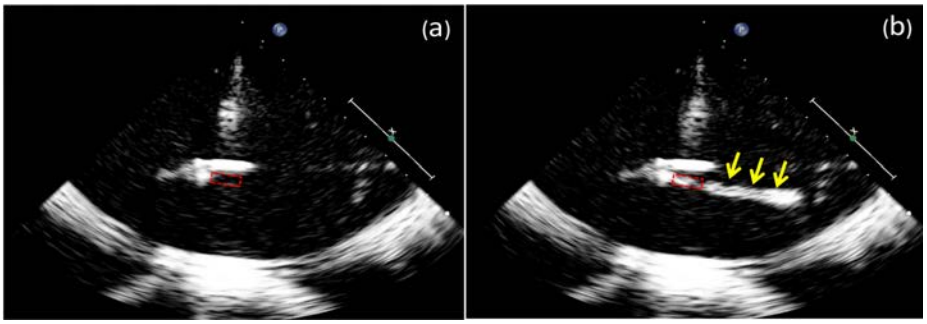

Figure 1.2: Contrast images, (a) before and (b) after 10 minutes of ultrasound treatment. The dashed red rectangle indicates the thrombus location; the yellow arrows indicate the location of the reestablished flow after recanalization. Figure from Shi *et al.* (2010).

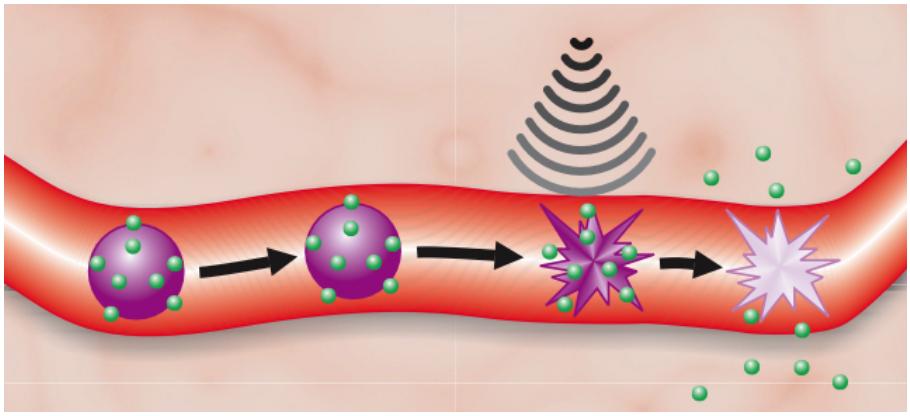

Figure 1.3: Gas-filled microbubbles (purple) covered with DNA (green) pass harmlessly and uneventfully through blood vessels until they are exposed to ultrasound. Then, the bubbles burst, causing not only the release of the DNA but also the opening of holes in the cells that line the vessel. (Courtesy of Ralph Shohet).

More recently, the idea of using UCA's as drug delivery vectors has been explored (Sutton *et al.*, 2013). The acoustic waves not only produce oscillations of the bubbles, but they are also able to displace the bubbles in the direction of the wave. The physical mechanism responsible for this is the radiation force, also known as the Bjerknes force. In this manner, UCA's can be directed to specific targets in the bloodstream. Certain drugs can be binded to the shell of the microbubbles or to the gas inside in order to treat pathologies such as thrombi or cancer tumors. Once the UCA's arrive at the desired target, they are broken down by means of cavitation so that the drug is delivered.

1.2 Background

1.2.1 An introduction to ultrasounds and bubbles

The term "ultrasonic" refers to sounds of frequency greater than 20 kHz, which is the upper limit of frequencies that the human ear can detect. An ultrasound field or an ultrasound wave is thus an acoustic pressure wave with frequencies greater than 20 kHz. To generate ultrasonic waves, piezoceramic materials, which transform electrical energy into mechanical energy, are commonly used. These ultrasound transducer are able to emit sound and also to receive it (in the latter case, they transform mechanical energy into electrical energy). They are used in a great variety of fields, ranging from surface cleaning and crack detection to, as we saw in the previous section, medical imaging diagnotics. The waves we are considering in this work are

travelling waves, since they transmit energy from one position to another. Nevertheless, if two identical travelling waves that are moving in opposite directions are superimposed, there will be no energy flux in any direction, resulting in a standing wave field (Leighton, 1994).

When a bubble is excited with a pressure wave, it oscillates. According to Flynn (1975) the bubble can experience three different motions: it can pulsate linearly about its equilibrium radius, it can oscillate in a nonlinear motion (what he refers to as a stable cavity), or it can expand quickly and then contract in such a fast way that it collapses (transient cavity). If the amplitude of the oscillation is small, the equation for the radial oscillation of the bubble can be linearized, yielding the equation for a harmonic oscillator. In this case, the natural frequency of the bubble is defined by Minnaert (1933) as

$$f_0 = \sqrt{\frac{3\gamma P_0}{\rho R_0^2}}, \tag{1.1}$$

where R_0 is the equilibrium radius of the bubble, γ is the polytropic exponent, ρ is the density of the surrounding fluid, and P_0 is the ambient pressure. When the amplitude of the excitation pressure is moderately high, the oscillations of the bubble will be nonlinear, being this behavior described by different nonlinear equations that we will see in chapter 2. The nonlinear response of the bubble is precisely what makes them good contrast agents. Also, the amplitude of their acoustical response will be higher and more easily detectable. Therefore, this is the regime we are going to focus on in this thesis.

If the amplitude of the pressure wave is very high, the oscillations will be strong and the bubble will be likely to suffer a strong expansion followed by a violent contraction that makes the bubble collapse. This oscillation regime is commonly known as inertial cavitation. In this violent regime, non-spherically-symmetric perturbations can appear that make the bubble lose its spherical symmetry. Plesset (1954) was the first who studied the stability of a spherical surface using spherical harmonics to describe the perturbations. Since then, many authors have addressed this topic. For example, Calvisi *et al.* (2007) used a boundary integral method to simulate nonspherical axisymmetric bubbles subject to acoustic driving, and studied the differences between the volumetric collapse of the bubbles and the collapse due to surfaces instabilities.

Due to the acoustic pressure, the bubble suffers an instantaneous radiation force which derives from the phase difference between the driving pressure and the volumetric oscillation of the bubble. The acoustic wave induces a pressure gradient on the bubble surface, causing an instantaneous force proportional to the pressure gradient and the volume of the bubble. When this instantaneous force is time-averaged during the excitation period, the resulting net force is different from zero. This time-

averaged force is known as the Bjerknes force and it is responsible for the translation that bubbles suffer in an acoustic field (Bjerknes, 1906). Bjerknes forces are classified into two types, primary forces that affect single bubbles, or secondary forces that affect clouds of bubbles and make them interact among them, sometimes attracting and forming clusters, other times repelling. There are several studies about the secondary Bjerknes force between two bubbles that attract or repel each other (Garbin *et al.*, 2009; Yoshida *et al.*, 2011). The effect of the primary Bjerknes force in a standing wave is also a well-studied phenomenon (Leighton *et al.*, 1990; Doinikov, 2002). Nevertheless, only a few studies can be found about the primary Bjerknes force induced by a travelling wave, (see, for example Dayton *et al.*, 2002).

In 1968, Gramiak & Shah (1968) reported that the injection of agitated saline in the aortic root greatly increased the backscattered ultrasound, and resulted in an enhanced contrast between the tissue and the blood. In order to use these microbubbles as contrast agents in echography studies, some improvements are neccesary. The bubbles should persist some minutes in the bloodstream and have a size smaller than 10 μm in diameter in order to navigate through the systemic circulation. In this way, the commercial contrast agents appear, being Albunex®(Molecular Biosystems, San Diego, CA, USA) the first one commercially availabel in 1994.

1.2.2 Noninvasive techniques for pressure measurement: a review

The response of bubbles to changes in the ambient pressure has been a subject of numerous studies. Measurements on bubbles clearly indicate a relationship between the ambient pressure and the acoustic behavior of the bubble. Several techniques have been proposed to measure the pressure in a noninvasive way. Indeed, the idea has been present in the literature for over 30 years, when it was suggested by Fairbank & Scully (1977). Nevertheless, a technique that provides reliable pressure measurements in a noninvasive way is yet to be developed. Below we examine the different methods that have been proposed, focusing on their advantages and disadvantages.

(a) Amplitude of the subharmonic

As mentioned above, when properly insonated with an acoustic wave, a bubble behaves as a weakly nonlinear oscillator. Therefore, the power spectral density of the acoustic signal scattered by the bubble exhibits peaks, not only at the main resonance frequency but also at half its value (subharmonic) as well as at higher multiples (harmonics). Shi *et al.* (1999) proposed that the amplitude of the subharmonic peak could be used to determine the ambient pressure. This technique was named

SHAPE (Sub-Harmonic Aided Pressure Estimation). Indeed, when the amplitude of the different peaks is plotted against the pressure, the subharmonic intensity exhibits a linear variation within the range of pressures relevant for medical applications (a few hundreds of millimetres of mercury). Taking advantage of this effect, the authors were able to successfully measure the pressure in their laboratory tank. More recently, Halldorsdottir *et al.* (2011) investigated *in vitro* the subharmonic response of different contrast microbubbles under different pressures and acoustic parameters, using the SHAPE technique. They concluded that subharmonic contrast signals are good indicators of hydrostatic pressure, making SHAPE an important, noninvasive clinical tool for measuring changes in pressure. Andersen & Jensen (2009) performed a parametric study to investigate how the energy of the subharmonic peak changes with ambient pressure. They concluded that there is a linear relation between this energy and the ambient pressure. One year later they also carried out experiments with Sonovue®, looking in this case how changes in ambient pressure affect the ratio between the energy of the subharmonic and the fundamental component of the spectrum (Andersen & Jensen, 2010). Despite the impressive results that the authors show in their papers, the technique of Shi *et al.* (1999) has some fundamental shortcomings, as the authors themselves point out in their work. Essentially, the problem lies in the fact that the amplitude of the subharmonic peak (actually any amplitude that can be measured) is not only very sensitive to the ambient pressure, but also to other parameters of the process, namely the bubble concentration and, more importantly, the acoustic pressure transmitted at the measurement point. The same conclusion can be extracted from the works of Andersen & Jensen (2009) and Andersen & Jensen (2010). It should be noticed that in many real applications, especially in medical diagnosis, the transmitted acoustic pressure at a given point is not known *a priori* and no reliable technique is available to predict it.

Adam *et al.* (2005) and Ganor *et al.* (2005) further explored the use of the amplitude of the subharmonic and other harmonics as a means to obtain the ambient pressure, but no conclusive results were shown in this regard. These works are nevertheless of great interest, as they perform an exhaustive theoretical and experimental investigation in order to model the nonlinear bubble behavior and the different possibilities to determine the ambient pressure.

This technique has proven to yield excellent results in a laboratory experiment, where both the bubble concentration and the transmitted acoustic pressure can be accurately controlled and characterized. We believe however that in any real situation it would be of limited use, since many factors affect the amplitude of the subharmonic.

(b) Disappearance time of bubbles

This idea was first proposed by Bouakaz *et al.* (1999). The method consists of insonating contrast microbubbles with a short high-intensity pulse, thus destroying the coating that prevents the gas inside the bubble from dissolving into the surrounding liquid, and then measuring the time required for the bubbles to disappear completely. It was shown by de Jong *et al.* (1993) that the radius of a gas bubble immersed into a stagnant liquid decreases at a rate that depends on the ambient pressure, among other parameters that can be easily characterized. Thus there is a direct relationship between dissolution time and pressure that can be exploited to compute the latter. Postema *et al.* (2004) performed more detailed numerical simulations in order to explore the suitability of different gases for measuring pressure.

It must be pointed out that the dissolution time of microbubbles in a liquid is typically short enough for the method to yield good temporal resolution in most practical applications, although this time could be too long for others. Consider for instance the measurement of blood pressure inside the human vascular system. Micrometer-sized air bubbles fully dissolve in blood in times of the order of 20-40 ms which is very short compared with the cardiac period, of the order of one second. Thus the technique would allow for a large number of measurements within the period of interest. Nonetheless this technique would be unable to yield good time resolution in certain phases of the cardiac cycle, such as systole and diastole, that occur in times of the order of 50 ms. Unfortunately, it is precisely during this phase that pressure measurements would be needed the most. Besides, there are other problems that, in our opinion, limit the applicability of the method. First of all, coated contrast bubbles are required. In medical applications this is not a problem, but in order for the technique to be useful in most industrial flows, it would be desirable to be able to employ free gas bubbles naturally existing in the flow. A second limitation concerns the applicability of the technique to flows rather than to a stagnant fluid. Indeed, if the bubbles are immersed in a flow with large velocity gradients, convective and unsteady terms have to be taken into account in order to properly predict the dissolution time of the bubbles. Unfortunately these terms are difficult to model and even to measure with the accuracy needed to correct the dissolution time, thus the technique cannot yield accurate results in such conditions. An example of this is the measurement of the pressure inside the heart, one of the applications where noninvasive pressure measurements are needed the most. Finally, the strongest disadvantage of the method is perhaps the difficulty of measuring dissolution times accurately. This issue arises from the fact that the bubble radius decreases as a negative power-law of the time. Therefore, the bubble concentration as a function of time exhibits a long tail that makes the measurement of the dissolution time highly imprecise. As a consequence, the pressure measurements reported in the work of Bouakaz *et al.* (1999) show errors of about 50 mmHg, which for the case of medical applications are unacceptable.

(c) Resonance frequency of microbubbles

This technique was proposed by Fairbank & Scully (1977). The idea is simple: a bubble insonated with an ultrasound wave of wavelength much larger than the bubble size behaves, for a wide range of acoustic pressures, as a weakly nonlinear oscillator. The resonance frequency of such an oscillator was shown by Minnaert (1933) to be proportional to the square root of the ambient pressure. Therefore, by measuring the frequency at which the acoustic signal scattered by the bubble shows a maximum in the power spectral density, the pressure at the position of the bubble can be obtained. The application of this technique to ultrasound medical diagnostics was explored by Bouakaz *et al.* (1999), who identified a series of accuracy issues. In their original work, Fairbank & Scully (1977) showed that the acoustic spectrum of air bubbles in water is shifted as a result of an increment of 0.2 atm in the ambient pressure, but they did not perform a systematic experimental study of the influence of the properties of the bubble on this effect. Leighton (1987) performed hydrophone recordings of a single air bubble in water, checking that the measured frequency corresponded to that given by Minnaert. It was not until 2010 when Aldham *et al.* (2010) reported a systematic experimental study in which the resonance frequency of a single bubble was measured for changes in ambient pressure as small as 1 kPa. They carried out experiments in which the bubble was placed on a plate and modified Minnaert's frequency to take into account the effect of this plate. They checked that effectively the resonance frequency of the bubble changes linearly with ambient pressure, although the ambient pressure measured using the resonance frequency did not match exactly with the existing ambient pressure. Furthermore, they performed the measurements with a bubble of 3 mm diameter. As they mentioned, for medical applications the bubble must be much smaller, and therefore the amplitude of the scattered pressure will be lower and more difficult to detect. Alternatively, other authors (Adam *et al.*, 2005; Ganor *et al.*, 2005) have recently performed experiments using commercial UCAs, whose physical properties cannot be changed and, in some cases, cannot even be measured. The coating shell affects the resonance frequency given by Minnaert, increasing this by about 50%, according to Van der Meer *et al.* (2007). Several equations have been proposed to incorporate the effect of the coating, however these models include the shell viscosity or shell elasticity, which are properties that are difficult to measure.

1.3 Scope of this thesis

The ultimate goal of this thesis was to develop a novel noninvasive method to experimentally determine the pressure in a liquid by measuring the resonance frequency of microbubbles in suspension. The highest impact of this technique would lie in the

field of medicine, in order to measure the pressure in the bloodstream, without the use invasive catheters. The achievement of this ambitious goal would definitely have meant a revolution in the medical field. Unfortunately, this has not been possible yet, due to several technical limitations. Nevertheless, our efforts have guided us towards the better understanding of the motion of bubbles in acoustic fields. We have carried out a complete numerical and theoretical study of the radial motion of bubbles, in order to determine the parameters that have the strongest effect on their resonance, and therefore, to learn what is the best way to make the bubble resonate. We have studied the effect of a polydisperse population of bubbles on their acoustical response in order to determine how accurately the resonance frequency can be determined. Futhermore, experiments have been carried out in order to study experimentally the acoustic response of a bubble cloud. These steps lay out the beginning of the path towards the ultimate goal.

In addition, we have developed an easy and inexpensive technique to generate microbubbles using water electrolysis, in order to experimentally study how these bubbles behave in acoustic fields. We have focused on the primary Bjerknes force that bubbles undergo when they are excited by a short travelling acoustic wave. Although the complete numerical and analytical study of the effect of the Bjerknes force is the scope of another thesis being carried out currently in our research group by Elena Igualada, in this dissertation we show several experimental results, and compare them with simple numerical simulations.

References

ADAM, D., SAPUNAR, M. & BURLA, E. 2005 On the relationship between encapsulated ultrasound contrast agent and pressure. *Ultrasound Med. Biol.* **31**, 673–686.

ALDHAM, B., MANASSEH, R., ILLESINGHE, S., LIFFMAN, K., OOI, A. & SUTALO, I. D. 2010 Measurement of pressure on a surface using bubble acoustic resonances. *Meas. Sci. Technol.* **21**, 027002.

ANDERSEN, K.S. & JENSEN, J.A. 2009 Ambient pressure sensitivity of microbubbles investigated through a parameter study. *J. Acoust. Soc. Am.* **126** (6), 3350–3358.

ANDERSEN, K.S. & JENSEN, J.A. 2010 Impact of acoustic pressure on ambient pressure estimation using ultrasound contrast agent. *Ultrasonics* **50**, 294–299.

BJERKNES, V. F. K. 1906 *Fields of Force*. Columbia University Press, New York.

BOUAKAZ, A., FRINKING, P. JA., DE JONG, N. & BOM, N. 1999 Noninvasive measurement of the hydrostatic pressure in a fluid-filled cavity based on the disappearance time of the micrometer-sized free gas bubbles. *Ultrasound Med. Biol.* **25**, 1407–1415.

CALVISI, M. L., LINDAU, O., BLAKE, J. R. & SZERI, A. J. 2007 Shape stability and violent collapse in acoustic travelling waves. *Physics of Fluids* **19**, 047101.

DAYTON, P.A., ALLEN, J.S. & FERRARA, K.W. 2002 The magnitude of radiation force on ultrasound contrast agents. *J. Acoust. Soc. Am.* **112**, 2183–2192.

DOINIKOV, A. 2002 Translational motion of a spherical bubble in an acoustic standing wave of high intensity. *Physics of Fluids* **14** (4), 1420–1425.

FAIRBANK, W. K. & SCULLY, M. O. 1977 A new noninvasive technique for cardiac pressure measurement: resonance scattering of ultrasounds for bubbles. *IEEE Trans. Biomed. Eng.* **24**, 107–110.

FLYNN, H. G. 1975 Cavitation dynamics i. a mathematical formulation. *J. Acoust. Soc. Am.* **57** (6), 1379–1396.

GANOR, Y., ADAM, D. & KIMMEL, E. 2005 Time and pressure dependence of acoustic signals radiated from microbubbles. *Ultrasound Med. Biol.* **31**, 1367–1374.

GARBIN, V., DOLLET, B., OVERVELDE, M., COJOC, D., DI FABRIZIO, E., VAN WIJNGAARDEN, L., PROSPERETTI, A., DE JONG, N., LOHSE, D. & VERSLUIS, M. 2009 History force on coated microbubbles propelled by ultrasound. *Physics of Fluids* **21**, 092003.

GRAMIAK, R. & SHAH, P. M. 1968 Echocardiography of the aortic root. *Invest. Radiol.* **3**, 356–388.

HALLDORSDOTTIR, V.G., DAVE, J.K., LEODORE, L.M., EISENBREY, J.R., PARK, S., HALL, A.L., THOMENIUS, K. & FORSBERG, F. 2011 Subharmonic contrast microbubble signals for noninvasive pressure estimation under static and dynamic flow conditions. *Ultras. Imag.* **33**, 153–164.

DE JONG, N., TEN CATE, F.J., VLETTER, W.B. & J.T.C.R., ROELANDT 1993 Quantification of transpulmonary echoconstrast effects. *Ultrasound Med. Biol.* **19**, 179–188.

LEIGHTON, T.G. 1994 *The acoustic bubble*. Academic Press, London.

LEIGHTON, T. G. 1987 An experimental study of the sound emitted from gas bubbles in a liquid. *Eur. J. Phys.* **8** (2), 98 – 104.

LEIGHTON, T. G., WALTON, A.J. & M.J.W., PICKWORTH 1990 Primary bjerknes forces. *Eur. J. Phys.* **11**, 47 – 50.

VAN DER MEER, S., DOLLET, B., VOORMOLEN, M.M., CHIN, C.T., BOUAKAZ, A., DE JONG, N., VERSLUIS, M. & LOHSE, D. 2007 Microbubble spectroscopy of ultrasound contrast agents. *J. Accoust. Soc. Am.* **121**, 648–656.

MINNAERT, M. 1933 On musical air bubbles and the sounds of running water. *Phil. Mag.* **26** (104), 235–248.

PLESSET, M. S. 1954 On the stability of fluid flows with spherical symmetry. *J. Appl. Phys.* **25**, 96–98.

POSTEMA, M., BOUAKAZ, A. & DE JONG, N. 2004 Noninvasive microbubble-based pressure measurements: a simulation study. *Ultrasonics* **42**, 759–762.

ROBERTS, G. O. 1975 A new method to cure thrombi by ultrasonic cavitation. pp. 273–5. Ultrasonics International 1975, J. Ultrasonics.

SHI, W.T., FORSBERG, F., RAICHLEN, J.S., NEEDLEMAN, L. & GOLDBERG, B.B. 1999 Pressure dependence of subharmonic signals from contrast microbubbles. *Ultrasound Med. Biol.* **25**, 275–283.

SHI, W. T., GAO, S., FRANCOIS, V., POWERS, J. E., DRVOL, L., JUNG, K.W., XIE, F., LOF, J., EVERBACH, E.C. & PORTER, T. R. 2010 Investigation of effectiveness of microbubble stable cavitation in thrombolysis. pp. 330–3. IEEE International Ultrasonics Symposium Proceedings, IEEE, Piscataway, NJ, USA.

SUTTON, J. T., HAWORTH, K.J., PYNE-GEITHMAN, G. & HOLLAND, C.K. 2013 Ultrasound-mediated drug delivery for cardiovascular disease. *Expert opinion in drug delivery* **10** (5), 573–592.

TRUBESTEIN, G. G. 1976 Thrombolysis by ultrasound. *Clinical science and molecular medicine* **51**, 697–698.

YOSHIDA, K., FUJIKAWA, T. & WATANABE, Y. 2011 Experimental investigation on reversal of secondary bjerknes force between two bubbles in ultrasonic standing waves. *J. Acoust. Soc. Am.* **130** (1), 135–144.

ZHA, Z., WANG, J., QU, E., ZHANG, S., JIN, Y., WANG, S. & DAI, Z. 2013 Polypyrrole hollow microspheres as echogenic photothermal agent for ultrasound imaging guided tumor ablation. *Scientific Reports* **3**, 2360.

CHAPTER

TWO

Radial oscillations of bubble clouds under ultrasound: problem formulation

2.1 Introduction

The dynamics of stable and non-stable bubbles in liquids has always been a phenomenon of interest. It is useful to introduce simple models that reproduce these small, dynamical systems, which are named "cavities" in general. We shall need different models for different extreme modes of behavior. Thus we shall represent bubbles which collapse violently by 'transient cavities' and bubbles that pulsate over relatively long intervals of time by 'stable cavities'.

There are three kinds of motions of cavities: they may pulsate linearly about their equilibrium radius; they may oscillate in a nonlinear motion or they may expand quickly and then contract in such a fast way that they collapse. The first motion is not interesting; the others can be represented by stable and transient cavities respectively. The stable cavity model has been showed to be a useful model for a pulsating bubble. A bubble will act as a stable cavity if the acoustic pressure amplitude is small enough to not make it collapse, but high enough so that the motion is non-linear.

2.2 Theoretical background

An isolated bubble in a liquid which is insonified (this is, it is under the influence of an acoustic field), can move in different ways: it might pulsate for a long interval maintaining its spherical symmetry, it may experience surface oscillations or it may collapse. Several nonlinear differential equations have been used to describe the motion of a bubble of such characteristics. Most of them consider volumetric oscillations of the bubble, that is, there is always spherical symmetry. In order to avoid treating the interaction of a sound wave with a free surface, the wavelength of the

sound field is assumed to be much longer than the bubble radius. This assumption enables us to represent the sound field by a time-varying pressure at infinity.

The simplest equation that describes the bubble's motion is the Rayleigh-Plesset equation. Other equations exist which take into account the compressibility of the liquid and other effects. But in general, it is not possible to obtain fully analytical solutions to these equations of motion. However, in the case of small amplitudes, we can linearize these equations of motion, obtaining those of linear damped oscillator, as we will see in the next section.

2.2.1 The Rayleigh-Plesset equation

Let's consider a single spherical bubble in an infinite liquid medium whose temperature and pressure far from the bubble are T_∞ and P_∞ respectively. We assume that the temperature and pressure within the bubble are uniform, and the gas inside the bubble behave as a perfect gas. There is also a vapor part inside the bubble, which is considered through a constant vapour pressure, p_v. We also consider the liquid incompressible with constant density ρ and constant viscosity μ. When this bubble is excited with an acoustic wave, it will oscillate varying its radius with time. If the bubble radius, R_0, is small compared with the acoustic wavelength, $\lambda = 2\pi c_0/\omega_c$, the sound field can be expressed as a time-varying pressure $P_\infty(t) = P_0 + p(t)$, being P_0 the static pressure in the liquid. The time dependant pressure $p(t)$ can be expressed in general form by $p(t) = P_A f(\omega_c t)$. Since the liquid is considered incompressible, the sound speed, c_0, can be assumed to be infinite. Therefore, any change in $P_\infty(t)$ is effective and immediately communicated to the bubble interface. We assume that the bubble remains spherical at all times and that there is no diffusion of the gas contained in the bubble into the liquid. The Rayleigh-Plesset equation (Rayleigh (1917), Plesset (1949)) thus describes the response of a spherical bubble in a time-varying pressure field in an incompressible, viscous fluid.

$$\rho(R\ddot{R} + \frac{3}{2}\dot{R}^2) = (P_0 - p_v)\left[\left(\frac{R_0}{R}\right)^{3\gamma} - 1\right] + \frac{2\sigma}{R_0}\left[\left(\frac{R_0}{R}\right)^{3\gamma} - \frac{R_0}{R}\right] - p(t) - 4\mu\frac{\dot{R}}{R} \quad (2.1)$$

where $\dot{R}$ and $\ddot{R}$ denotes $\mathrm{d}R/\mathrm{d}t$ and $\mathrm{d}^2R/\mathrm{d}t^2$ respectively. Making use of the dimensionless variables $\tau = \omega_c t$ and $a(\tau) = R(t)/R_0$, we can write the equation in non-dimensional form:

$$\ddot{a} = \Pi_0\left(\frac{1}{a^{3\gamma}} - 1\right)\frac{1}{a} + \frac{1}{We}\left(\frac{1}{a^{3\gamma}} - \frac{1}{a}\right) - \epsilon f(\tau)\frac{1}{a} - \frac{1}{Re}\frac{\dot{a}}{a^2} - \frac{3}{2}\frac{\dot{a}^2}{a} \quad (2.2)$$

where the following dimensionless parameters appear: the Euler number Π_0, the Webber number *We*, the Reynolds number *Re* and the parameter ϵ which represents the dimensionless amplitude of the pressure wave. These parameters are defined as:

$$\begin{aligned} Re &= \frac{\rho {R_0}^2 \omega_c}{4\mu}, \quad We = \frac{\rho {R_0}^3 {\omega_c}^2}{2\sigma} \\ \Pi_0 &= \frac{P_0 - P_v}{\rho {R_0}^2 \omega_c^2}, \quad \epsilon = \frac{P_a}{\rho {R_0}^2 \omega_c^2} \end{aligned} \tag{2.3}$$

2.2.2 The Flynn equation

This equation (Flynn (1975)) is very similar to the previous one (see equation (2.1)), but it takes into account the effect of the compressibility of the liquid in the far field. The flow near the bubble however is still considered as incompressible. In this equation a new parameter appears: the sound speed, c_0, which is supposed to be constant and finite.

$$\begin{aligned} \rho(R\ddot{R} + \frac{3}{2}\dot{R}^2) = (p_0 - p_v)\left[\left(\frac{R_0}{R}\right)^{3\gamma} - 1\right] + \frac{2\sigma}{R_0}\left[\left(\frac{R_0}{R}\right)^{3\gamma} - \frac{R_0}{R}\right] \\ - p(t) - 4\mu\frac{\dot{R}}{R} + \frac{R}{c_0}\left(1 - \frac{\dot{R}}{c_0}\right)\frac{dp_l}{dt} \end{aligned} \tag{2.4}$$

where p_l is the liquid pressure at the wall of the bubble and it has the following expression:

$$(p_0 - p_v + \frac{2\sigma}{R_0})\left(\frac{R_0}{R}\right)^{3\gamma} + p_v - \frac{2\sigma}{R} \tag{2.5}$$

Using the variables and dimensionless parameters (2.3) already defined, and introducing a new dimensionless parameter, the called Mach number

$$M = \frac{R_0 \omega_c}{c_0} \tag{2.6}$$

the equation can be written in a non dimensional form:

$$\begin{aligned} \ddot{a} = \Pi_0\left(\frac{1}{a^{3\gamma}} - 1\right)\frac{1}{a} + \frac{1}{We}\left(\frac{1}{a^{3\gamma}} - \frac{1}{a}\right)\frac{1}{a} - \epsilon f(\tau)\frac{1}{a} - \\ \frac{1}{Re}\frac{\dot{a}}{a^2} - \frac{3}{2}\frac{\dot{a}^2}{a} + M(1 - M\dot{a})\left[\frac{1}{We}\left(\frac{1}{a} - 3\gamma\right) - 3\gamma\Pi_0\frac{1}{a^{3\gamma}}\right]\frac{\dot{a}}{a} \end{aligned} \tag{2.7}$$

2.2.3 The Keller-Miksis equation

Keller & Miksis (1980) derived a new equation for large amplitude forced radial oscillations of a free bubble in an incident sound field. It includes the effect of of acoustic radiation, viscosity and surface tension. They assumed the pressure within the bubble is uniform. They formulated the problem in function of the velocity potential, the density of the liquid and the pressure, variables that must satisfy continuity, Navier-Stokes equation and the equation of state. Solving the wave equation and a modified Bernoulli integral, they obtained the following equation:

$$\left(1-\frac{\dot{R}}{c_0}\right)R\ddot{R}+\frac{3}{2}\dot{R}^2\left(1-\frac{\dot{R}}{3c_0}\right)= \left(1+\frac{\dot{R}}{c_0}\right)[P(R,t)-p_{\text{ext}}(t)]\rho^{-1}+\frac{R}{\rho c_0}\frac{\mathrm{d}}{\mathrm{d}t}P(R,t) \tag{2.8}$$

being $P(R,t)$ the pressure at the wall of the bubble:

$$P(R,t)=\left(P_0+\frac{2\sigma_0}{R_0}-P_v\right)\left(\frac{R_0}{R}\right)^{3\gamma}+P_v-P_0-\frac{2\sigma_0}{\rho R}-\frac{4\mu\dot{R}}{R} \tag{2.9}$$

and $p_{\text{ext}}(\omega_c t)$ is the incident pressure wave, which can be expressed in generic way as an amplitude P_A and a function which depends of the product $\omega_c t$, $p_{\text{ext}}(\omega_c t)=P_A f(\omega t)$. Developing all the terms the equation yields:

$$\begin{aligned}\ddot{R}\left[\frac{4\mu}{\rho c_0}+R\left(1-\frac{1}{c_0}\dot{R}\right)\right]+\frac{3}{2}\dot{R}^2\left(1-\frac{1}{3c_0}\dot{R}\right)& \\ =\frac{1}{\rho}\left[\left(P_0-p_v+\frac{2\sigma_0}{R_0}\right)\left(\frac{R_0}{R}\right)^{3\gamma}-P_0+p_v-\frac{2\sigma_0}{R}-\frac{4\mu\dot{R}}{R}\right]& \\ +\frac{\dot{R}}{\rho c_0}\left[(1-3\gamma)\left(P_0-p_v+\frac{2\sigma_0}{R_0}\right)\left(\frac{R_0}{R}\right)^{3\gamma}-P_0+p_v\right]& \\ -\frac{1}{\rho}\left(1+\frac{\dot{R}}{c_0}\right)p_{\text{ext}}(\omega_c t)&\end{aligned} \tag{2.10}$$

Equation (2.10) is a nonlinear second-order ordinary differential equation for the bubble radius $R(t)$.

We now rewrite equation (2.10) in dimensionless variables. In doing so we define

the following dimensionless variables:

$$\begin{aligned} a &= \frac{R}{R_0}, & \tau &= \omega_c t, & M &= \frac{R_0 \omega_c}{c} \\ Re &= \frac{\rho {R_0}^2 \omega_c}{4\mu}, & We &= \frac{\rho {R_0}^3 {\omega_c}^2}{2\sigma} \\ \Pi_0 &= \frac{P_0 - P_v}{\rho {R_0}^2 \omega_c^2}, & \epsilon &= \frac{P_a}{\rho {R_0}^2 \omega_c^2} \end{aligned} \tag{2.11}$$

$$\begin{aligned} \ddot{a}\left[\frac{M}{Re} - a(\dot{a}M - 1)\right] + \frac{3}{2}\dot{a}^2\left(1 - \frac{M}{3}\dot{a}\right) &= \Pi_0\left(\frac{1}{a^{3\gamma}} - 1\right) \\ &+ We^{-1}\left(\frac{1}{a^{3\gamma}} - \frac{1}{a}\right) - Re^{-1}\frac{\dot{a}}{a} - (1 + M\dot{a})\,\epsilon f(\tau) \\ &+ M\dot{a}\left[\Pi_0\left((1-3\gamma)\frac{1}{a^{3\gamma}} - 1\right) + We^{-1}\left((1-3\gamma)\frac{1}{a^{3\gamma}} - \frac{1}{a}\right)\right] \end{aligned} \tag{2.12}$$

Equation (2.12) is a nonlinear second-order ordinary differential equation for the dimensionless radius $a(\tau)$, where $\dot{a}$ denotes the derivative of a with respect to the dimensionless variable τ, i.e. $\dot{a} = \mathrm{d}a/\mathrm{d}\tau$

2.2.4 Other non-linear equations

There exist more equations which describe the oscillatory motion of a bubble in an incident acoustic field. For example, the Herring-Trilling equation (Herring (1941), Trilling (1952)), or the Gilmore equation (Gilmore (1952)), written as a function of the liquid enthalpy. Prosperetti & Lezzi (1986) studied the radial dynamics of a spherical bubble in a compressible liquid by to means of a simplified singular-perturbation method to first order in the bubble-wall Mach number, M. It is shown that a one-parameter family of approximate equations, all of them accurate to first order in the Mach number, for the bubble radius exists, which includes those previously derived by Herring and Keller. Prosperetti & Lezzi (1986) proposed to refer this equation as the general *Keller-Herring equation*.

$$\begin{aligned} \left[1 - (\delta+1)\frac{\dot{R}}{c_0}\right]R\ddot{R} + \frac{3}{2}\left[1 - \frac{1}{3}(3\delta+1)\frac{\dot{R}}{c_0}\right]\dot{R}^2 \\ = \left[1 + (1-\delta)\frac{\dot{R}}{c_0}\right]\left(h_B - \frac{p_v}{\rho}\right) + \frac{R}{c_0}\frac{\mathrm{d}}{\mathrm{d}t}\left(h_B - \frac{p_v}{\rho}\right) \end{aligned} \tag{2.13}$$

where $p_v(t)$ denotes the variable part of the pressure in the liquid at the location of the bubble centre in the absence of the bubble and δ is an arbitrary parameter. Any member of this one-parameter family of equations is *a priori* an acceptable form of the radial equation of motion correct to first order in the Mach number. But no criteria exist to choose a more suitable value of δ. Nevertheless, comparing the results obtained with this equation with the results of the full problem, they concluded that an equation close to the Keller form, but written in terms of the enthalpy of the liquid at the bubble wall, h_B, rather than the pressure, is the most accurate, at least for the case of bubble collapse.

The equations described are valid for free bubble. Since the contrast agents used in many experiments are coated microbubbles, these equations must be modified to take into account for the effect of the shell. One of the models more frequently used is the proposed by Marmottant *et al.* (2005), which uses a modified RP equation taking into account the physical properties of a lipid monolayer coating. Khismatullin & Nadim (2002) also proposed a model that incorporates a viscoelastic shell, and even considers the liquid as slightly compressible and viscoelastic, in order to model the human tissue and blood more accurately.

Since in this work we are not considering bubble collapse or coated microbubbles, we have chosen the Keller-Miksis equation to simulate the radial bubble motion, seen that this equation is the most accurate.

2.2.5 Pressure radiated by a bubble

The pressure scattered or radiated by the bubble at a distance d is related to the velocity potential in the liquid, χ by $P_{\text{sc}} = -\rho\,\partial\chi/\partial t$. For a small pulsating bubble the velocity potential can be expressed as (Landau & Lifshitz (1959))

$$\chi(r,t) = -\frac{R^2\dot{R}}{d(1+ikR_0)}e^{-ik(d-R_0)} \tag{2.14}$$

where the distance d is measured from the center of the bubble and k is the wave number. Therefore, the radiated pressure yields

$$P_{\text{sc}} = \rho\frac{R}{d}\left(2\left(\frac{\mathrm{d}R}{\mathrm{d}t}\right)^2 + R\frac{\mathrm{d}^2R}{\mathrm{d}t^2}\right)(1+ikR_0)\,e^{-ik(d-R_0)}. \tag{2.15}$$

Following the analysis of Vokurka, explained by (Leighton (1994)) a similar equation is found, valid at distances far from the bubble

$$P_{\text{sc}}(d,t) = \rho\frac{R}{d}\left(2\left(\frac{\mathrm{d}R}{\mathrm{d}t}\right)^2 + R\frac{\mathrm{d}^2R}{\mathrm{d}t^2}\right) \tag{2.16}$$

which written in dimensionless variables yields

$$P^*_{\mathrm{sc}} = \frac{P_{sc}}{\rho\,\omega_{\mathrm{c}}^2 R_0^2} = \frac{a}{d^*}\left(2\dot{a}^2 + a\ddot{a}\right) \tag{2.17}$$

being $d^* = d/R_0$.

2.3 Linearization of the equations

If we suppose that the amplitude of the oscillations is weak enough, the dimensionless instantaneous radius can be written as $R = R_0(1+\epsilon x(t))$, with $\epsilon \ll 1$. Equation (2.10) can then be linearized, yielding

$$\epsilon\frac{\mathrm{d}^2x}{\mathrm{d}t^2}\left(1+\frac{4\mu}{\rho R_0 c_0}\right)+\epsilon 2\beta\frac{\mathrm{d}x}{\mathrm{d}t}+\epsilon\omega_0^2 x = -\frac{p_{\mathrm{ext}}(\omega_{\mathrm{c}}t)}{\rho R_0^2}, \tag{2.18}$$

where we have neglected all ϵ^2 order terms. Since the viscosity of water is small, its density is large and the sound speed in water is large, we can consider that the term $\frac{4\mu}{\rho R_0 c_o} \sim \epsilon \ll 1$. We also are considering oscillations of small amplitude, therefore the amplitude of the sound field should be very small. Remember that $p_{\mathrm{ext}}(\omega_{\mathrm{c}}t) = P_A f(\omega_{\mathrm{c}}t)$ and the dimensionless amplitude is $\epsilon = P_A/(\rho R_0^2\omega_{\mathrm{c}}^2)$. The resulting equation corresponds to a driven harmonic oscillator,

$$\frac{\mathrm{d}^2x}{\mathrm{d}t^2}+2\beta\frac{\mathrm{d}x}{\mathrm{d}t}+\omega_0^2 x = -\omega_{\mathrm{c}}^2 f(\omega t) \tag{2.19}$$

Here, ω_0 is the undamped angular frequency of the oscillator and β the damping ratio

$$\omega_0^2 = 3\gamma\frac{P_0}{\rho R_0^2}+(3\gamma-1)\frac{2\sigma_0}{\rho R_0^3}$$
$$2\beta = \frac{4\mu}{\rho R_0^2}+\frac{R_0}{c}\omega_0^2.$$

Note that for a particular driven frequency, the resonance frequency, $\omega_R = \omega_0\sqrt{1-2\frac{\beta^2}{\omega_0^2}}$, the amplitude of the oscillations will be maximum.

By means of a Fourier transform $x(t) = \int_{-\infty}^{\infty}\mathscr{X}(\omega)e^{i\omega t}\mathrm{d}\omega$, the equation (2.19) can be written in frequency domain as

$$-\omega^2\mathscr{X}(\omega)+i2\beta\,\omega\mathscr{X}(\omega)+\omega_0^2\mathscr{X}(\omega) = -\omega_c^2\mathscr{P}_{\mathrm{in}}(\omega) \tag{2.20}$$

from where the response of the bubble is:

$$\mathscr{X}(\omega) = \frac{-\omega_c^2 \mathscr{P}_{\text{in}}(\omega)}{\omega_0^2 - \omega^2 + i2\beta\omega} \tag{2.21}$$

being $\mathscr{P}_{\text{in}}(\omega)$ the fourier transform of the dimensionless incident pressure wave, which could be expressed as a wave package with a central frequency ω_{c}.

The pressure scattered by the bubble can also be linearized

$$P_{\text{sc}} \simeq \rho \frac{R_0}{d} R_0^2 \epsilon \ddot{a} \tag{2.22}$$

and written in frequency domain as

$$\mathscr{P}_{\text{sc}}(\omega) = -\frac{\rho R_0^3}{d} \epsilon \omega^2 \mathscr{X}(\omega) \frac{e^{-ik(d-R_0)}}{1+ikR_0} \tag{2.23}$$

with $k = \omega_{\text{c}}/c_0$ the wave number, and considering $\epsilon = P_A/(\rho R_0^2 \omega_c^2)$.

Combining both expressions (2.21) and (2.23) we can write the dimensionless scattered pressure as

$$\frac{\mathscr{P}_{\text{sc}}(\omega)}{P_A} = \frac{R_0}{d} e^{-ikd} \frac{\omega^2}{\omega_0^2 - \omega^2 + i2\beta\omega} \mathscr{P}_{\text{in}}(\omega) \tag{2.24}$$

where we have assumed that $kR_0 << 1$ and therefore $e^{ikR_0} \simeq 1 + ikR_0$.

2.4 Collective effects

2.4.1 Motivation

In most applications, it is difficult or even impossible to have an isolated bubble in a liquid medium. Some examples are the bubbles behind the turbine of a ship, the suspended bubbles in a bubbly liquid, the solution of ultrasound contrast agents used in medicine, etc. In all these cases we find not a single bubble but a bubble cloud. Due to this, it seems logical to apply the previous equations to a population of bubble instead of to only one bubble. If we assume that the interaction between neighboring bubbles is negligible, then we can treat each bubble as isolated and to sum their responses in order to compute the total response of the cloud. Zheng *et al.* (2006) proposed a method consisting of a size-integration (SI) technique. The method uses a weighting scheme based on the histogram of bubble size distribution to determine the cumulative backscatter.

It is not possible *a priori* to neglect the interaction between neighboring bubbles, as many authors showed. They developed different models taking into account the multiple interaction between bubbles in order to compute the response of a cloud. Omta (1987) studied the oscillations and sound emission of a bubble cloud containing a large number of bubbles. He showed that the frequency spectrum is determined mainly by the total volume of gas in the cloud, and that the natural frequency of the cloud is lower than the eigenfrequency of the individual bubbles. Simultaneously, D'Agostino & Brennen (1988*b*) studied the response of a spherical bubble cloud subject to harmonic far-field pressure excitation using, as Omta (1987), linear equations. They also showed that the sound speed in the medium is drastically modified by the presence of bubbles. Moreover, they identified different modes of collective oscillations. Later, the same authors (D'Agostino & Brennen (1988*a*)) investigated how the acoustical absorption and scattering cross sections of spherical bubble clouds significantly differ from those of individual bubbles in the cloud, as well as from the acoustical cross section of a single large bubble with the same volume of vapor and gas. More recently, Zeravcic *et al.* (2011) analyzed theoretically the collective oscillations of a bubble cloud using concepts and techniques of condensed matter physics.

Most of these models work in frequency domain and use linearized equations, which introduce a strong limitation, not providing accurate results in the case of large amplitudes. As D'Agostino & Brennen (1988*b*) point out in their work, if the linear hypothesis were omitted, only numerical solutions could be realistically attempted. Moreover, it is not easy to try to apply these models to our non-linear equations and solve them numerically. In addition, it is unusual to find populations of bubbles with uniform sizes. Normally, bubble clouds are polydisperse, making more difficult its treatment. However, we can proceed using the size integration (SI) technique proposed by Zheng *et al.* (2006) in the time domain. The question here is if it is adequate to neglect the multiple interactions between bubbles. In the next subsection we are going to show how it is possible to neglect multiple interaction only in some conditions.

2.4.2 Dynamics of bubble clusters

To calculate the pressure scattered by a bubble cloud, Zheng *et al.* (2006) proposed the SI method. According to his formulation, the total scattered pressure is just a superposition of that scattered individually by each bubble, neglecting interaction between bubbles. Suppose we have a bubble cloud with characteristic size D and a number of bubbles N. The bubbles have different sizes with a probability density

function $f(R_0)$ such that $\int_0^\infty f(R_0)\mathrm{d}R_0 = 1$. The total scattered pressure will be

$$P_{\mathrm{sc,T}} = \int_0^\infty P_{\mathrm{sc}}(R_0) N f(R_0)\mathrm{d}R \tag{2.25}$$

Writing this expression in the frequency domain and using 2.24 we get the total scattered pressure as

$$\mathscr{P}_{\mathrm{sc},T} = \frac{\pi}{6}\frac{D^3 n}{d} e^{-ikd} P_A \mathscr{P}_{\mathrm{in}}(\omega)\omega^2 \int_0^\infty \frac{R_0 f(R_0)}{\omega_0^2 - \omega^2 + i2\beta\omega}\mathrm{d}R_0 \tag{2.26}$$

where we have assumed that the cloud is spherical with volume $V_c = \pi/6D^3$ and n is the density number of bubbles such that $n = N/V_c$. As we have seen before, both ω_0 and β depend on bubble size. In order to simplify, let us call $I(\omega) = \int_0^\infty \frac{R_0 f(R_0)\mathrm{d}R_0}{\omega_0^2 - \omega^2 + i2\beta\omega}$ from now on.

This model is valid as long as there are not multiple interactions between bubbles. Nevertheless, a bubble cloud can oscillate as a whole, as we mentioned, and the resonance frequency associated to this motion could hide the resonance frequency of the bubble. Following the computations of Omta (1987) and Commander & Prosperetti (1989) we can get a similar equation in the linear regime and frequency domain. Suppose we have a spherical bubble cloud with characteristic size D. The bubbles have different sizes with a probability density function $f(R_0)$ such that $\int_0^\infty f(R_0)\mathrm{d}R_0 = 1$. Let $n(\mathbf{r})f(R_0)$ be the density number of bubbles with size R_0 that can be found in some region $\mathbf{r}$ of the cloud. We consider the cloud as a continuous field, such that $\eta << \lambda$ being η the characteristic distance between bubbles inside the cloud and λ the wave length of the incident pressure wave. The only effect that the bubbles have in the flow field is to provide a void fraction $\alpha(\mathbf{r}, t)$ which will be different at each point $\mathbf{r}$ of the field. This void fraction is defined as the ratio between the sum of the volumes of all the bubbles and the total volume, gas and liquid, that the cloud occupies. The volume of the bubbles can be calculated as $V_b = \int_0^\infty \upsilon(R_0) f(R_0)\mathrm{d}R_0$, where $\upsilon(R_0)$ is the volume of one bubble with radius R_0.

Let ρ_m and $\mathbf{u}$ denote the average density of the mixture and the velocity. The equation for the conservation of total mass in the mixture can be written in the usual form,

$$\frac{\partial \rho_m}{\partial t} + \nabla\cdot(\rho_m \mathbf{u}) = 0. \tag{2.27}$$

The average density for the mixture liquid and gas is written in terms of the void fraction, considering that $\alpha \ll 1$ and that the gas density is negligible compared to the density of the liquid,

$$\rho_m \simeq \rho(1-\alpha). \tag{2.28}$$

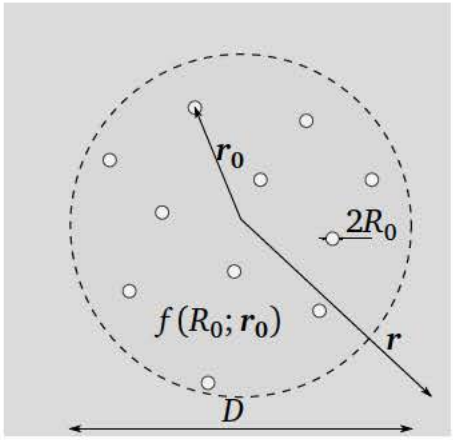

Figure 2.1: Bubble cloud

Substituting (2.28) into (2.27) and rearranging terms, the continuity equation yields

$$\frac{1}{\rho}\frac{D\rho}{Dt} + \nabla \cdot \mathbf{u} = \frac{1}{1-\alpha}\frac{D\alpha}{Dt} \tag{2.29}$$

where $\frac{D}{Dt}$ denotes the convective derivative. According to Commander & Prosperetti (1989), the acoustic theory of small perturbations leads to the approximation $D/Dt \simeq \partial/\partial t$, and therefore equation (2.29) becomes

$$\frac{1}{\rho}\frac{\partial\rho}{\partial t} + \nabla \cdot \mathbf{u} = \frac{\partial\alpha}{\partial t}, \tag{2.30}$$

which is equivalent to the continuity equation of the van Wijngaarden-Papanicolau model (van Wijngaarden (1968)). According to this model, the momentum equation states

$$\rho\frac{\partial \mathbf{u}}{\partial t} + \nabla P = 0, \tag{2.31}$$

which is derived form the general momentum equation for the cloud neglecting the convective term since the terms quadratic in $\mathbf{u}$ are small for the conditions considered. If we take the divergence of equation (2.31) and use equation (2.30) in order to eliminate $\mathbf{u}$ we have

$$\frac{\partial}{\partial t}\left(\frac{\partial\alpha}{\partial t} - \frac{1}{\rho}\frac{\partial\rho}{\partial t}\right) + \nabla \cdot (\frac{1}{\rho}\nabla P) = 0. \tag{2.32}$$

Defining the sound speed in the bubble-free liquid as $c^2 = (\partial P/\partial\rho)$ and making use of the acoustic approximation, such that the variation of liquid density and pres-

sure are small and therefore their quadratic terms are negligible, we find the wave equation for the mixture liquid and gas bubbles:

$$\frac{1}{c^2}\frac{\partial^2 P}{\partial t^2} - \nabla^2 P = \rho \frac{\partial^2 \alpha}{\partial t^2}. \tag{2.33}$$

We have defined the void fraction α as the total volume of the bubbles that form the cloud divided by the volume of the cloud. Taking into account that the number density of bubbles is $n = N/V_c$, the void fraction can be calculated as

$$\alpha = n\frac{4}{3}\pi \int_0^\infty R^3(\mathbf{r}, t; R_0) f(R_0) \mathrm{d}R_0 \tag{2.34}$$

being R the instantaneous radius of the bubble, which is different from the equilibrium radius R_0. Now, an equation for R is needed, so we use the solution x to the linearized Keller-Miksis equation (2.19), such that $R = R_0(1+\epsilon x)$. Differentiating α with respect to time, and considering we are in linear regime,

$$\begin{aligned}\frac{\partial^2 \alpha}{\partial t^2} &= \frac{4}{3}\pi n \int_0^\infty \frac{\mathrm{d}^2 R^3}{\mathrm{d}t^2} f(R_0)\mathrm{d}R_0 \\ &= 4\pi n \int_0^\infty R_0^3 \epsilon \frac{\mathrm{d}^2 x}{\mathrm{d}t^2} f(R_0)\mathrm{d}R_0,\end{aligned} \tag{2.35}$$

the equation (2.33) yields

$$\frac{1}{c^2}\frac{\partial^2 P}{\partial t^2} - \nabla^2 P = \frac{4\pi n}{\omega_c^2} P_A \int_0^\infty R_0 \frac{\mathrm{d}^2 x}{\mathrm{d}t^2} f(R_0)\mathrm{d}R_0. \tag{2.36}$$

By mean of the Fourier transform and making use of (2.21), the previous equation can be written in the frequency domain yielding

$$\frac{-\omega^2}{c^2}\mathscr{P}(\omega) - \nabla^2 P(\omega) = 4\pi n \omega^2 \mathscr{P}(\omega) \int_0^\infty \frac{R_0 f(R_0)\mathrm{d}R_0}{\omega_0^2 - \omega^2 + i2\beta\omega}, \tag{2.37}$$

which can be expressed in a simplified way as:

$$\frac{\omega^2}{c_{\text{eff}}^2}\mathscr{P}(\omega) + \nabla^2 \mathscr{P}(\omega) = 0 \tag{2.38}$$

with $1/c_{\text{eff}}^2 = 1/c^2 + 4\pi n I(\omega)$ the effective sound speed in the bubble cloud. Note

that this equation can be written as the inhomogeneous Helmholtz equation,

$$k^2\mathscr{P}(\omega)+\nabla^2\mathscr{P}(\omega)=-4\pi nI(\omega)\mathscr{P}(\omega) \tag{2.39}$$

with $k=\omega/c_0$ the wave number and the right term the inhomogeneous term, F_{NH}, whose solution can be obtained through the Green function:

$$\mathscr{P}(\mathbf{r},\omega)=(G*\mathscr{P}(\omega))(\mathbf{r})=\int_{\upsilon}G(\mathbf{r}-\mathbf{r_0})F_{\mathrm{NH}}(\mathbf{r_0})\mathrm{d}\upsilon \tag{2.40}$$

where υ represents volume and G is the Green function, that is, the solution of the Helmholtz equation with the inhomogeneous term F_{NH} equal to the Dirac delta function,

$$\frac{1}{c^2}\frac{\partial^2 G}{\partial t^2}-\nabla^2 G=\delta(\mathbf{r}-\mathbf{r_0}) \tag{2.41}$$

whose solution is expressed as

$$G=\frac{e^{-i\mathbf{k}\,(\mathbf{r}-\mathbf{r}_0)}}{4\pi|\mathbf{r}-\mathbf{r_0}|} \tag{2.42}$$

where $\mathbf{k}=\frac{\omega}{c_0}\vec{e}_r$ is the wave vector, the vector $\mathbf{r}$ represents the distance between the center of the cloud and the point where the pressure is going to be measured; and the vector $\mathbf{r_0}$ represents the distance between the center of the cloud and the point where a certain bubble is located.

Substituting in (2.40) the expression for G and $F_{\mathrm{NH}}(\mathbf{r_0})$, we find a solution for the pressure in the bubble cloud

$$\mathscr{P}(\mathbf{r},\omega)=\int_{\upsilon}\frac{e^{-i\mathbf{k}\,(\mathbf{r}-\mathbf{r}_0)}}{4\pi|(\mathbf{r}-\mathbf{r_0})|}4\pi n\omega^2 I(\omega)\mathscr{P}(\mathbf{r_0},\omega)\mathrm{d}\upsilon \tag{2.43}$$

This equation tell us that the pressure measured in a point $\mathbf{r}$ is due to the contributions of all the bubbles in the cloud, located at points $\mathbf{r_0}$. $\mathscr{P}(\mathbf{r_0},\omega)$ is the pressure that a bubble located in point $\mathbf{r_0}$ feels. *A priori* this pressure will be function of the incident pressure as well as the pressure radiated by neighbouring bubbles; therefore, it will be different for every bubble. If we assume that the magnitude of the vector $\mathbf{r}$ is of the order of the distance from the center of the cloud to the receptor point, d, meaning that the pressure is going to be measured far from the cloud, we can write $e^{-i\mathbf{k}\,(\mathbf{r}-\mathbf{r}_0)}\approx e^{-ikd}e^{i\mathbf{k}\,\mathbf{r}_0}$ and $|\mathbf{r}-\mathbf{r_0}|=|\mathbf{r}|(|1-\mathbf{r}/\mathbf{r_0}|)\approx d(1-r_0/d)$. Then, the

equation 2.43 turns to

$$\mathscr{P}(\omega) = n\omega^2 I(\omega)\frac{e^{\frac{-i\omega d}{c_0}}}{d}\int_{\upsilon}\frac{e^{i\mathbf{k}\,\mathbf{r_0}}}{1-\frac{r_0}{d}}\mathscr{P}(\mathbf{r_0},\omega)\mathrm{d}\upsilon \tag{2.44}$$

To simplify this expression and try to recover equation (2.26), several considerations must be done. First, $\mathbf{k}\cdot\mathbf{r_0}$ should be small enough in order to $e^{i\mathbf{k}\,\mathbf{r_0}} \simeq 1$. This condition is satisfied provided that $r_0 \ll \lambda_0$, since $k = \omega/c_0 = 2\pi/\lambda_0$, and therefore $kr_0 \sim r_0/\lambda_0$, with λ_0 the wavelength of the pressure wave outside the bubble cloud. Second, r_0/d must be much smaller than 1, which is satisfied as $r_0 \sim D \ll d$. Third and last, if the pressure inside the cloud can be considered uniform , we can approximate $\mathscr{P}(\mathbf{r_0},\omega) \simeq \mathscr{P}(\omega)$. This implies that all bubbles feel the same pressure, independently of the position $\mathbf{r_0}$ we are looking at. The condition for this fact is that the wavelength in the cloud, defined as $\lambda_{\text{eff}} = 2\pi c_{\text{eff}}/\omega$ must be larger than the characteristic size of the cloud, $\lambda_{\text{eff}} \gg D$. Under these assumptions, the previous equation reads

$$P_{sc,T}(w) = \upsilon n\omega^2 I(\omega)\frac{e^{\frac{-i\omega d}{c_0}}}{d}\mathscr{P}(\omega) \tag{2.45}$$

which is equal to equation (2.26) considering that $\mathscr{P}(\omega)$ is the incident pressure, that is, the external excitation and υ is the volume of the cloud.

Previously we had seen that $c_0^2/c_{\text{eff}}^2 = 1 + 4\pi n c_o^2 I(\omega)$. If $n \to 0$, then the effective sound speed inside the cloud would be very similar to that outside the cloud, that is, we can approximate the wave length inside the cloud as that outside in the pure liquid. Alternatively, when n is large enough the effective velocity can be approximate by $c_{\text{eff}} \simeq (4\pi n I(\omega))^{-1/2}$, so the effective wave length inside the bubble cloud will be $\lambda_{\text{eff}} = \frac{2\pi c_{\text{eff}}}{\omega} = \frac{\pi(\pi n I(\omega))^{-1/2}}{\omega}$. Since $\lambda_{\text{eff}} \gg D$, we can write the relation

$$\frac{1}{nI(\omega)\omega^2} \gg D^2 \quad \text{or} \quad n \ll \frac{1}{D^2\omega^2 I(\omega)} \equiv \frac{1}{D^2\sigma_s^{1/2}} \tag{2.46}$$

where $\sigma_s^{1/2} = \omega^2 I(\omega)$ is the effective scatter cross-section that the average bubble of the distribution would have. Since $n \simeq N/D^3$, the previous relation can also be written as $N \ll D/\sigma_s^{1/2}$.

We see that the density of bubbles n must be large enough in order to approximate $c_{\text{eff}} \simeq (4\pi n I(\omega))^{-1/2}$, but also must satisfy the above criteria ((2.46)). If it does not and n becomes larger, then the wave length inside the cloud would become small enough to induce spatial variations in pressure, in other words, the hypothesis $\lambda_{\text{eff}} \gg D$ would not be satisfied.

Since in our computations we neglect multiple interactions and use Zheng model,

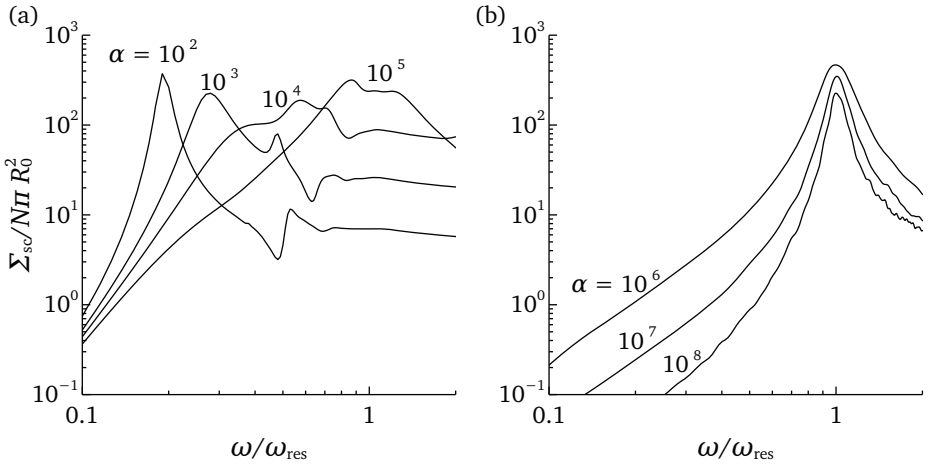

Figure 2.2: Scatter cross-section spectra produced by a monodisperse bubble cloud with $N = 2000$ and $R_0 = 3\mu$m, for different void fractions α.

we must prove that the criteria (2.46) is satisfied. For that, we should calculate the effective scatter cross-section. Parrales (2013), in his PhD thesis, obtains an expression to calculate the scatter cross-section Σ_s of a monodisperse bubble cloud, considering multiple interactions. He plots this cross-section versus the frequency normalized with the resonance frequency (figure 2.2) for different values of the void fraction α, observing that for values $\alpha \geq 10^{-5}$ there exist collective modes of resonance in the spectrum, meanwhile for $\alpha \leq 10^{-6}$ its effect is negligible being the resonance corresponding to that of the individual bubble the only visible in the spectrum.

In figure 2.3, obtained from Parrales (2013), the acoustic dispersion map radiated by a monodisperse bubble cloud is represented. In this map the different regimes of collective modes are shown. We see that for values of void fraction $\alpha < 10^{-6}$, all the acoustical dispersion take place at resonance frequency, indicating that the multiple interaction and coupling between bubbles are negligible and the cloud is acoustically diluted.

2.5 Thermal effects

2.5.1 Introduction

The previous equations consider uniform pressure and temperature inside the bubble and do not take into account thermal effects. According to Prosperetti (1977), thermal damping can be the dominant mechanism of energy disipation under some conditions. Moreover, he maintains that the pressure inside the bubble cannot be

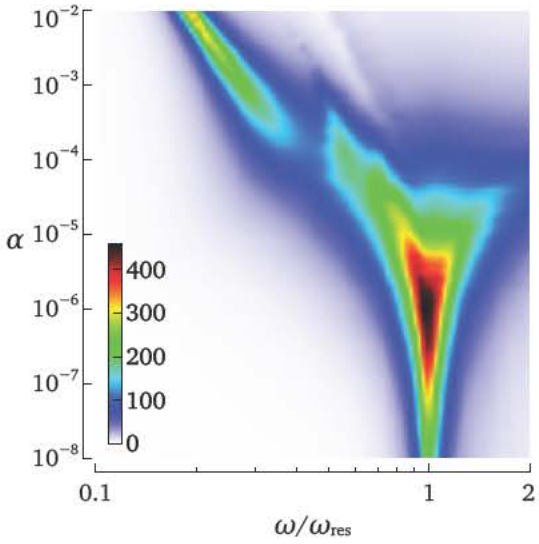

Figure 2.3: Acoustic dispersion map produced by a monodisperse bubble cloud with $N = 1000$ and $R_0 = 3\mu$m. The dimensionless scatter cross-section, $\Sigma_s/N\pi R_0^2$ is represented in the color bar.

considered spatially uniform, at least *a priori*. His analysis is based on a linearized formulation of the problem. On the one hand, to compute the pressure inside the bubble, he solves mass and momentum equations in the gas and also the energy equation both in the gas and in the liquid. From this method he obtains an equation for the amplitude of the radial oscillation x, which depends, among others parameters, of the complex quantity φ which is a function of the frequency, the initial radius and the properties of gas and liquid, and it describes all the thermal effects associated to small-amplitude bubble oscillation.

$$\varphi = \frac{\frac{k_l}{k_g} f(\Gamma_1 - \Gamma_2) + \lambda_2\Gamma_2 - \lambda_1\Gamma_1}{\frac{k_l}{k_g} f(\lambda_2\Gamma_1 - \lambda_1\Gamma_2) - \lambda_1\lambda_2(\Gamma_2 - \Gamma_1)} \tag{2.47}$$

where:

$$\begin{aligned}
\Gamma_{1,2} &= i + G_1 \pm \left[(i-G_1)^2 + 4iG_1/\gamma\right]^{1/2} \\
\lambda_i &= \beta_i \coth\beta_i - 1, \quad i = 1,2 \\
\beta_{1,2} &= \left(\frac{1}{2}\gamma G_2 \left\{ i - G_1 \pm \left[(i-G_1)^2 + 4iG_1/\gamma\right]^{1/2} \right\}\right)^{1/2} \\
f &= 1 + (1+i)(\tfrac{1}{2}G_3)^{1/2} \\
G_1 &= \left[\frac{(D_g/\omega)^{1/2}}{c_g/\omega}\right]^2, \quad G_2 = \omega R_0^2/D_g \\
G_3 &= \omega R_0^2/D_l, \quad k_f = k_l/k_g
\end{aligned} \tag{2.48}$$

In the dimensionless parameters G_1, G_2, and G_3, D_g is the thermal diffusivity of the gas, c_g is the sound speed in the gas, and D_l is the thermal diffusivity in the liquid. k_f is the ratio between the liquid and the gas thermal conductivities. G_1 represents the ratio between the thickness of the layer in which conduction causes significant temperature changes and the wavelength of the sound in the gas. G_2, and G_3 represent the ratios between the bubble radius and the thermal penetration depth in the gas and in the liquid, respectively.

Alternatively, since $D_g \sim \bar{\lambda} c_g$, where $\bar{\lambda}$ is the mean free path of the molecules in the gas, we can approximate $G_1 \sim \frac{\bar{\lambda}}{c_g/\omega}$, so that it can be expected to be a very small quantity. In view of the smallness of G_1 the above expressions can be simplified:

$$\begin{aligned}
\Gamma_1 &= 2(i + G_1/\gamma) \\
\Gamma_2 &= 2[(\gamma-1)/\gamma]G_1 \\
\beta_1 &= (1+i)(\tfrac{1}{2}\gamma G_2)^{1/2}\left\{1 + \tfrac{1}{2}i\,[(\gamma-1)/\gamma]\,G_1\right\} \\
\beta_2 &= (G_1 G_2)^{1/2}\left\{i + \tfrac{1}{2}\,[(\gamma-1)/\gamma]\,G_1\right\}
\end{aligned} \tag{2.49}$$

On the other hand, in order to make the problem treatable, instead of solving the whole conservation equation, he simplifies the problem calculating the pressure inside the bubble assuming a pressure-volume relationship of polytropic type, and incorporating an *ad-hoc* term that includes thermal losses, $P_{in} = P_{in,eq}(R_0/R)^{3\kappa} - 4\mu_{\text{th}}\dot{R}$. In this way he gets the following differential equation for the amplitude of

the radial oscillation:

$$\ddot{x}+\left(4\frac{\mu+\mu_{\text{th}}}{\rho R_0^2}+\frac{\omega R_0/c_0}{1+(\omega R_0/c_0)^2}\omega\right)\dot{x}+\left(\frac{3\kappa P_0}{\rho R_0^2}-(3\kappa-1)\frac{2\sigma}{\rho R_0^3}+\frac{(\omega R_0/c)^2}{1+(\omega R_0/c)^2}\omega^2\right)x=-\epsilon\alpha e^{i\omega t}, \tag{2.50}$$

which compared to that of a damped harmonic oscillator, gives us an expression for the damping term β and the natural frequency ω_0. The damping term is the sum of the viscous damping, β_{vis}, the thermal damping, β_{th} and the acoustic damping, β_{ac}. The first one, β_{vis}, depends on bubble size only, meanwhile the other two depend on the frequency also.

$$\begin{aligned}\beta_{\text{vis}} &= 2\mu/\rho R_0^2\\ \beta_{\text{th}} &= 2\mu_{th}/\rho R_0^2\\ \beta_{\text{ac}} &= \tfrac{1}{2}\omega(\omega R_0/c)\left[1+(\tfrac{\omega R_0}{c})^2\right]^{-1}\end{aligned}$$

The natural frequency, ω_0, depends on both bubble size and frequecy too. If the acoustical radiation is neglected and $\kappa=\gamma$, its value is equal to the well-known Minnaert's frequency.

$$\omega_0^2=\tfrac{3\kappa P_0}{\rho R_0^2}-(3\kappa-1)\tfrac{2\sigma}{\rho R_0^3}+(\tfrac{\omega R_0}{c})^2\left[1+(\tfrac{\omega R_0}{c})^2\right]^{-1}\omega^2$$

For very small bubbles the viscous damping is the dominant damping mechanism, but its importance decreases quickly with bubble size. The importance of the acoustical damping increases with frequency and bubble size, becoming dominant for very high frequencies and relatively large bubbles (50-100 microns). The thermal damping is the dominant mechanism for relatively small bubbles, a few tens of microns in diameter, and not very high frequency, around 100 kHz. This information is collected in figure 2.4 for air bubbles in water. It is worth to mention that the expressions for the damping have been obtained assuming uniform pressure. This assumption fails, as we will explain below, when the acoustic wavelength inside the bubble, $\lambda_g=c_g/\omega$, is of the order of the bubble size R_0; in these cases the expression for the thermal damping produces incoherent values as we can see in the two bottom graphics of figure 2.4 (a).

In order to calculate the unknown quantities κ and μ_{th}, he compares the solution for the equation (2.50) with the solution previously obtained solving the energy equation. Doing so, he gets two expressions to calculate an effective polytropic exponent κ and an effective thermal viscosity μ_{th}. These quantities depend on both driving frequency and bubble radius, as well as the physical properties of the gas

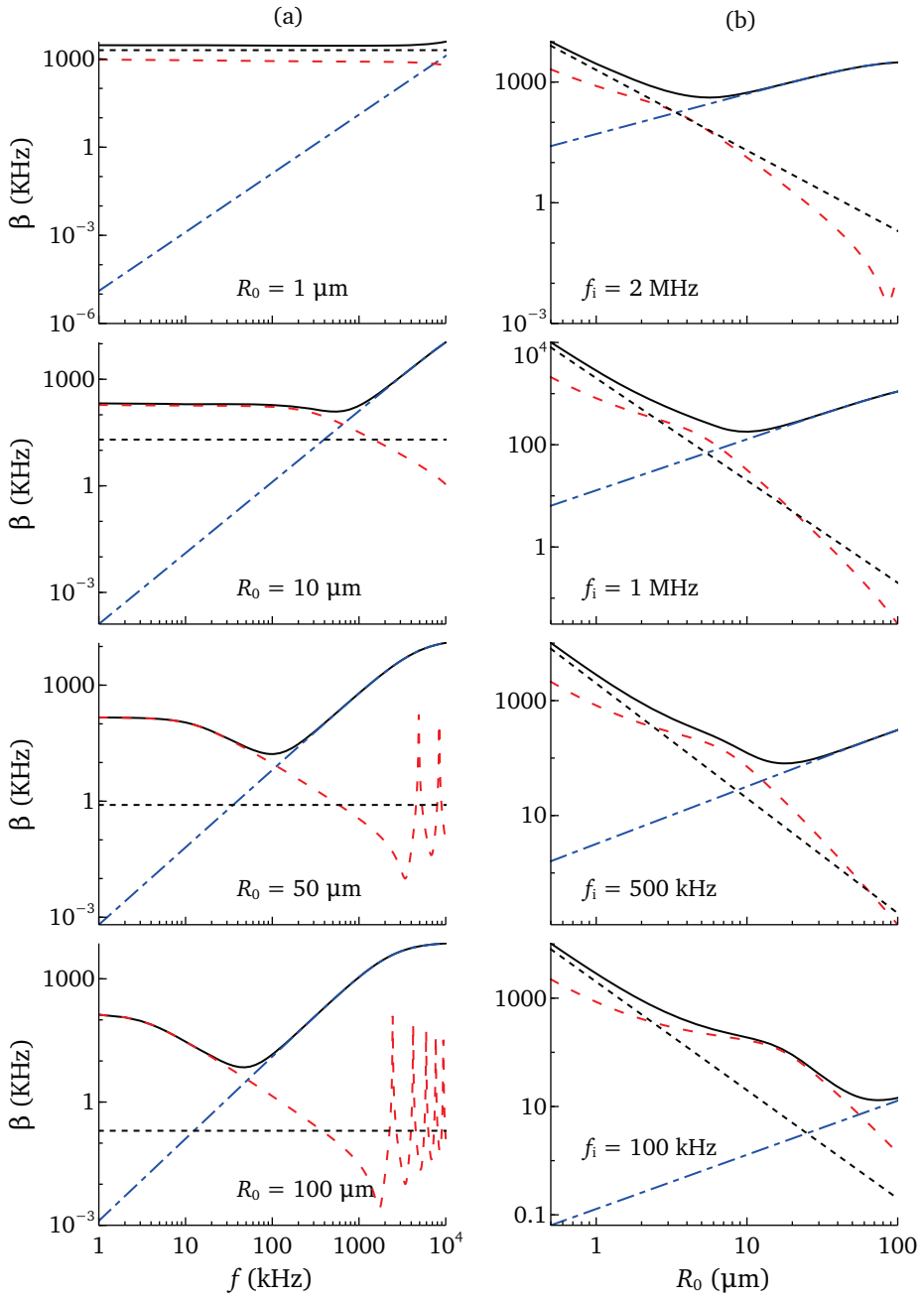

Figure 2.4: The dependence of the damping coefficient β on frequency f_i and bubble size R_0 is shown in (a) and (b) respectively. The black dotted line represents β_{vis}, the blue dash-dotted line β_{ac} and the red dashed line β_{th}. The sum of the three is the total damping, β, which is represented with the black solid line.

and the liquid. This dependence with frequency and bubble size has been plotted for air bubbles in water and for hydrogen bubbles in water in figures 2.5 and 2.6, respectively.

$$\begin{aligned} \mu_{\text{th}} &= \tfrac{1}{4}\omega\rho_g R_0^2 \text{Im}(\varphi) \\ \kappa &= \tfrac{1}{3}\left(\omega^2\rho_g R_0^2/(P_0 + \tfrac{2\sigma}{R_0})\right)\text{Re}(\varphi) \end{aligned}$$

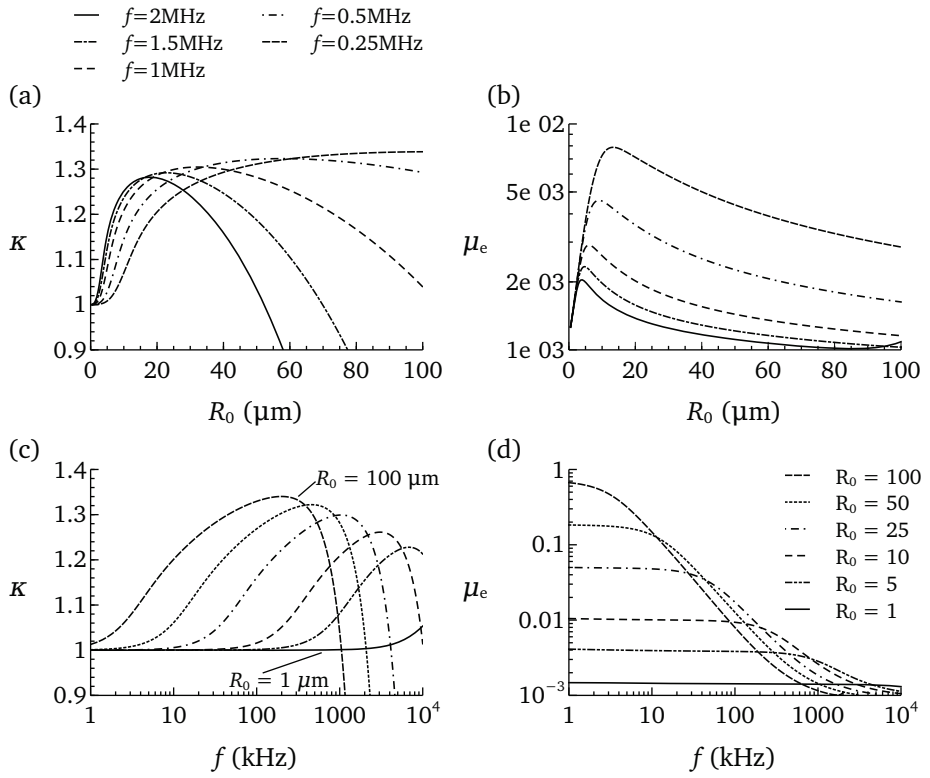

Figure 2.5: The effective polytropic exponent, κ and the effective thermal viscosity, μ_{th}, as a function of bubble size, R_0, for different driving frequencies (figures (a) and (b) respectively), and as a function of frequency f, for different initial radii (figures (c) and (d)). Results for air bubbles in water.

To understand the thermal behavior of the bubble we should note that there are three different time scales involved in the problem, namely, the characteristic oscillation time, ω^{-1}, the time needed to propagate the pressure changes inside the bubble, $t_g = R_0/c_g$, and the characteristic thermal diffusion time, $t_D = R_0^2/D_g$. If $t_g/\omega^{-1} \ll 1$

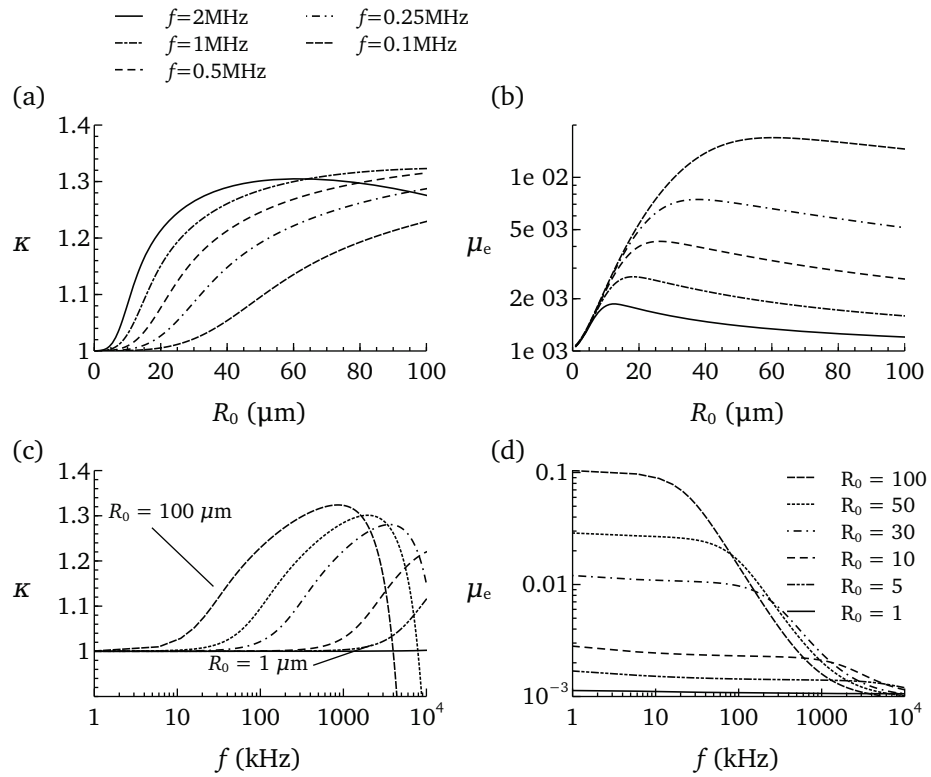

Figure 2.6: The effective polytropic exponent, κ and the effective thermal viscosity, μ_{th}, as a function of bubble size, R_0, for different driving frequencies (figures (a) and (b) respectively), and as a function of frequency f, for different initial radii (figures (c) and (d)). Results for hydrogen bubbles in water.

(or what it is the same, $R_0 \ll \lambda_g$), then the pressure inside the bubble can be assumed uniform. This implies that the pressure change is radially propagated within the bubble instantaneously, therefore the bubble feels the same pressure in its motion. This condition is satisfied for very small bubbles and for not relatively large frequencies. In this case, the behaviour of the bubble can be isothermal, adiabatic or a mix of both, depending of the characteristic diffusion time. If $t_D << \omega^{-1}$ the bubble behaves as isothermal ($\kappa \simeq 1$), while if $t_D >> \omega^{-1}$ the bubble behaves as adiabatic ($\kappa \simeq \gamma$). In the first case, oscillations are too slow to maintain an appreciable temperature gradient in the bubble; when the bubble is compressed the temperature changes, but this change is immediately propagated towards the wall and diffused to the liquid, being the temperature uniform inside the bubble and equal to the liquid temperature at the bubble wall. In the second case the oscillations are fast enough to keep the bubble isolated thermally from the liquid. In this case, before the temperature variation

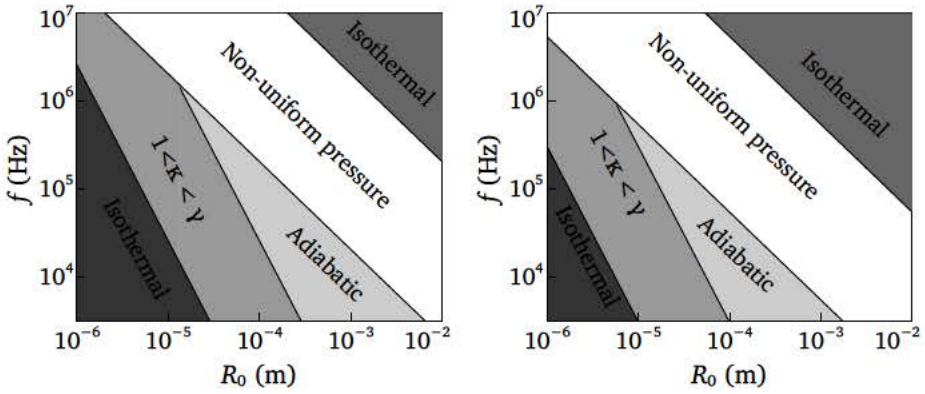

Figure 2.7: Behavior diagram as a function of size and excitation frequency for hydrogen (left) and air bubbles (right). In the dark, medium and light gray regions $t_g/\omega^{-1} << 1$ and the pressure is uniform. In the dark gray region on the top, $t_g/\omega^{-1} >> 1$ and pressure can be considered also uniform. In the white region, $t_g/\omega^{-1} \sim 1$, the pressure inside the bubble is not spatially uniform.

due to the compression can be propagated towards the wall, the bubble is expanding again, thus the bubble wall can be assumed to have the same temperature always. When $t_D \sim \omega^{-1}$, then the bubble behaves nor isothermal neither adiabatically but like a combination of both and $1 < \kappa < \gamma$.

However, if $t_g/\omega^{-1} \gtrsim 1$, the pressure inside the bubble cannot be considered uniform. As we mentioned before, $R_0 \sim \lambda_g$ and the uniform pressure assumption fails. Indeed, a polytropic law to model the pressure-volume relation makes no sense anymore, and the effective polytropic exponent takes values out of the range $1 < \kappa < \gamma$ (Plesset & Prosperetti (1977)), as can be seen in figure 2.5. The question is how is the thermodynamic behavior of the bubble as a whole at very high frequencies, when $t_g/\omega^{-1} >> 1$. This regime implies that the characteristic time of oscillations is much smaller than t_g, this is, before the pressure can change during the compression, the bubble is expanding again. Therefore, the pressure can be assumed uniform again, not only spatially but also in time, and the bubble behaves as isothermal. Effectively, if the pressure does not change, temperature neither, being this inside the bubble the same that the one at the bubble wall. To summary this information, a phase diagram has been plotted in fig. 2.7, where the different behaviour of hydrogen and air bubbles is represented as a function of size and frequency. Effectively, in this plot we can see that a bubble of 100μm irradiated at a frequency higher than 1MHz is located in the non-uniform pressure regime, both for hydrogen and air bubbles. This explains the oscillations of the thermal damping, β_{th}, in figure 2.4.

Looking at figures 2.5 and 2.6 we check that for very small bubbles, lower than 10μm, both κ and μ_{th} do not change significantly with frequency, and $\kappa \simeq 1$. Nev-

ertheless, for relatively larger bubbles, the variations with frequency are really important. In this case it makes no sense to talk about a constant effective polytropic exponent or a constant effective viscosity. This is more remarkable if we consider a bubble population with different sizes instead of only one bubble, since κ and μ_{th} vary with bubble size. To incorporate the thermal effects to our problem, instead of solving the complete problem, this is, solving the full equations for the gas inside the bubble, we integrate an ordinary differential equation which models the heat transfer between the bubble and the liquid, as we will see in next section.

Many authors incorporate the thermal effects using an effective viscosity coefficient, and an effective polytropic exponent (Dayton, etc.). This is valid only, as we have seen, if the bubbles are very small and they are driving at high frequencies, of the order of 1MHz. This is normally the case when working with typical ultrasound contrast agents, where common values for the polytropic exponent and the effective viscosity are $\kappa = 1$ and $\mu_{\text{eff}} = 2\mu_{\text{water}}$. Moreover, this UCA's are normally coated microbubbles, being the damping due to the elasticity of the shell more important than the thermal one. Also, most UCA's are filled with high molecular weight gases, thus the isentropic exponent is already close to 1.

2.5.2 Thermal model for the bubble oscillations

In order to take into account the thermal problem, we should solve the energy equation in the liquid, outside the bubble, as well as full continuity, momentum and energy equations in the gas inside the bubble. This implies to solve numerically partial differential equations (PDE), which is highly expensive from the computational point of view. Because of this, to incorporate thermal effects we use an ordinary differential equation (ODE) model described by Stricker *et al.* (2011), in order to model the temperature, and also the pressure, inside the bubble. This model makes no attempt to describe the spatial gradient of the temperature inside the bubble, considering this as an averaged value which depends on time only. As they describe in their work, the results obtained using ODE model are very similar to those obtained integrating the full system of PDE's. It is worth pointing out that they are using this ODE model to study sonoluminescence, what implies high amplitudes of oscillation and a strong non-linear behavior, while we are interested in lower amplitudes. Therefore, the limitations of this model will be more severe in that case than in ours. Moreover, we have adapted the model to our conditions, as explained following.

To describe the gas pressure inside the bubble we use the usual equation of state for ideal gases, instead of using Van der Waals equation, as it is done in some references (Stricker *et al.*, 2011; Dayton *et al.*, 2002),

$$P_g = \rho_g R_g T \tag{2.51}$$

The temperature inside the bubble, considered spatially uniform, is described using a control volume that contains the gas inside the bubble. Neglecting reaction and dissolution, the energy equation for the gas can be written as

$$m_g c_v \frac{\mathrm{d}T}{\mathrm{d}t} = \dot{Q} - P_g \dot{V} \tag{2.52}$$

being m_g the mass of gas inside the bubble, c_v the constant-volume specific heat of the gas and $V = \frac{4}{3}\pi R^3$ the volume of the bubble.

We model the net heat flux in the problem through the heat transport equation, where the temperature gradient has been approximated as the expected temperature difference through a thermal boundary layer,

$$\dot{Q} = 4\pi R^2 \lambda_g \frac{T_0 - T}{l_{\text{th}}}, \quad \text{with } l_{\text{th}} = \min\left(\sqrt{\frac{RD_g}{\dot{R}}}, \frac{R}{\pi}\right) \tag{2.53}$$

where l_{th} is an estimate of the thickness of the thermal boundary layer in the gas, D_g and λ_g are the thermal diffusivity and thermal conductivity of the gas, respectively. Regarding the value of l_{th}, the general properties of diffusion processes suggest $l_{\text{th}} \sim \sqrt{D_g t_{\text{th}}}$, where t_{th} is a characteristic time scale. Since we are interested in knowing how the temperature varies with the radius of the bubble, a logical scale is $t_{\text{th}} = R/\dot{R}$. If $\dot{R}$ becomes very small, then l_{th} will be very big and does not make sense to talk about thermal boundary layer in that case, being the size of the bubble the characteristic length scale. Then, an appropriate cutoff suggested by Stricker *et al.* (2011) is $l_{\text{th}} = R/\pi$.

The mass of gas contained inside the bubble is assumed constant and it can be calculated as:

$$m_g = \rho_g \mathcal{V} = \rho_g 4/3\pi R^3 = \rho_{g,0} 4/3\pi R_0^3 \tag{2.54}$$

which, combined with the equation of state (2.51) and knowing that the pressure inside when it is at rest is $P_{g0} = p_0 + 2\sigma/R_0$, may be written as:

$$m_g = \frac{4\pi}{3} R_0^3 \frac{p_0 + 2\sigma/R_0}{R_g T_0} \tag{2.55}$$

To model the radial oscillations of the bubble we use the well-known Keller-Miksis equation formulated as:

$$\begin{aligned}\left(1 - \frac{\dot{R}}{c}\right) R\ddot{R} + \frac{3}{2}\dot{R}^2\left(1 - \frac{\dot{R}}{3c}\right) &= \left(1 + \frac{\dot{R}}{c}\right)\frac{1}{\rho}\left(P_g - P_a f(\omega_c \tau) - P_0\right) + \\ &+ \frac{R\dot{P}_g}{\rho c} - 4\frac{\nu\dot{R}}{R} - 2\frac{\sigma}{\rho R}\end{aligned} \tag{2.56}$$

Note that thermal effects appear in the terms related with the pressure inside the bubble and its time derivative. Using the usual notation to make the problem dimensionless, we can rewrite the problem as:

$$(1-M\dot{a})\,a\ddot{a}+\frac{3}{2}\dot{a}^2\left(1-\frac{M\dot{a}}{3}\right)=(1+M\dot{a})\left(\Pi_g-\epsilon\sin\tau-\Pi_0\right)+$$
$$+aM\Pi_g\left(\frac{\dot{T}}{T}-3\frac{\dot{a}}{a}\right)-1/Re\frac{\dot{a}}{a}-1/We\frac{1}{a} \tag{2.57a}$$
$$\Pi_g=\Pi_{g,0}\frac{T}{a^3} \tag{2.57b}$$
$$\dot{T}=Fo\frac{a^2}{l_{th}}(1-T)-3(\gamma-1)\frac{\dot{a}}{a}T \tag{2.57c}$$
$$l_{th}=\min\left(\left(Pe^{-1}\frac{a}{|\dot{a}|}\right)^{1/2},\quad\frac{a}{\pi}\right) \tag{2.57d}$$

where the new dimensionless parameters are $\Pi_{g,0}=\frac{m_g R_g T_0}{\gamma\rho R_0^2\omega_c^2}$, which represents the dimensionless pressure of the gas when the bubble is at rest and it is denoted by Euler number, which compares the pressure with the kinetic energy, the Fourier number $Fo=3\frac{\lambda_g/\rho_{g,0}c_v}{R_0^2\omega_c}$, which compares the heat diffusion with the heat storage; and finally the gas Peclet number $Pe=\frac{R_0^2\omega_c}{D_g}$, which is the ratio between the convective term and the diffusion term.

Solving the equation system (2.57) we obtain the time evolution of the average temperature inside the bubble. Therefore, we can calculate the pressure using (2.51). If we assume an isentropic law for the pressure inside the bubble, such that $PV^\kappa=cte$, we can compute an effective polytropic exponent for different initial bubble radius and different frequencies in order to check if $1<\kappa<\gamma=1.4$ for the range of sizes and frequencies we simulate.

$$PV^\kappa=cte\rightarrow P_gV^\kappa=P_{g0}V_0^\kappa\rightarrow P_gR^{3\kappa}=P_{g0}R_0^{3\kappa} \tag{2.58}$$
$$\frac{P_g}{P_{g0}}=\frac{R}{R_0}^{-3\kappa}\Rightarrow\log\frac{P_g}{P_{g0}}=-3\kappa\log\frac{R}{R_0} \tag{2.59}$$

We can check in figure 2.8 that effectively the value of κ is in the range $1\leq\kappa\leq\gamma$, and also that its value depends on the driving frequency. Please note that the goal of this comparison is merely qualitative. As we said before, it makes no sense to use a polytropic pressure-volume relationship to model pressure inside the bubble.

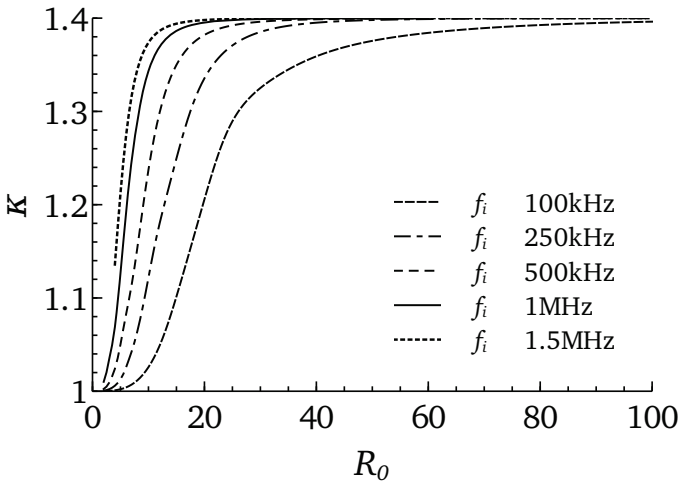

Figure 2.8: The polytropic exponent as a function of the bubble size, for different driving frequencies.

Validation of the model

We check that, in the isothermal and adiabatic limits, the thermal model produces the same results that the Keller-Miksis equation considering $\kappa = 1$ and $\kappa = \gamma$ respectively. Effectively, if the thermal diffusion is important, the bubble behaves as isothermal, meanwhile if this effect is negligible, it behaves as adiabatic. In figure 2.9, the power spectra density for a bubble of 100 and 300 μm has been plotted. The thermal problem has been solved imposing a small and a large value for the constant λ_g and the results are compared to that obtained with KM equation with $\kappa = 1.4$ and $\kappa = 1$, respectively.

Leighton (1994) uses the Rayleight-Plesset equation to simulate the oscillations of a 10 microns air bubble in water at 20C and under one atmosphere static pressure, which is subjected to a 10 kHz sound-field with pressure amplitude $P_A = 2.4$ bar. He shows how the radius of the bubble grows exponentially to a maximum size ($R \simeq 300\mu$m) and after that, it rapidly collapses (it takes a value lower than zero). The thermal model also predicts the collapse of that bubble for the same conditions, as can be seen in the figure 2.10, although the maximum size reached before the collapse in smaller, $R \simeq 100\mu$m, which is more realistic.

Effectively, for highly nonĺinear conditions, the acceleration of the bubble wall reaches large values very quickly and the numerical code diverges to NaN numbers. Even if we use a very short time step, the radius reaches values lower than zero,

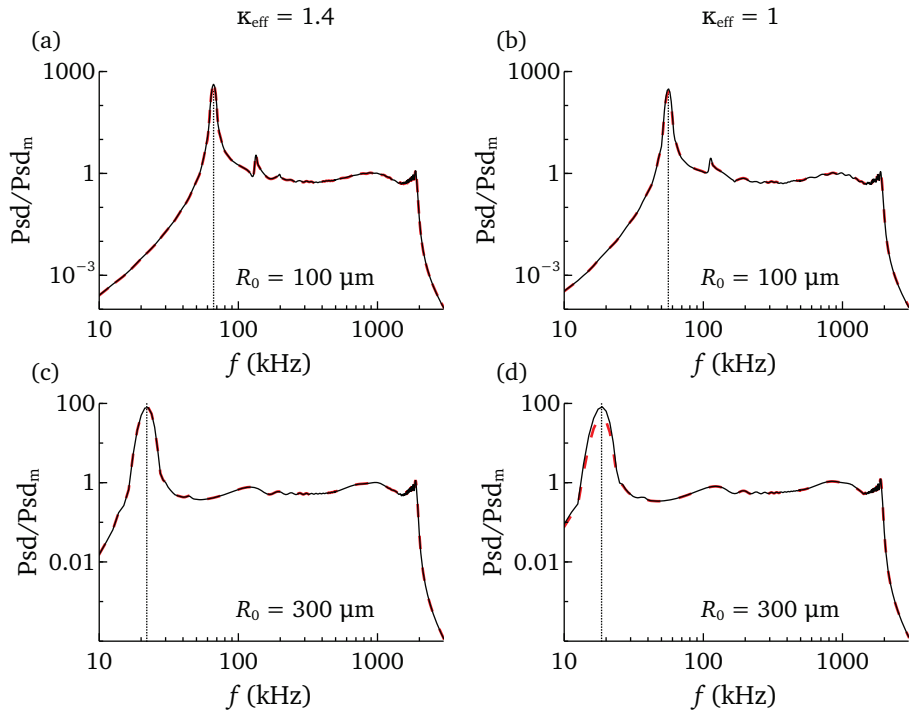

Figure 2.9: At the left, the thermal problem has been solved imposing a small value for the constant λ_g and the result is compared to that obtained with KM equation with $\kappa = 1.4$. At the right, a large value of λ_g is used to solve the thermal problem and the result compared to the KM equation with $\kappa = 1$.

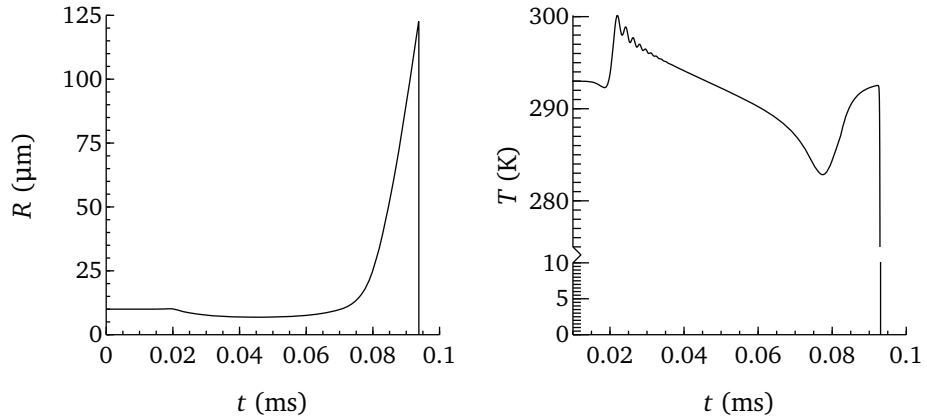

Figure 2.10: Radial and temperature oscillations of an air bubble with $R_0 = 10\mu$m, excited with a 10 kHz sound-field with pressure amplitude $P_A = 2.4$ bar. After some time the bubble grows up exponentially to immediately collapse.

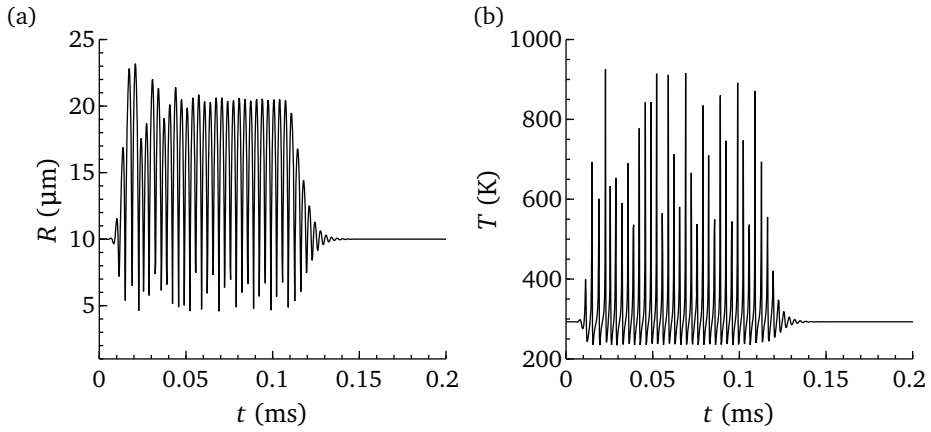

Figure 2.11: Radial and temperature oscillations of an air bubble with $R_0 = 10\mu$m, excited with a 300 kHz sound-field with pressure amplitude $P_A = 100$ kPa. The oscillations of the bubble are highly non-linear.

meaning that the bubble collapses. Therefore, we remark here that this model does contemplate the volumetric collapse of the bubble. However, it cannot predict the stability of the surface of the bubble and therefore a possible collapse for that. For example, a bubble excited at a frequency close to the resonance and with a large pressure amplitude will show a behavior highly nonlinear, as we can observe in figure 2.11. In this case the amplitude of the oscillation is very large, and consequently the temperature changes a lot, oscillating between 250K and 900K. These values of temperature are consistent with the reported by Stricker *et al.* (2011). Also, Calvisi *et al.* (2007) study the temperature reached by the bubble before the collapse, reporting values of thousands of Kelvin, in consistency with the values reported by Yasui *et al.* (2011). Therefore, although the oscillation is highly non-linear, this behavior of the bubble is perfectly possible. But, as Stricker *et al.* point out in their work, near resonances the bubble is doubtful to retain its integrity, and it is likely that shape instabilities occur and the bubble breaks up. Therefore, although the model can reproduce a highly nonlinear behavior, we cannot guarantee the total reliability since it does not contemplate shape instabilities of the bubble surface. Anyhow, this scenario is far from our interest since, as we will focus on linear to weakly-nonlinear oscillations.

2.5.3 Linearized problem

If the amplitude of the radial oscillations is really small, we can consider that the radial and temperature fluctuations are in a linear regimen. In this case, the variations

of the temperature will be very small, too, so we can linearize the variables of the problem as:

$$\begin{cases} a = 1 + \epsilon\, x \\ T = 1 + \epsilon\, \theta \end{cases} \tag{2.60}$$

Substituting variables a and T in the previous equations yields:

$$\dot{\theta} = -\pi Fo\theta - 3(\gamma-1)\dot{x} \tag{2.61a}$$

$$\ddot{x} - M\Pi_{g,0}\left(\dot{\theta} - 3\dot{x}\right) - \left(\frac{M}{We} - \frac{1}{Re}\right)\dot{x} - \Pi_{g,0}(\theta - 3x) - \frac{1}{We}x = -p_{\text{ext}}(\omega_c t) \tag{2.61b}$$

where the linearization of l_{th} is shown following:

$$\begin{aligned} \frac{1}{l_{th}} &\approx \left(\frac{1}{Pe^{-1}\frac{\dot{a}}{a}}\right)^{1/2} + \frac{1}{a/\pi} \approx \left(\frac{Pe}{\frac{1+\epsilon x}{\epsilon \dot{x}}}\right)^{1/2} + \frac{\pi}{1+\epsilon x} \\ &\simeq \sqrt{Pe}\sqrt{\epsilon\dot{x}}(1 - \tfrac{1}{2}\epsilon x) + \pi(1-\epsilon x) = \pi - \pi\epsilon x + Pe^{\frac{1}{2}}\epsilon^{\frac{1}{2}}\dot{x}^{\frac{1}{2}} \end{aligned}$$

If we substitute that expression for $1/l_{th}$ in the previous equation, we observe that the only term with an order of magnitude lower than ϵ^2 is π, therefore we can conclude that $1/l_{th} \sim \pi$.

This system can be solved in the frequency domain taking Fourier transform of the variable x and θ, which transform into $\mathscr{X}(\Omega)$ and $\Theta(\Omega)$, respectively.

$$i\Omega 3(\gamma-1)\mathscr{X}(\Omega) + (\pi Fo + i\Omega)\Theta = 0 \tag{2.62a}$$

$$\begin{aligned} \left\{-\Omega^2 + i\Omega\left(3M\Pi_{g,0} - \frac{M}{Re}\right) + 3\Pi_{g,0} - \frac{1}{We}\right\}\mathscr{X}(\Omega) \\ -\left(i\Omega M\Pi_{g,0} + \Pi_{g,0}\right)\Theta = -P_A \end{aligned} \tag{2.62b}$$

Clearing out the variable Θ of (2.62a) and substituting in (2.62b) we get the following equation for the variable $\mathscr{X}(\Omega)$ that represents the radial response:

$$\begin{aligned} &\left\{-\Omega^2 + i\Omega\left(3M\Pi_{g,0} - \frac{M}{We} + \frac{1}{Re}\right) + \frac{i\Omega^3 3(\gamma-1)\Pi_{g,0}M}{\Omega^2 + (\pi Fo)^2} + 3\Pi_{g,0} - \frac{1}{We} + \right. \\ &\left. \Omega^2\frac{\Pi_{g,0}3(\gamma-1)(1 - M\pi Fo)}{\Omega^2 + (\pi Fo)^2} + \frac{3i\Omega(\gamma-1)\Pi_{g,0}\pi Fo}{\Omega^2 + (\pi Fo)^2}\right\}\mathscr{X}(\Omega) = p_{\text{ext}}(\omega_c t) \end{aligned} \tag{2.63}$$

where Ω represents the dimensionless frequency ω/ω_c. We can check that if $\Lambda \to 0$, effectively we recover the linearized Keller-Miksis equation. We can compute the resonance frequency of the bubble doing $\mathrm{d}\mathscr{X}(\Omega)/\mathrm{d}\Omega = 0$. The response $\mathscr{X}(\Omega)$ can be written as

$$\mathscr{X}(\Omega) = \frac{1}{\sqrt{(\Omega_0^2 - \Omega^2)^2 + (\beta\Omega)^2}} \tag{2.64}$$

with

$$\Omega_0^2 = 3\Pi_{g,0} - \frac{1}{We} + 3(\gamma-1)\Pi_{g,0}(1 - M\pi Fo)\frac{\Omega^2}{\Omega^2 + (\pi Fo)^2}$$
$$\beta = M\left(3\Pi_{g,0} - \frac{1}{We}\right) + \frac{1}{Re} + 3(\gamma-1)\Pi_{g,0}\frac{M\Omega^2 + \pi Fo}{\Omega^2 + (\pi Fo)^2}$$

such that

$$\frac{\mathrm{d}}{\mathrm{d}\Omega}(\Omega^2 - \Omega^2)^2 + (\beta\Omega)^2 = 0$$

Note that Ω_0 and β depend on Ω, therefore care should be taken in the differentiation.

In order to simplify, we are going to assume that $Fo^2 \ll \Omega^2$, therefore the previous equation yields

$$\left(-\Omega^2 + i\Omega\hat{\beta} + \hat{\Omega}_0^2\right)\mathscr{X}(\omega) = p_{\mathrm{ext}}(\omega_c t) \tag{2.65}$$

where

$$\hat{\Omega}_0^2 = 3\gamma\Pi_{g,0} - \frac{1}{We} - 3\Pi_{g,0}M(\gamma-1)\pi Fo$$
$$\hat{\beta} = \frac{1}{Re} + \left(3\gamma\Pi_{g,0} - \frac{1}{We}\right)M + 3\Pi_{g,0}(\gamma-1)\frac{\pi Fo}{\Omega^2} \tag{2.66}$$

which differs from the linearized Keller-Miksis equation due to the Fourier number Fo that incorporates the thermal effects. Note that the thermal and the acoustic damping are coupled, therefore it seems not possible to separate an expression for thermal damping and another one for the acoustic one and compare with the expressions deduced by Prosperetti. We can check that the new thermal terms also affect

the resonance frequency of the bubble, being this

$$\left(\frac{f_{\text{res}}}{f_i}\right)^2 = 3\gamma\Pi_{\text{g},0} - \frac{1}{We} - 3\Pi_{\text{g},0}M(\gamma-1)\pi Fo$$
$$-\frac{1}{2}\left[\frac{1}{Re} + \left(3\gamma\Pi_{\text{g},0} - \frac{1}{We}\right)M + 3\Pi_{\text{g},0}(\gamma-1)\frac{\pi Fo}{\Omega^2}\right]^2 \tag{2.67}$$

References

CALVISI, M. L., LINDAU, O., BLAKE, J. R. & SZERI, A. J. 2007 Shape stability and violent collapse in acoustic travelling waves. *Physics of Fluids* **19**, 047101.

COMMANDER, K.W. & PROSPERETTI, A. 1989 Linear pressure waves in bubbly liquids: Comparison between theory and experiments. *J. Acoust. Soc. Am.* **85** (2), 732–746.

D'AGOSTINO, L. & BRENNEN, C. E. 1988*a* Acoustical absorption and scattering cross sections of spherical bubble clouds. *J. Acoust. Soc. Am.* **84** (6), 2126–2134.

D'AGOSTINO, L. & BRENNEN, C. E. 1988*b* Linearized dynamics of spherical bubble clouds. *J. Fluid Mech.* **199**, 155–176.

DAYTON, P.A., ALLEN, J.S. & FERRARA, K.W. 2002 The magnitude of radiation force on ultrasound contrast agents. *J. Acoust. Soc. Am.* **112**, 2183–2192.

FLYNN, H. G. 1975 Cavitation dynamics i. a mathematical formulation. *J. Acoust. Soc. Am.* **57** (6), 1379–1396.

GILMORE, F.R. 1952 The collapse and growth of a spherical bubble in a viscous compressible liquid. *California Imtitute of Techdogy Hydrodynumica Laboratory, Rep* **26-4**.

HERRING, C. 1941 Theory of the pulsations of the gas bubble produced by an underwater explosion. *OSRD Rep.* **236**.

KELLER, J. B. & MIKSIS, M. 1980 Bubble oscillations of large amplitude. *J. Acoust. Soc. Am.* **68** (2), 628–633.

KHISMATULLIN, D. B. & NADIM, A. 2002 Radial oscillations of encapsulated microbubbles in viscoelastic liquids. *Physics of Fluids* **14**, 3534–3556.

LANDAU, L. & LIFSHITZ, E. 1959 *Fluid Mechanics*. Adison-Wesley, Reading, MA.

LEIGHTON, T.G. 1994 *The acoustic bubble*. Academic Press, London.

MARMOTTANT, P., VAN DER MEER, S., EMMER, M., VERSLUIS, M., DE JONG, N., HILGENFELDT, S. & LOHSE, D. 2005 A model for large amplitude oscillations of coated bubbles accounting for buckling and rupture. *J. Acoust. Soc. Am.* **118** (6), 3499–3505.

OMTA, R. 1987 Oscillations of a cloud of bubbles of small and not so small amplitude. *J. Acoust. Soc. Am.* **82** (3), 1018–1033.

PARRALES, MIGUEL 2013 Propagación y dispersión de ondas acústicas a través de nubes de microburbujas. PhD thesis, Universidad de Sevilla.

PLESSET, MS. & PROSPERETTI, A. 1977 Bubble dynamics and cavitation. *Annu. Rev. Fluid Mech.* **9**, 145–185.

PLESSET, M. S. 1949 The dynamics of cavitation bubbles. *J. Appl. Mech.* **16**, 277–282.

PROSPERETTI, A. 1977 Thermal effects and damping mechanisms in the forced radial oscillations of gas bubbles in liquids. *J. Acoust. Soc. Am.* **61** (1), 17–27.

PROSPERETTI, A. & LEZZI, A. 1986 Bubble dynamics in a compressible liquid. part 1. first-order theory. *J. Fluid Mech.* **168**, 457–478.

RAYLEIGH, LORD 1917 On the pressure developed in a liquid during the collapse of a spherical cavity. *Phil. Mag.* **34** (200), 94–98.

STRICKER, L., PROSPERETTI, A. & LOHSE, D. 2011 Validation of an approximate model for the thermal behavior in acoustically driven bubbles. *J. Acoust. Soc. Am.* **130** (5), 3243–3251.

TRILLING, L. 1952 The collapse and rebound of a gas bubble. *J. Appl. Phys.* **23**, 14–17.

VAN WIJNGAARDEN, L. 1968 On equations of motion for mixtures of liquid and gas bubbles. *J. Fluid Mech.* **33**, 465–474.

YASUI, K., TOWATA, A., TUZIUTI, T., KOZUKA, T. & KATO, K. 2011 Effect of static pressure on acoustic energy radiated by cavitation bubbles in viscous liquids under ultrasound. *J. Acoust. Soc. Am.* **130** (5), 3233–3241.

ZERAVCIC, Z., LOHSE, D. & VAN SAARLOOS, W. 2011 Collective oscillations in bubble clouds. *J. Fluid Mech.* **680**, 114–149.

ZHENG, H., BARKER, A. & SHANDAS, R. 2006 Predicting backscatter characteristics from micron- and submicron-scale ultrasound contrast agents using a size-integration technique. *IEEE Trans. Ultrasonics, Ferroelectrics and Freq. Control* **53**, 639–644.

CHAPTER

THREE

Acoustic spectrum of polydisperse diluted clouds of bubbles

3.1 Introduction

As we have seen in chapter 2, there are several equations to model the radial oscillations of the bubbles, which have not analytical solution. In this chapter, we are going to solve numerically the Keller-Miksis equation, to compare it with the linear regime, for which is possible to find an analytical solution, as we have seen in section 2.3. Also, we solve the simplified thermal problem explained in section 2.5 in order to compare the results with those obtained with Keller-Miksis equation neglecting thermal effects, or considering them through the use of an effective polytropic exponent and an effective viscosity.

In order to determine the instantaneous radii of the bubble, we integrate numerically the previous equations with suitable initial conditions. Note that in case we neglect thermal effects, we only have to solve an ODE; in the case we take into account thermal effects, we should integrate a system of two ODEs. The initial conditions are the radius and temperature at rest, and that the wall velocity is zero, since the bubble is considered to be quiescent.

The numerical method used is a fourth order Runge Kutta with constant time step. The time integration is done in Fortran while the previous and posterior analysis is done in Matlab. Once the evolution of the radius with time is known, we can compute the pressure radiated by the bubble and then the power density spectrum in order to detect the resonant frequency.

In the first section, we study the oscillations of a single bubble. Firstly, we difference between linear and non-linear regime. Secondly, we compare the results obtained with Keller-Miksis equation with the ones produced by the thermal model. We will see how both equations produce different results in general. However, when oscillations can be considered linear, the results produced by both Keller-Miksis and

linear equation, using the effective values of κ and μ_{eff} match well with the results provided by the thermal model. Alternatively, we probe how the resonance frequency is affected by the ambient pressure, maintaining the other parameters fixed.

In the second section, we will study the response of a bubble cloud. For this case, we use the thermal model since it provides more accurate results. Also, when studying a cloud instead of a single bubble, it makes no sense to take an effective value of κ or μ_{eff}. In addition, we will study the effect of the kind of excitation pressure wave. We will also study the effect of the size distribution of the bubble cloud on the accuracy of the determination of the resonance frequency.

Lastly, we develop an analytic formulae based on a linear analysis in order to calculate the acoustic spectrum of a bubble cloud. The results will be compared to that obtained with the numerical simulations.

3.2 Radial oscillations of a single bubble

3.2.1 Linear and non-linear regimes

We have already seen in section 2.3 that if the radius departs slightly from its initial or equilibrium value and it can be written as $R = R_0(1+\epsilon x)$, with $\epsilon \ll 1$, we can assume that the bubble oscillates in the linear regime. In the linear analysis, we have defined the behavior of the bubble as linear or not linear depending on the dimensionless amplitude of the pressure wave, $\epsilon = \frac{P_A}{\rho\omega^2 R_0^2}$, such that if $\epsilon \ll 1$, the oscillations are linear. But certainly, the dimensionless parameter for the acoustic pressure is not adequate to differ between linear and nonlinear oscillations. For the case in which we study a bubble of a few microns under a low driving frequency, a hundreds of kHz, the oscillations of the bubble will be weak, since the driving frequency is far from the resonance. This implies that the quantity $\rho\omega^2 R_0^2$ is small, therefore for a not relatively large pressure amplitude P_A, $\epsilon \geq 1$ and even so, the oscillation will be linear. By the contrary, if the driving frequency is close to the resonance associated to that size of bubble, even with a low pressure amplitude such that $\epsilon \ll 1$, the amplitude of the oscillation is such that they cannot be considered linear. In figure 3.1 we can see an example of this. Here, a bubble of $R = 1\mu$m is excited with a driving frequency of $f = 100$kHz and an amplitude of $P_A = 10$kPa. The oscillations are linear and therefore the linear equation produces the same result than the Keller-Miksis equation. However, for a bubble of $R = 3\mu$m excited at a driving frequency of $f_i = 1$MHz, which is near the resonance frequency, and a pressure amplitude of $P_A = 10$kPa, the oscillations are clearly non-linear. In effect, the linear equation does not reproduce the results obtained with the non-linear equation.

In order to distinguish between linear and non-linear regimes, we should choose

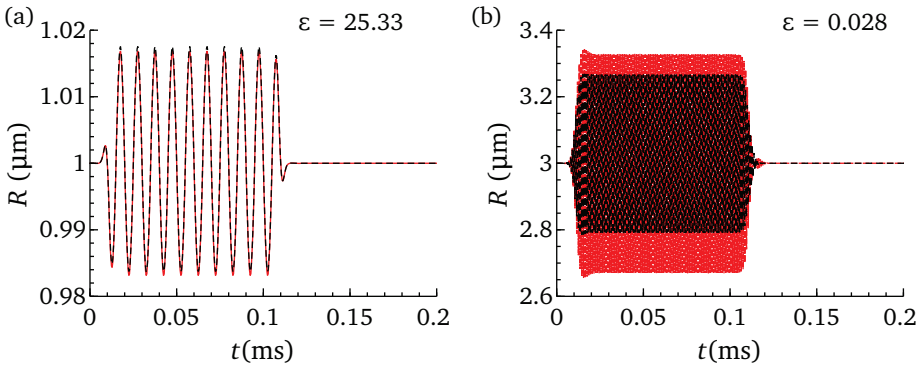

Figure 3.1: (a) Bubble in linear regime with large value of ϵ. The linear solution, red solid line, matches perfectly with the solution of the Keller-Miksis equation, represented by the black dashed line. (b) Bubble in non-linear regime with small value of ϵ. The linear solution is the red solid line and the KM solution is the black dashed line.

another parameter which take into account if the driving frequency is far from the resonance. As we will see in the last section of the chapter, the parameter $P_A F$, where $F(\omega; R_0) = 1/\left(\left(\frac{\omega_0}{\omega}\right)^2 - 1 + i\frac{2\beta}{\omega}\right)$ must be evaluated at $\omega = \omega_i$, is a good option, since it presents its maximum at resonance frequency. Therefore, if we are exciting with a frequency close to the resonance of the bubble, $F(\omega_i)$ will be large, meanwhile if we use a frequency far from the resonance, its value is small.

When the radial oscillations of the bubbles are such that $(R-R_0)/R_0 = \epsilon x \geqq 0.1$, we consider that the behavior of the bubble is lightly non-linear. This behavior is important because it is precisely the non-linearity of the bubbles what makes them good contrast agents. Also, the non-linear response is stronger in amplitude, which is important in order to detect the resonance frequency from the acoustical response of the bubble.

3.2.2 Keller-Miksis equation versus Thermal model

As we anticipated in 2.5, thermal damping becomes the most important damping mechanism under some conditions. In this cases, the differences between the results obtained with the thermal model and with the Keller-Miksis (KM) equation should be noticeable, since the KM equation neglects the heat transfer. However, if we correct this equation with the values of κ and μ_{eff} explained before, both equations should provide similar results, as least for the the cases in which we can assume linear regime.

To study the differences between the two methods, we analyze several cases.

For them, we plot the radial response of a forced bubble obtained with the thermal model, as well as the evolution of the temperature in order to observe if this is constant and the case can be considered isothermal, or by the contrary, the temperature changes notably. Then, we compare this solution with the radial response obtained with the KM equation assuming adiabatic or isothermal case, blue line in the following plots, and also with the one obtained with KM equation using the effective polytropic exponent and viscosity, κ and μ_{eff} (red line). In table 3.1 the different studied cases have been summarized.

R_0 (μm)	f_c (kHz)	P_A (kPa)	μ_{eff} (kg/(m s))	κ	ΔR(%)
1	100	10	1	1	2
20	900	10	0.002	1.3	0.1
40	500	300	0.0025	1.33	2.5
10	300	10	0.007	1.1	12
3	1000	10	0.002	1	10

Table 3.1: Different conditions studied to analyze the difference between thermal model and Keller-Miksis equation.

According to figure 2.4, for a bubble with size $R_0 = 1\mu$m driving at a frequency of 100 kHz, the most important damping mechanism is the viscous damping followed by the thermal one with similar order of magnitude. The acoustic damping is negligible since the bubble is small and the driving frequency is low. This frequency is very far from the resonance frequency of the bubble, and the pressure amplitude is low, $P_A = 10$ kPa, therefore the behavior of the bubble is linear, as can be seen in figure 3.2. Also, we can observe that the temperature remains constant and the process can be assumed isothermal. Indeed, the value for the effective polytropic exponent is $\kappa = 1$, and the effective viscosity is equal to that for the water. Using these effective values in the KM equation we obtained exactly the same result than that provided by the thermal model. By the contrary, if we use wrongly the value for γ, the oscillations obtained are too damped and they do not match with the thermal solution.

We examine now the case of a bubble with radius $R_0 = 20\mu$m excited with $P_A =$ 10 kPa and driving frequency $f_i = 900$ kHz. As can be observed in figure 3.3, the radial oscillations are linear and the temperature remains constant, therefore we can classify the process as isothermal. Indeed, if we solve KM equation with $\kappa = 1$ and water viscous coefficient, the result for the radial oscillation is equal to the one obtained by the thermal model. Taking a look at the effective values according to the analysis of Prosperetti (1977), we see that these are $\kappa = 1.3$ and $\mu_{\text{eff}} = 0.002$ kg/ms. Integrating the KM equation with these values we also have the same result. This is justified because the acoustic damping is much more important than the thermal or the viscous damping, being these considerably smaller.

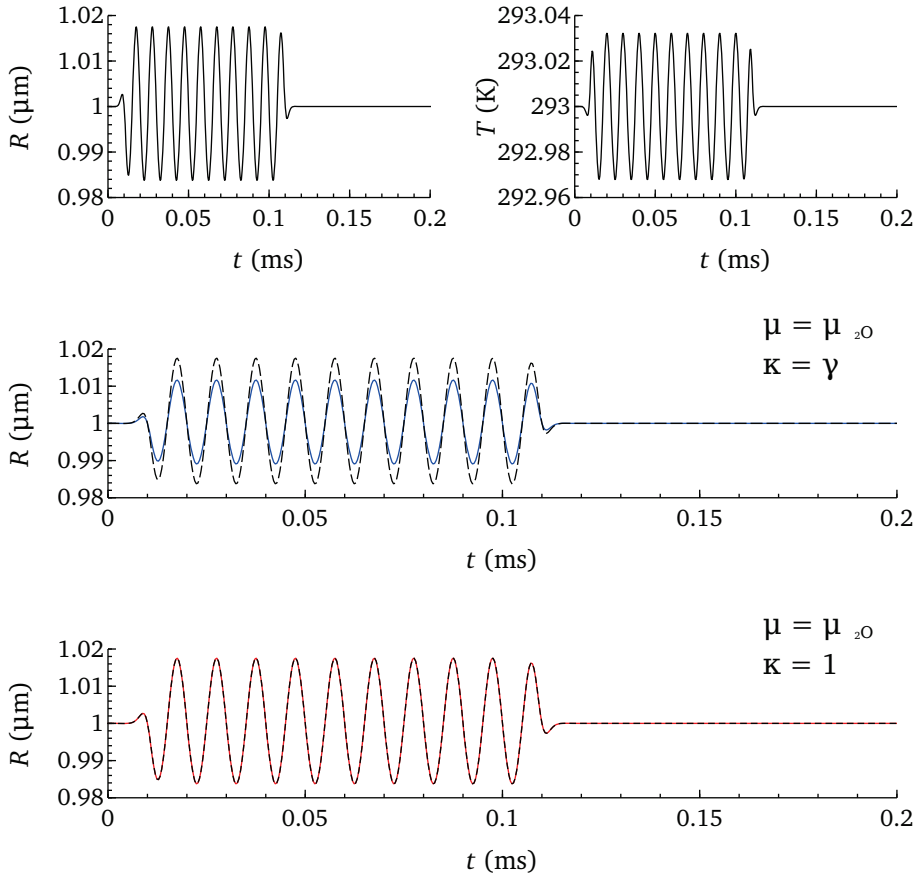

Figure 3.2: Bubble with $R_0 = 1\mu$m excited with a sinusoidal pressure wave with amplitude $P_A = 10$ kPa and driving frequency $f_i = 100$ kHz. At the top, the results of instantaneous radius (left) and temperature (right) are observed. The radial oscillations provided by the thermal model are compared with the Keller-Miksis equation, taking values of water viscosity and $\gamma = 1.4$ (middle, blue solid line) and effective values of μ_{eff} and κ(bottom, red solid line). It can be checked that the latter yields same results than the thermal model.

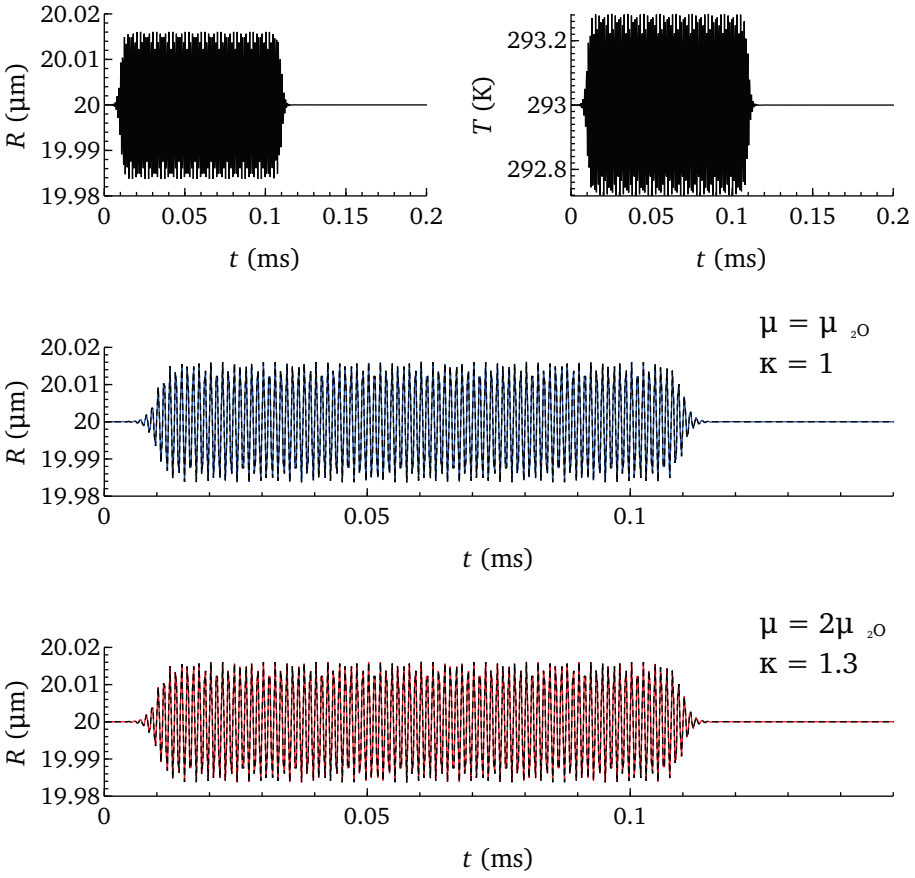

Figure 3.3: Bubble with $R_0 = 20\mu$m excited with a sinusoidal pressure wave with amplitude $P_A = 10$ kPa and driving frequency $f_i = 100$ kHz. At the top, the results of instantaneous radius (left) and temperature (right) are observed. The radial oscillations provided by the thermal model are compared with the Keller-Miksis equation, taking values of water viscosity and $\gamma = 1$ (middle, blue solid line), since the behaviour is isothermal, and effective values of μ_{eff} and κ(bottom, red solid line). It can be checked that both results match perfectly with the solution provided by the thermal model.

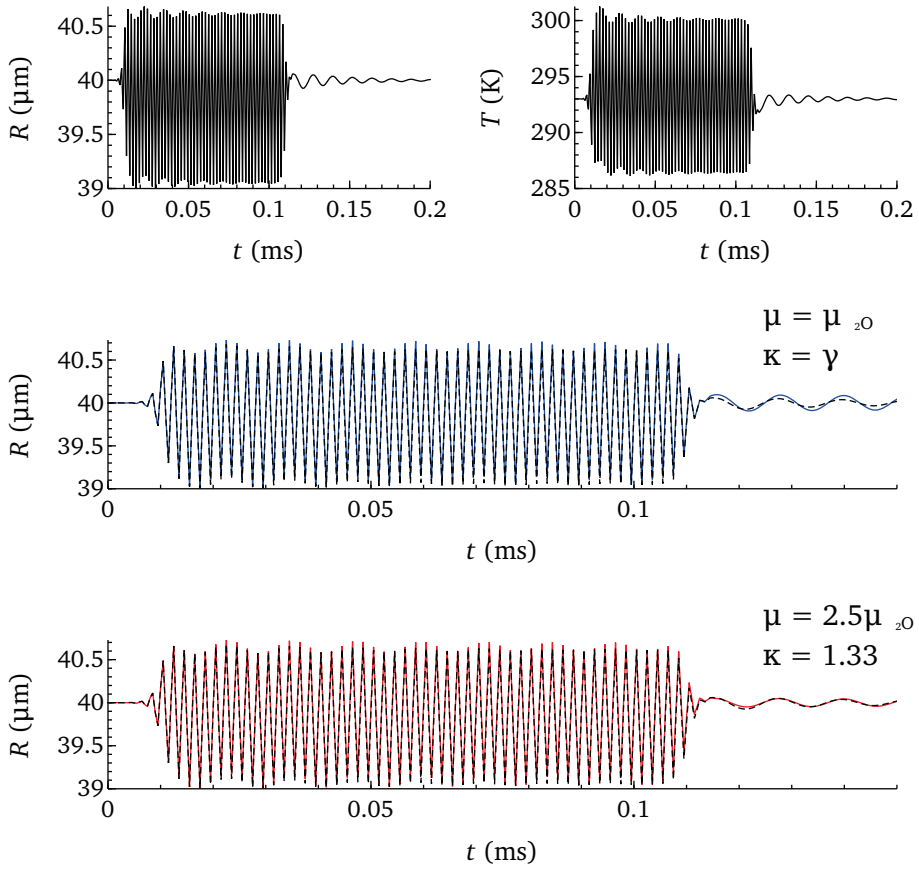

Figure 3.4: Bubble with $R_0 = 40\mu$m excited with a sinusoidal pressure wave with amplitude $P_A = 300$ kPa and driving frequency $f_i = 500$ kHz. At the top, the results of instantaneous radius (left) and temperature (right) are observed. The radial oscillations provided by the thermal model are compared with the Keller-Miksis equation, taking values of water viscosity and $\gamma = 1.4$ (middle) and effective values of μ_{eff} and κ(bottom). It can be checked that the latter yields the same results than the thermal model.

The oscillations suffered by a bubble of 40μm of radius excited by a pressure wave with frequency $f_c = 500$ kHz, and amplitude $P_A = 300$ kPa, are linear even with such a high amplitude, since the driving frequency is far from the resonance associated to this bubble (see figure 3.4). According to figure 2.4, the most important damping mechanism for these values of bubble size and driving frequency is the acoustic one, being the viscous and the thermal damping of the order of a hundred times smaller. We can check in figure 3.4 that the temperature varies notably, therefore we could consider *a priori* the case as adiabatic. The response from the bubble obtained with KM equation with $\kappa = \gamma = 1.4$ is very similar to that obtained with the thermal model. However, if we use the effective values of $\kappa = 1.33$ and $\mu_{\text{eff}} = 0.0025$ kg/ms derived from Prosperetti's expressions explained in chapter 2, section 2.5, the response is exactly equal to that of the thermal model.

For a bubble with radius $R_0 = 10\mu$m, excited with a pressure wave with amplitude $P_A = 10$kPa and driving frequency $f_c = 300$kHz close to the resonance, the radial oscillations cannot be considered linear; indeed, the variation of the radius is a 10% of the initial radius. Also, the temperature changes significantly, as can be seen in figure 3.5. According to figure 2.4, the thermal damping is the most important, therefore, we can anticipate that the KM equation does not reproduce well the results obtained with the thermal model. In fact, if we integrate the KM equation considered the case as adiabatic, the radial response shows a lower amplitude than that obtained for the thermal model. Also we observe that a larger time is necessary so that the oscillations are damped. This is explained because we are neglecting the thermal effects, when we observe that they are very important in this case. Even if we resolve KM equation considered $\kappa = 1.1$ and $\mu_{\text{eff}} = 0.007$ kg/ms, the radial oscillation does not match the solution obtained with the thermal model. This is due to the response of the bubble cannot be considered linear, meanwhile these effective values are derived from the linear analysis.

Looking at figure 2.4, we check that for a bubble of radius $R = 3\mu$m driving at a frequency of $f_i = 1$MHz, the thermal and viscous damping are equally important, meanwhile the acoustic damping can be neglected. In addition, the driving frequency is close to the resonance frequency of this bubble size, therefore the oscillations are not linear, even when the amplitude of the pressure wave is low ($P_A = 10$kPa), as can be observed in figure 3.6. Because of this, the effective values for the polytropic exponent and viscous coefficient, $\kappa = 1$ and $\mu_{\text{eff}} = 0.002$ kg/ms, obtained from the analysis of Prosperetti do not produce good results. Indeed, according to these values the process is isothermal; however, we can check in figure 3.6 that the temperature does not remain constant but changes notably. If we consider the process as adiabatic, and use $\kappa = \gamma$ in the KM equation, the oscillations are highly damped compared with the thermal model result.

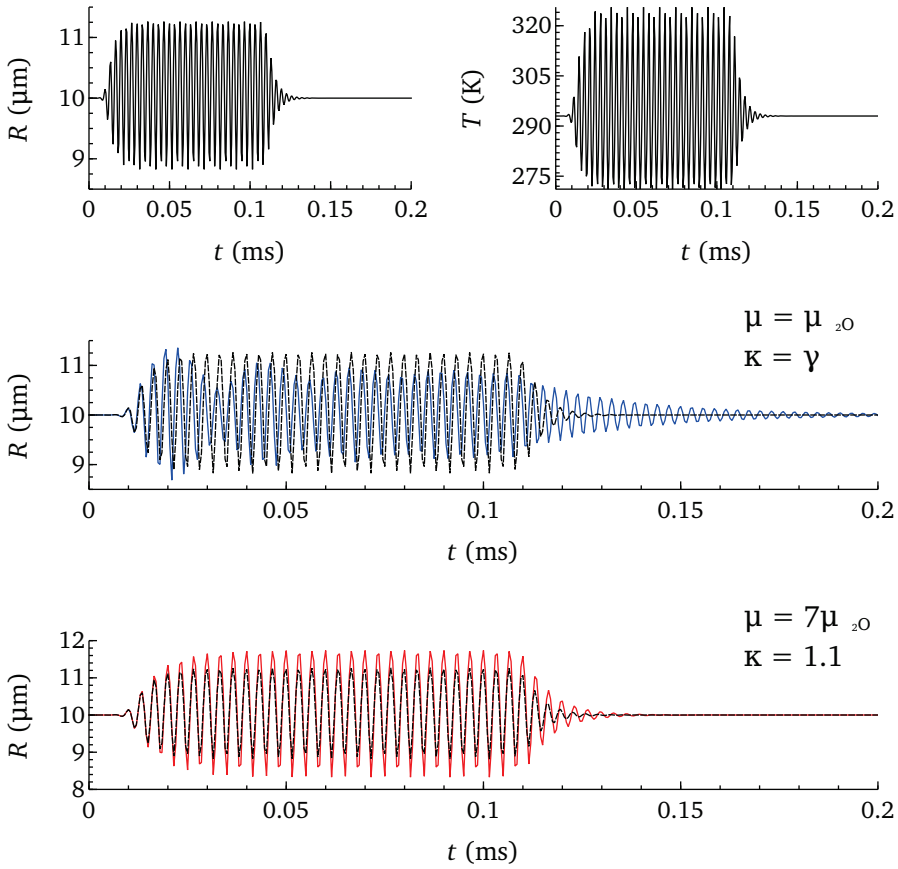

Figure 3.5: Bubble with $R_0 = 10\mu$m excited with a sinusoidal pressure wave with amplitude $P_A = 10$ kPa and driving frequency $f_i = 300$ kHz. At the top, the results of radius (left) and temperature (right) are observed. The radial oscillations provided by the thermal model are compared with the Keller-Miksis model, taking values of water viscosity and γ and effective values (bottom)

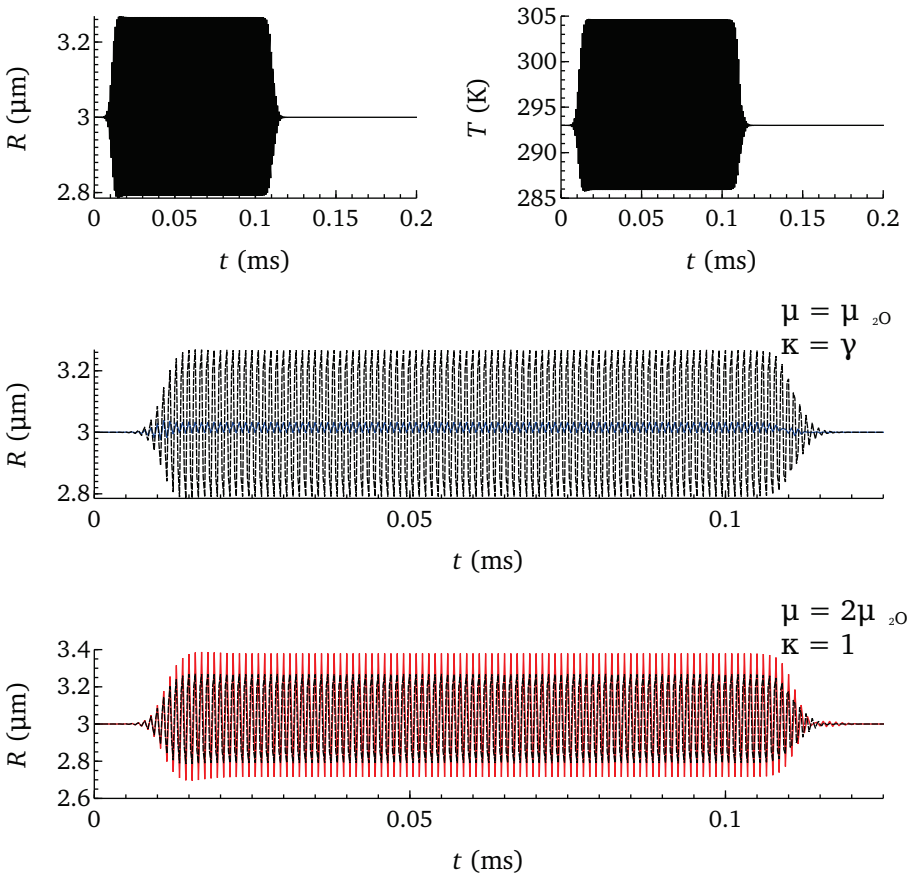

Figure 3.6: Bubble with $R_0 = 3\mu$m excited with a sinusoidal pressure wave with amplitude $P_A = 10$ kPa and driving frequency $f_i = 31$ MHz. At the top, the results of radius (left) and temperature (right) are observed. The radial oscillations provided by the thermal model are compared with the Keller-Miksis model, taking values of water viscosity and γ and effective values (bottom)

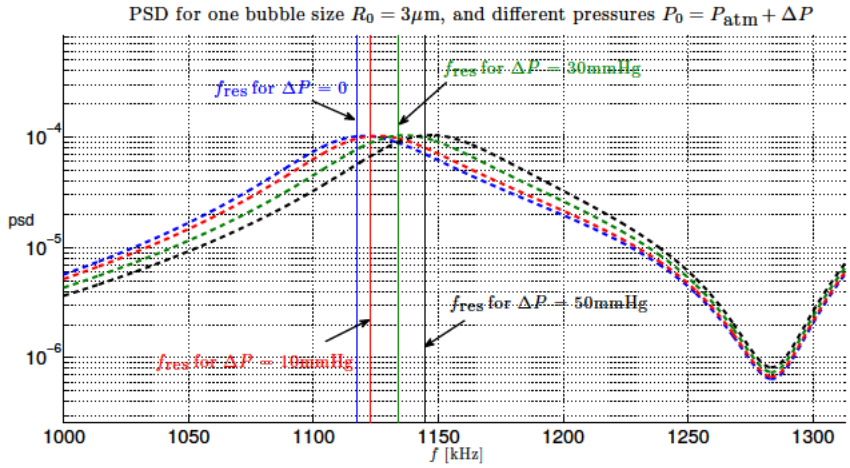

Figure 3.7: Effect of the ambient pressure in the resonance frequency.

3.3 Effect of the ambient pressure on the resonance of a single bubble

As we remark in chapter 1, the resonance frequency is strongly related to the ambient pressure. In figure 3.7, a bubble of $R_0 = 3\mu$m is subjected to the same acoustic pulse, but we change the ambient pressure in the range of pressure increments observed in the cardiac cycle. We can check how the resonance peak moves to higher frequencies when the static pressure of the medium is increased. Nevertheless, the variation in the resonance due to an increment in pressure of 10 mmHg is not very remarkable, and other effects exist which influence the position of the resonance peak, making difficult its accurate determination. Specially significant is the effect of the polydispersity when we have a bubble cloud instead of a single bubble, as we will see in the next section. In order to develop a non invasive technique of pressure measurement, useful in the field of medicine, to measure the pressure inside the circulatory system, we should be able to detect changes of pressure of 10 mmHg.

3.4 Numerical simulations for bubble clouds

Different insonation parameters, such that pulse length, insonation frequency, pressure amplitude, have been study. As we will see in the results, depending on the bubble population we need to excite, some parameters are better than others, meanwhile some of them are not good at all.

3.4.1 Preliminary considerations

Size Distribution

To model the size of the bubble population, normally weibull or gamma probability distributions are used (Parrales *et al.*, 2014). In our case, we choose the gamma distribution to model the size distribution since it has nice math properties. Then, the probability function is computed as:

$$f(R_0) = \frac{\theta^{-k}}{\Gamma(k)} D^{k-1} e^{-D/\theta} \tag{3.1}$$

being θ and k the scale and shape parameters of the distribution, which are related with the mean and variance through the expressions $D_m = k\theta$ and $var = k\theta^2$. When the value of k is large, the value of $\Gamma(k) = (k-1)!$ cannot be computed numerically in matlab so we use the following approximation:

$$f(R_0) = \frac{1}{D}\sqrt{\frac{k}{2\pi}} e^{-k\varepsilon^2/2}; \tag{3.2}$$

with $\varepsilon = D/D_m - 1$.

Pressure scattered by a cloud

As we explained in section 2.4, under some conditions we can neglect the multiple interactions between bubbles and assume that the total scattered pressure can be computed as the sum of the individual contribution of each bubble. In the following analysis, therefore, we will use the size integration technique proposed by Zheng *et al.* (2006) in order to compute the scattered pressure by the bubble cloud. We make sure that the necessary conditions in order that this method is valid are satisfied, especially we calculate the value of the void fraction $\alpha = V_b/V_c$ as the ratio between the volume of all the bubbles and the volume of the cloud. The volume of bubbles can be calculated as

$$V_b = N \int_0^\infty 4\pi/3 R_0^3 f(R_0) \mathrm{d}R_0, \tag{3.3}$$

where N is the total number of bubbles, $f(R_0)$ is the size distribution and R_0 is the initial radius of the bubble. For the different size distributions used, we have considered a number of bubbles of 50 or 100. The values for the total volume of the bubbles oscillates between $V_b = 10^{-5} - 6 \times 10^{-3} \mu\mathrm{m}^3$. In order to compute the pressure scattered at a distance, we are considering in allcases that $d = 1\mathrm{cm}$, and the criteria $d \sim D$, being D the characteristic length of the cloud, must be satisfaid.

Therefore, we can assume that $V_c \approx 10^3 \text{mm}^3$. In the worse case, the value for the void fraction is $\alpha \approx 6 \times 10^{-6}$. In the figure we saw that for $\alpha = 10^{-6}$ the predominant frequency in the spectrum was the resonance frequency.

Thermal Model

When studying a bubble cloud with different sizes, to use an effective value of κ and μ_{eff} to take into account the thermal effects makes no sense, since we have seen that these values depend on the bubble size. Moreover, in order to detect the resonance frequency in the acoustic spectrum, we are working in the lightly non-linear regime, and these effective values are derived from a linear analysis. To achieve a better accuracy, we use the thermal model in the following analysis.

3.4.2 Influence of the kind of excitation wave

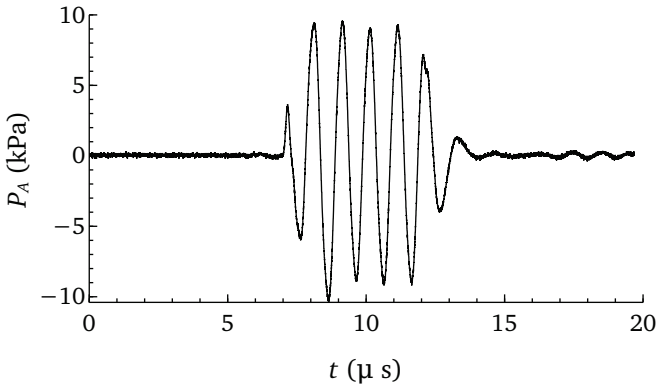

Figure 3.8: Example of a signal produced by a pulse generator machine, with $f_i = 1$ MHz and number of cycles $N_c = 6$.

When the bubble is excited with a sinusoidal wave package, this is, with a large number of cycles, then the only detectable frequency in the spectra is the driving one. Since we are interested in detecting the resonance frequency in the spectra, we need to excite with a pulse with a length as short as possible. To excite with a Dirac delta function would be ideal; in this way, the only remarkable peak would be located at the resonance frequency in the spectrum. Unfortunately, this is not possible with the commercial US machines that are available currently, which produce a sinusoidal wave packet with a variable number of pulses. In figure 3.8 an example of a wave produced by one of these machines can be seen. It is defined by the driving frequency f_i and the number of cycles N_c. In order to try to model this kind of waves, we use

a sinusoidal pulse modulated with a gaussian function, with a very short length. Instead of using the number of cycles we define the pulse length, which is related with the former through the expression $L_p = N_c/f_i$. The pulse length needed to detect the resonance frequency depends on the insonation frequency. The larger the driving frequency is, the shorter the pulse length must be.

Besides the most common pulse produced by US machines is the one already described, Van der Meer (2007) showed in his PhD dissertation that to excite with a linear frequency chirp is more useful in order to detect the resonance frequency. In this kind of wave, there is not a main frequency that will stand out in the spectrum, but a range of frequency with the same energy level. In figure 3.9 a gaussian pulse with central frequency $f_c = 2$MHz is compared with a linear chirp with the same central frequency and a bandwidth of $BW = 3.9$MHz. We see that the first signal has a high amplitude peak located at the central frequency, meanwhile the chirp does not present a peak. Then, when a bubble is excited with a frequency chirp, if the resonance frequency belongs to the driving frequency range in the chirp, this will be notable in the spectra. In figure 3.10 we observe the response of a bubble cloud with mean size $D_m = 20\mu$m and variance $\sigma^2 = 0.1\mu\text{m}^2$ excited with the gaussian pulse (top) and the chirp (bottom) described above.

3.4.3 Effect of the mean size and variance on the spectra

When a monodisperse bubble cloud, this is, all bubbles have the same size, is excited with a pressure wave, the resonance frequency of the cloud is that one corresponding to the size of the bubble. When the cloud is formed by bubbles with different sizes, the resonance frequency depends of the size distribution. The resonance peak corresponds to the resonance of the mean size. If the polydispersity index is low, the resonance peak will be narrow. When the variance of the size distribution increases, the resonance peak will be wider and wider, becoming not notable in the spectrum. In figure 3.11 both scattered pressure and power spectral density for a monodisperse and a polydisperse bubble cloud are shown. The excitation signal is the same for both cases, as well as the number of bubbles forming the cloud, $N = 100$. We can appreciate that the scattered pressure by the monodisperse cloud has a higher amplitude than the pressure radiated by the polydisperse cloud. Regarding to the spectra, the resonance peak is narrower for the monodisperse population and its amplitude is also higher.

The goal of this section is to study the influence of the mean size of the cloud as well as the variance in the acoustic spectrum. We will try with different acoustic waves, namely, kind of wave, driving frequency and amplitude.

We start exciting a cloud of $N = 100$ bubbles with a gaussian pulse with central frequency $f_c = 2$ MHz and $P_A = 10$ kPa, the same represented in figure 3.9.

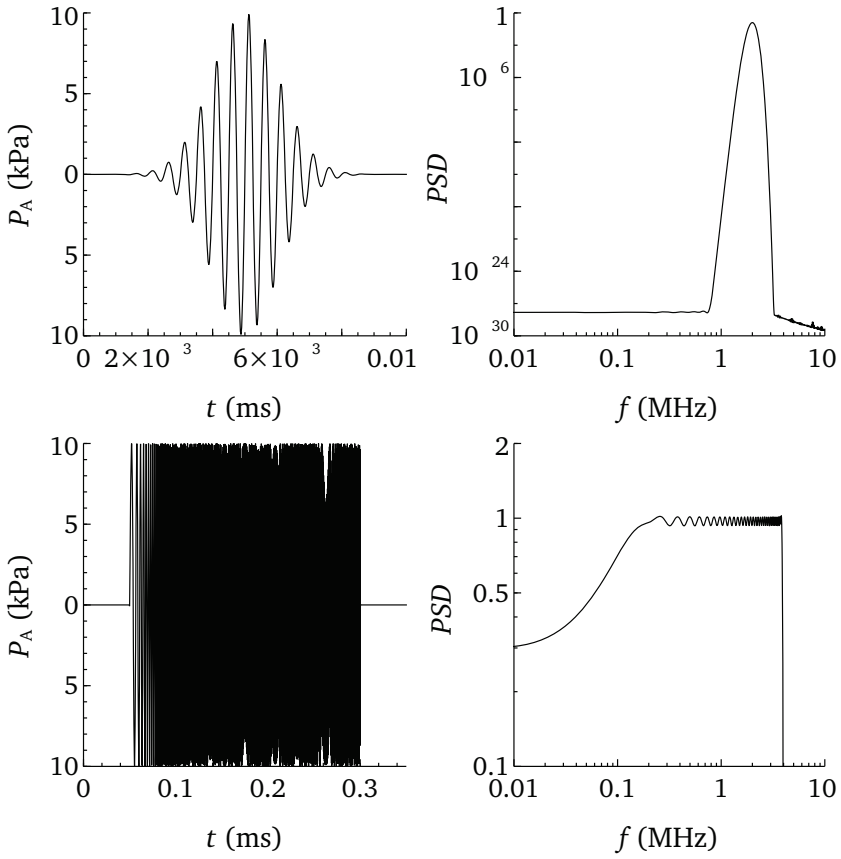

Figure 3.9: Gaussian pulse with central frequency $f = 2$MHz and pressure amplitude $P_A = 10$ kPa (upper left) and its spectrum (upper right). Linear chirp in frequency with $f_c = 2$ MHz and bandwidth $BW = 3.9$ MHz (lower left) and its spectrum (lower right).

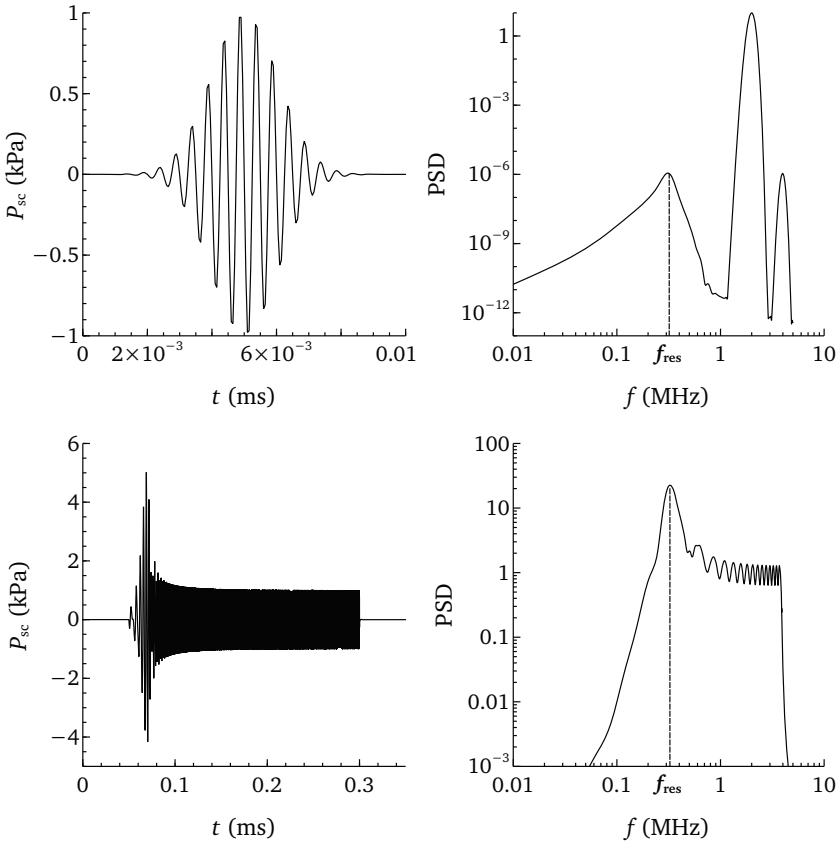

Figure 3.10: Bubble cloud excited with the two signals showed in figure 3.9. The resonance peak of the population is eclipsed by the driving peak in the case of the gaussian pulse (top) meanwhile it is clearly noticeable in the case of excitation with chirp (bottom).

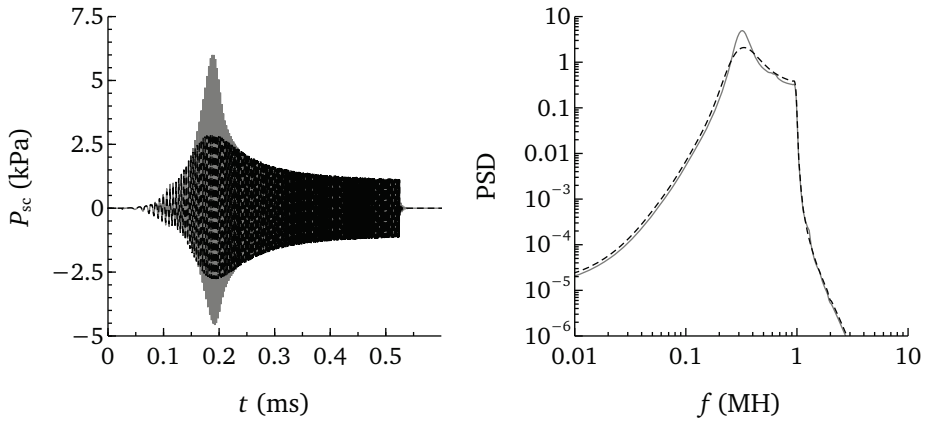

Figure 3.11: At the left, pressure scattered by a monodisperse (gray solid line) bubble cloud with size $D_0 = 20\mu$m, and by a polydisperse bubble cloud (black dashed line) with mean size $D_m = 20\mu$m. At the right, the spectra of the scattered pressures.

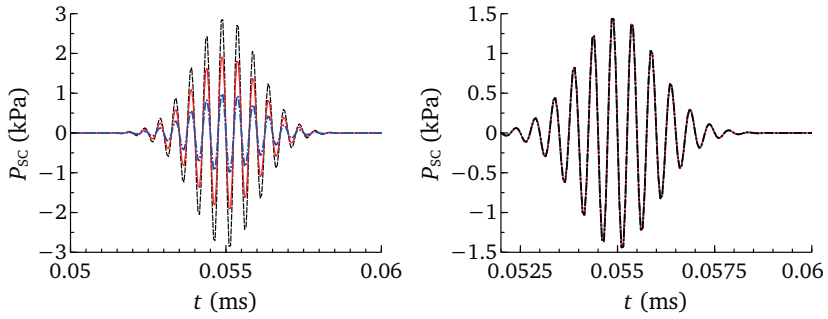

Figure 3.12: Scattered pressures for different bubble clouds with different mean sizes and fix variance $\sigma^2 = 1\mu m^2$ (left), and equal mean sizes ($D_m = 30\mu$m) and different variances (right). The blue line corresponds to $D_m = 20\mu$m, the read line to $D_m = 40\mu$m and the dashes black line to $D_m = 60\mu$m in the left graphic.

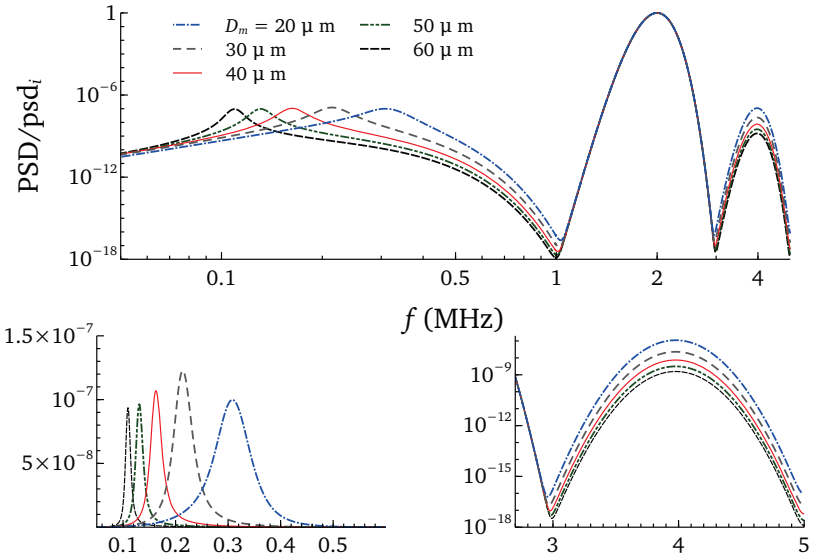

Figure 3.13: Spectra of bubble clouds excited with a pressure wave with $P_A = 10$ kPa and $f_i = 2$ MHz. In order to compare the resonance peak with the driving peak, the power spectral density has been made dimensionless with the energy value corresponding to this driving peak. The position of the resonance peak changes with the mean size, but also the amplitude. At the left bottom, a zoom of the resonance peak has been represented in order to appreciate the different amplitudes. Also a zoom of the harmonic peaks can be noticed at the right bottom. It is noticeable that the subharmonic amplitude increases when the mean size decreases.

We change the mean size as well as the variance of the cloud, this is, the size distribution. In figure 3.12 the pressure waves scattered by clouds with different size distributions have been plotted. These scattered pressures have been computed at a distance $d = 1$cm from the center of the bubble cloud. At the left, several populations with different mean size and equal variance are represented. We can note that the amplitude of the pressure is very low, of the order of 1 kPa and it decreases with the mean bubble size, D_m. The mean size not only affects the resonance frequency, but also the harmonics, as can be seen in figure 3.13. Here, several clouds with different mean sizes but equal variances have been excited with the same pressure wave. The number of bubbles is $N_b = 100$ in all the clouds. Obviously, the position of the resonance peak changes with mean size, but also its amplitude changes. All the mean sizes considered have associated resonance frequency very far from the insonation one ($f_i = 2$MHz), therefore, the response to the excitation is weak and the amplitudes of the resonance peaks are low compared to the driving peak. Curiously the higher amplitude is the one corresponding to $D_m = 30\,\mu$m. This is due to the resonance frequency of this size is $f_{\text{res}} \approx 200$ kHz, which is a subharmonic of the driving frequency.

If we maintain the mean size constant and vary the variance of the size distribution, the scattered pressure does not seem to be affected (figure 3.12). Nevertheless, when we look to the power spectral density of this signal, figure 3.14, we see that the resonance peak becomes wider and its amplitude lower when the variance increases. Also, the maximum moves to the left displacing the resonance to lower frequencies, what means that larger bubbles have more effect in the acoustical response. Respect to the driving peak and its harmonics, we can see that there is not appreciable difference.

Now, we use another excitation wave also gaussian kind but with a lower driving frequency closer to the resonance frequencies of the mean sizes, $f_c = 500$ kHz, to study what happens with the spectra for different mean sizes and variances. In figure 3.15, the scattered pressure for different populations have been plot. At the left we can see the response of bubble clouds with mean size $D_m = 25\,\mu$m and different variances and at the right the response for clouds with mean size $D_m = 10\,\mu$m. We observe how the amplitude of the scattered pressure is higher for larger mean sizes, and therefore, it takes the oscillations more time to be damped. When the variance increases the amplitude of the pressure wave decreases indicating that the smaller bubbles have more effect on the scattered pressure, and therefore in the spectra. The acoustical spectra of several clouds with different mean sizes and equal variance $\sigma^2 = 0.1\,\mu\text{m}^2$ and for equal mean size but different variances have been represented in figures 3.16 and 3.17, respectively.

The resonance frequency for a bubble with $D = 10\,\mu$m is $f_{\text{res}} = 600$ kHz, which is close to the driving frequency. If we look at the spectrum (3.16) of the scattered

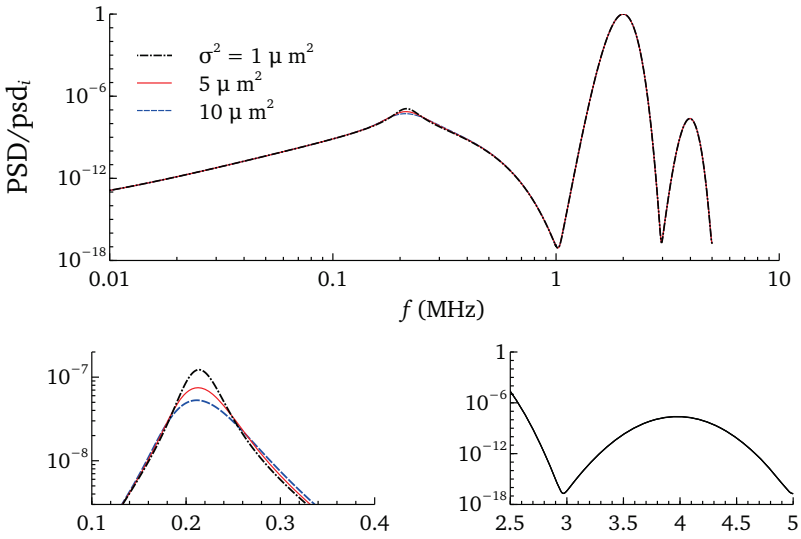

Figure 3.14: Spectra of bubble clouds with equal mean size, $D_m = 30\,\mu$m, and different variances. The value of the variance affects the resonance peak, as we can see in the graph at the bottom left, but not the harmonics of the driving frequency (bottom right).

pressure with $D_m = 10\,\mu$m and $\sigma^2 = 0.1\,\mu$m^2, we check that only one peak is detected, corresponding to the resonance frequency. When the mean size is increased, the associated resonance decreases and it is far from the driving frequency. In the spectra we can check that when the mean size increases, the peak corresponding to the driving frequency is being more notorious meanwhile the amplitude of the resonance peak decreases.

We shall now study what happens to the spectra when the variance increases. We choose the mean sizes $D_m = 10\,\mu$m, since there is only one peak in the spectrum, and $D_m = 25\,\mu$m, since here there are two peaks, the resonance one and the driving one. In the first case, we see in figure 3.17, right, that increasing the variance makes the resonance peak wider and wider at the same time that the maximum moves toward the driving frequency, that is, the resonance peak moves to lower frequencies. In the second case, the resonance peak is weaker and weaker until it becomes mixed with the peak at the driving frequency for a certain value of $\sigma^2 = 10\,\mu$m^2, turning indistinguishable.

As we have checked, the most noticeable peak in the spectra usually is the driving one, independently of the driving frequency. Although the resonance peak is easily detectable in the numerical spectra, we think that in a real signal, where electronic noise exists, the resonance peak is not going to be detectable since its amplitude is

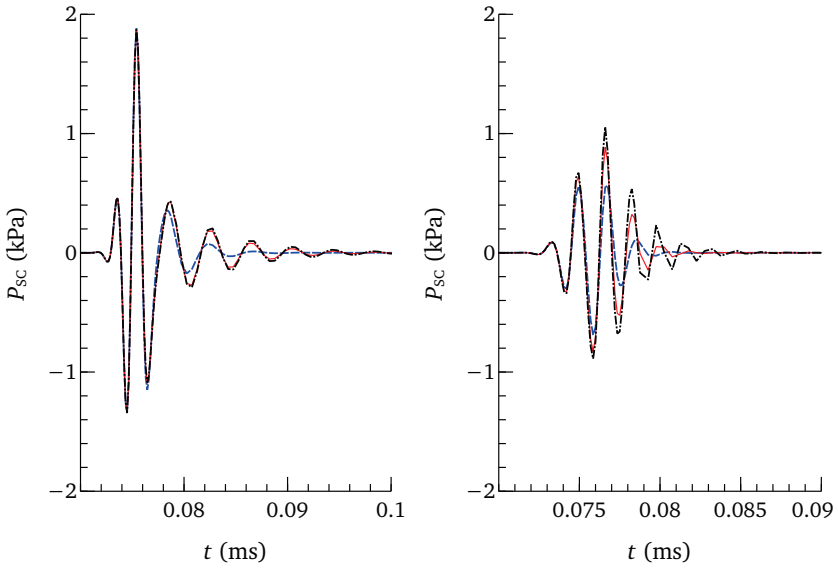

Figure 3.15: Scattered pressures for different bubble clouds. At the left, the mean size of the bubble distributions is $D_m = 25\,\mu$m. At the right, the mean size is $D_m = 10\,\mu$m. We can observe that the amplitude of the scattered pressure increases with bubble size. For a fix mean size, when increasing the variance, the amplitude decreases

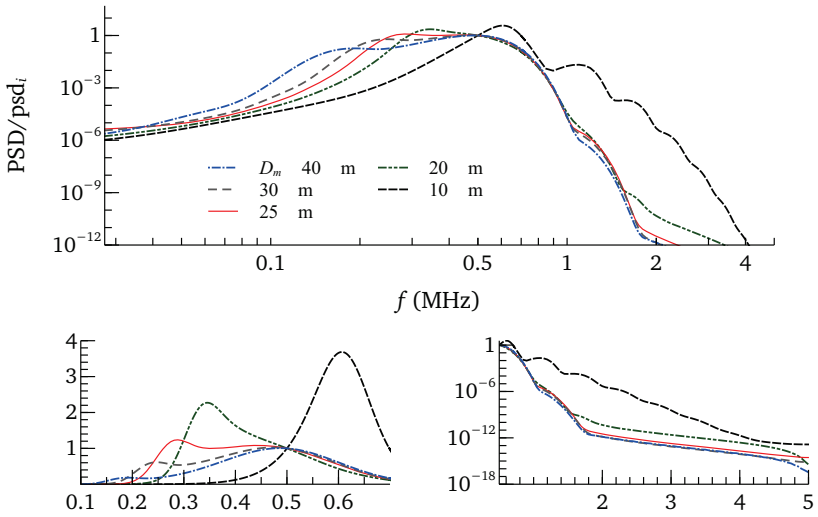

Figure 3.16: Spectra of bubble clouds excited with a pressure wave with $P_A = 10$kPa and $f_i = 500$kHz. The variance for all distributions is $\sigma^2 = 0.1\mu m^2$. In order to compare with the driving peak, the power spectral density has been made dimensionless with the energy value corresponding to this driving peak. For mean sizes $D_m = 10$, 20 and 25 μm the resonance peak is the most remarkable in the spectrum. For $D_m \geq 30\mu$m the driving peak stands out in the spectrum and the resonance cannot be detected. At the left bottom a zoom of the amplitudes of the driving and resonance peaks is shown in linear scale, to a greater clarity.

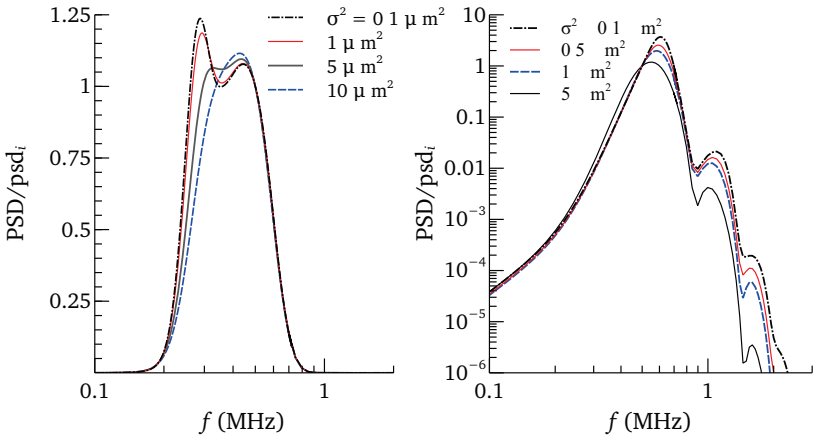

Figure 3.17: Spectra of bubble clouds with mean size $D_m = 25\,\mu$m (left) and $D_m = 10\,\mu$m (right), and different variances. When the variance increases, the resonance peak is wider.

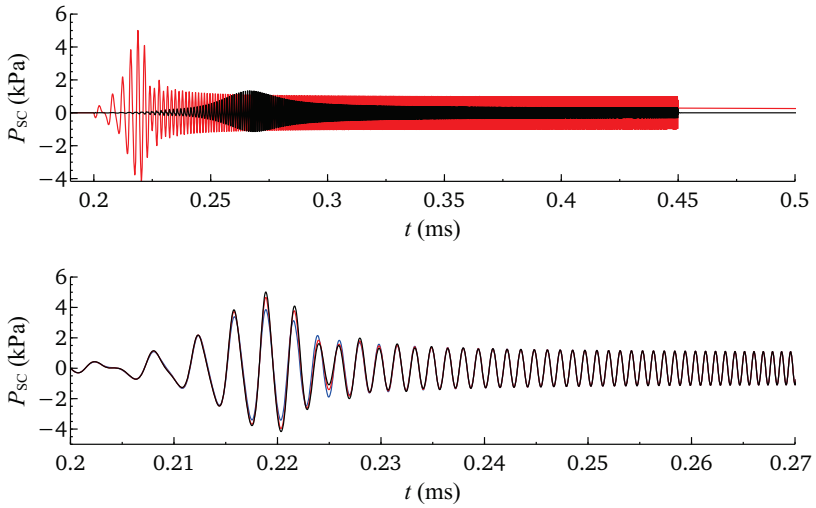

Figure 3.18: Different bubble populations excited with the linear frequency chirp described in fig. 3.9. Upper, two bubble clouds of $\sigma^2 = 0.1\mu\text{m}^2$ and mean sizes $D_m = 6$ and $20\,\mu$m. Lower, three population with mean size $D_m = 20\,\mu$m and $\sigma^2 = 0.1$, 1 and $4\,\mu\text{m}^2$.

too low. For this reason, we try to excite the same population but now using the linear frequency chirp represented in figure 3.9, with central frequency $f_c = 2$ MHz, a bandwidth of $BW = 3.8$ MHz, and a pulse length of $Lp = 0.5$ ms.

As we observe in figure 3.18, bigger bubbles have a stronger response, this is, the amplitude of the scattered pressure is higher. The larger is the bubble, the lower is its resonance frequency. Since the frequency of the excitation pulse increases in time, larger bubbles are excited sooner than smaller bubbles, which response to larger frequencies. Effectively, in figure 3.19, where the spectra for different clouds with different mean sizes have been plotted, we see that smaller bubbles present larger resonance frequencies. Also, the amplitude of the resonance peak is higher for larger bubbles, as predicted by the scattered pressure, except for the size $D_m = 25\,\mu$m, which shows a lower amplitude then that corresponding to $D_m = 20\,\mu$m. According to the variance, when this is increased the amplitude of the scattered pressure decreases. This means that smaller bubbles gain more importance, and the resonance peak moves to higher frequencies, as can be observed in the spectrum (figure 3.20).

As we did with the gaussian pulse, we are going to use another chirp with central frequency $f_c = 500$ kHz, pulse length $L_p = 0.5$ ms, and bandwidth $BW = 980$ kHz, such that the frequency swaps form 10 kHz to 990 kHz, in order to excite bubble clouds with mean sizes of a few tens of microns. Again, the larger the bubble and the smaller the variance are, the higher the amplitude of the scattered pressure is, as can be checked in figure 3.21. Taking a look to the spectra (figure 3.22), we see

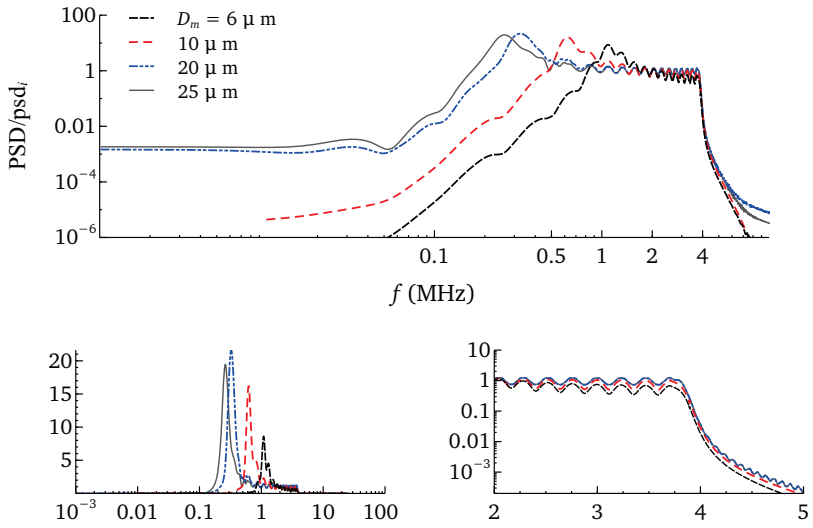

Figure 3.19: Spectra of bubble clouds excited with a chirp with pressure amplitude P_A = 10 kPa and f_c = 2 MHz. The variance for all distributions is $\sigma^2 = 0.1\,\mu m^2$. In order to compare with the driving peak, the power spectral density has been made dimensionless with the energy value corresponding to the flat frequency range. At the left bottom a zoom of the amplitude of the resonance peaks is shown in linear scale, to a greater clarity.

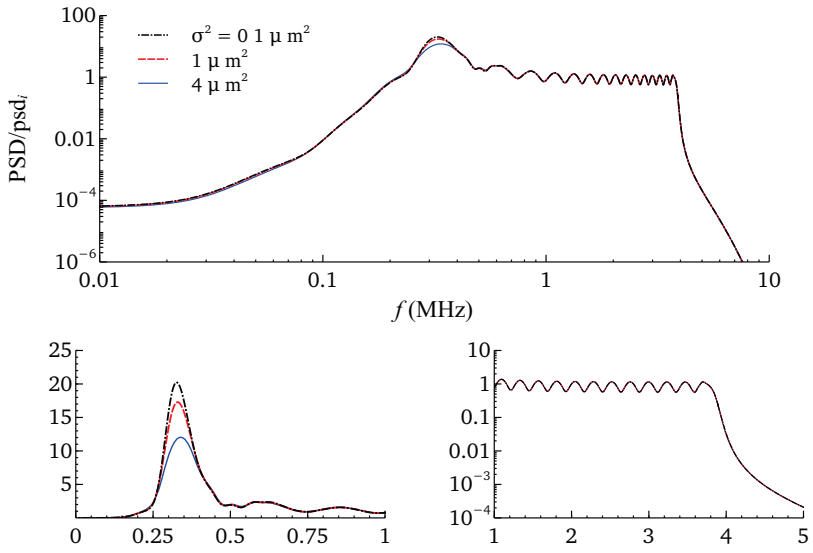

Figure 3.20: Spectra of bubble clouds with mean size $D_m = 20\,\mu$m and different variances. When the variance increases, the resonance peak is wider and moves to higher frequencies. Also, its amplitude decreases.

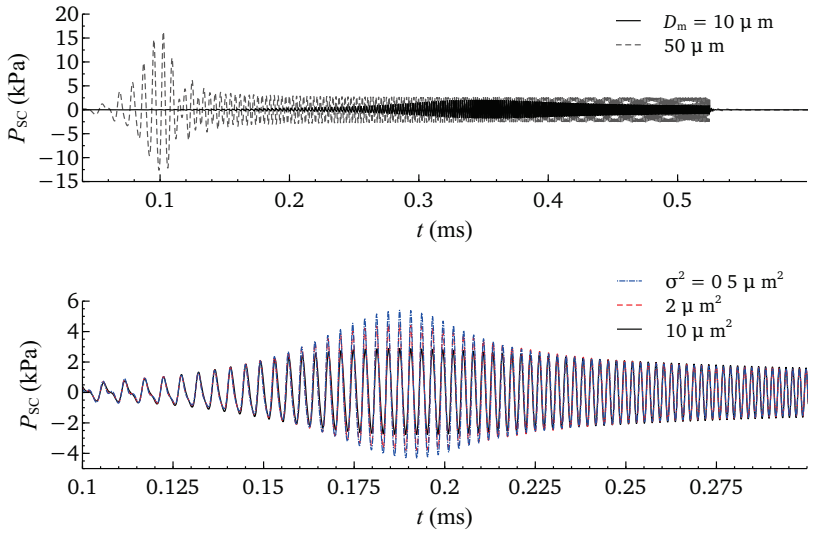

Figure 3.21: Pressure scattered by different bubble populations excited with a linear frequency chirp with $f_c = 500$ kHz, pulse length $L_p = 0.5$ ms and bandwidth $BW = 980$ kHz. Upper, two bubble clouds of $\sigma^2 = 0.5\mu$m^2 and mean sizes $D_m = 10$ and 50μm. Lower, three population with mean size $D_m = 20\mu$m and $\sigma^2 = 0.5,\quad 2\quad$ and $\quad 10\mu$m^2.

that larger bubbles present lower resonance frequencies and that the amplitude of the resonance peak is higher. Regarding to the variance, when this increases the resonance peak becomes wider and the maximum moves to higher frequencies, the same that happened with the chirp with $f_c = 2$ MHz.

When the cloud is excited with a gaussian pulse, increasing the variance makes the resonance move towards the driving frequency, if this is close to the resonance. In the case that the resonance is far from the driving frequency, then this displaces to frequencies lower than the resonance corresponding to $\sigma^2 = 0$, indicating that larger bubbles affect more the spectrum. However, when the cloud is excited by a chirp, to increase the index of polydispersity originates that the resonance, the maximum peak, moves to slightly higher frequencies, indicating that in this case the smaller bubbles affect more the spectrum, just the opposite behavior.

The goal is to study how the resonance peak changes with the distribution parameters, namely, variance and mean size and how it is affected by excitation parameters. Trying to find a relationship, we fit the resonance peak to a cubic parabole and compute the frequency at which the maximum is located as well as the curvature, as shown in figure 3.24. For this analysis we chose the cases in which we excite with a linear chirp, since the spectra of the pressure radiated by the cloud presents just the

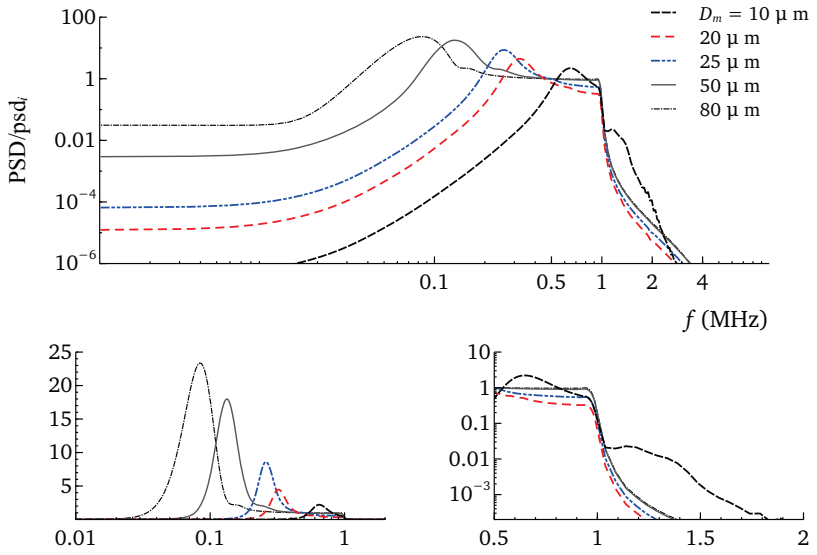

Figure 3.22: Spectra of bubble clouds with different mean sizes and equal variance $\sigma^2 = 0.5\mu\text{m}^2$. When the diameter increases, the maximum peak moves to lower frequencies and also its amplitude increases.

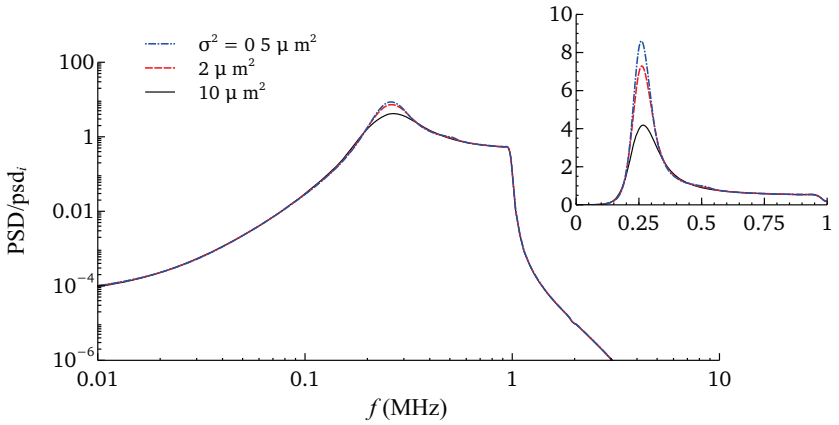

Figure 3.23: Spectra of bubble clouds with the same mean size $D_m = 25\mu$m and different variances. The maximum displaces to the right with increasing variances.

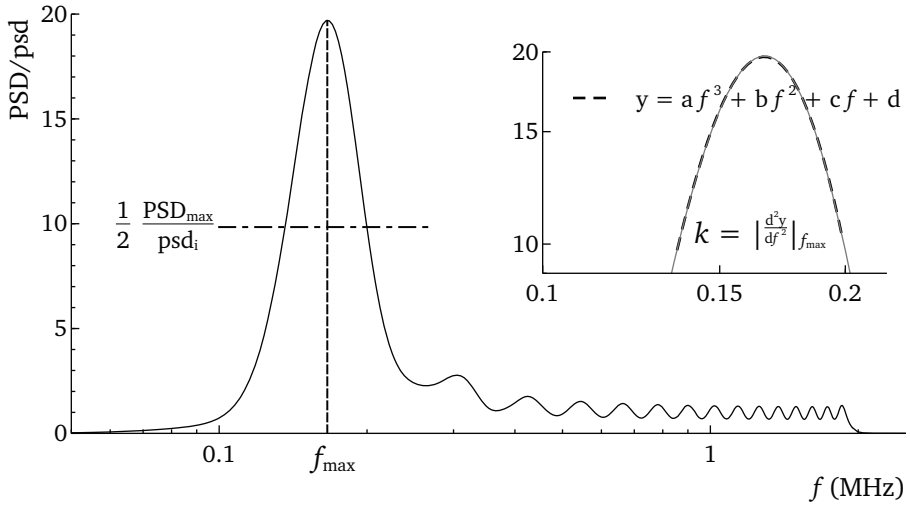

Figure 3.24: Acoustic spectrum of a bubble cloud with $N = 100$, subjected to a chirp excitation with central frequency $f_c = 1$MHz and pressure amplitude $P_A = 10$ kPa. The resonance peak is fitted to a hyperbole, taking the range of frequencies for which the amplitude of the maximum reduces to the half. The location of the maximum f_{max}, and the curvature k are obtained from the fitting.

resonance peak.

In figures 3.25, 3.26, 3.27 and 3.28 we show the position of the maximum peak, corresponding to the resonance frequency, for different bubble clouds and for different insonation parameters. Also an estimation of the width of the peak, calculated as $k_\sigma = -1/k$ is represented. The general tendency is that, when the variance is increased, the maximum peak moves to higher frequencies and the peak becomes wider. Moreover we can check that the lower is the resonance frequency, the slower is the variation of k_σ with the variance σ^2 of the size distribution. In table 3.2 a summary of the studied cases is shown.

Case	f_c (MHz)	BW (MHz)	Lp (ms)	P_A (kPa)
1	0.5	0.98	0.5	10
2	0.5	0.98	0.25	10
3	1	1.9	0.25	10
4	2	3.8	0.25	10

Table 3.2: Different conditions studied to analyze the dependency of the resonance peak on the excitation parameters

There are several parameters that affect the resonance frequency of a bubble with

a certain size. The most important is maybe the variance of the size distribution, but we can check how the driving frequency also affect, as well as the duration of the acoustic pulse. For example we check that bubble clouds with equal parameters of the size distribution do not present the same resonance peak (frequency and width) when they are irradiated with different parameters. In order to find a relationship between the variance and the width and maximum of the resonance peak, these are made dimensionless. The variance is normalized with the diameter square. To normalize the curvature is not so easy, since there are many parameters that affect the spectra. The more trivial is to make the curvature dimensionless with the square of the frequency at which the maximum of the resonance peak is located. But other frequencies can be taken into account, such us the natural frequency of the bubble, the central frequency of excitation, or the width of the peak. In figures from 3.25 to 3.28, two different normalization are shown, $k_\sigma/f_{\max}^2$ and $k_\sigma \Delta f/(f_{\max} f_{\text{res}}(f_{\max}-f_c))$.

The intention of the normalization is to check if we observe a self-similar behavior for the different cases considered. In general, the dimensionless parameter $k_\sigma/f_{\max}^2$ as a function of σ^2/D_m^2 shows a great dispersion. However, when the dimensionless parameter $k_\sigma \Delta f/(f_{\max} f_{\text{res}}(f_{\max}-f_c))$ is plotted versus σ^2/D_m^2, most of the different points can be fitted by the same curve.

For the case 1, the matching is very good for the clouds with mean sizes $D_m = 40-80\mu$m. The excitation used in case 2 is almost the same that in case 1, except for the pulse length that is the half. However, in this case there is a great dispersion, as we can check in figure 3.26. The fitting is the same than in case 1 just for the mean sizes $D_m = 80$ and $D_m = 60\,\mu$m. The bad fitting can be due to that the pulse length is too short for the bandwidth considered, not being this excitation adequate to excite these bubble clouds. With regard to the case 4, the matching is also good and similar to those seen in case 1 and 2, but the values of the parameter $k_\sigma \Delta f/(f_{\max} f_{\text{res}}(f_{\max}-f_c))$ are smaller by an order of magnitude for the same values of σ^2/D_m^2. In this case, the bubble clouds excited have smaller average sizes, and therefore, larger resonance frequencies. Regarding the case 3, we can appreciate in figure 3.27 that there are two curves that match with the different points. Curiously, the larger mean sizes are not fitted by the same curve, but the results corresponding to $D_m = 30\,\mu$m have a weird behavior, since they agree with the curve for the largest size.

Although more research about this self-similar behaviour must be done, we can anticipate that the good fitting is related to a proper choice of the acoustic parameters to excite a determined bubble cloud.

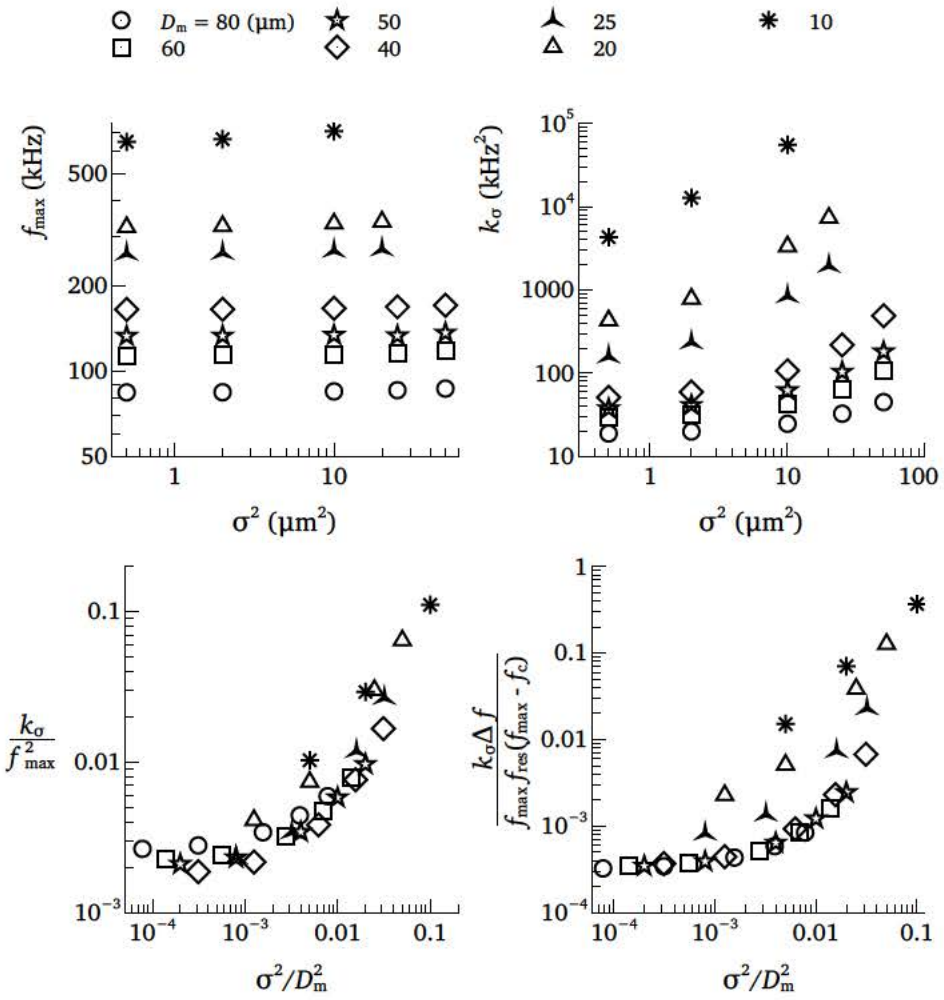

Figure 3.25: Case 1 (f_c = 500 kHz, L_p = 0.5 ms). Resonance frequency and width of the resonance peak as a function of the variance, for different mean sizes (top). Normalized curvature as a function of the normalized variance (bottom).

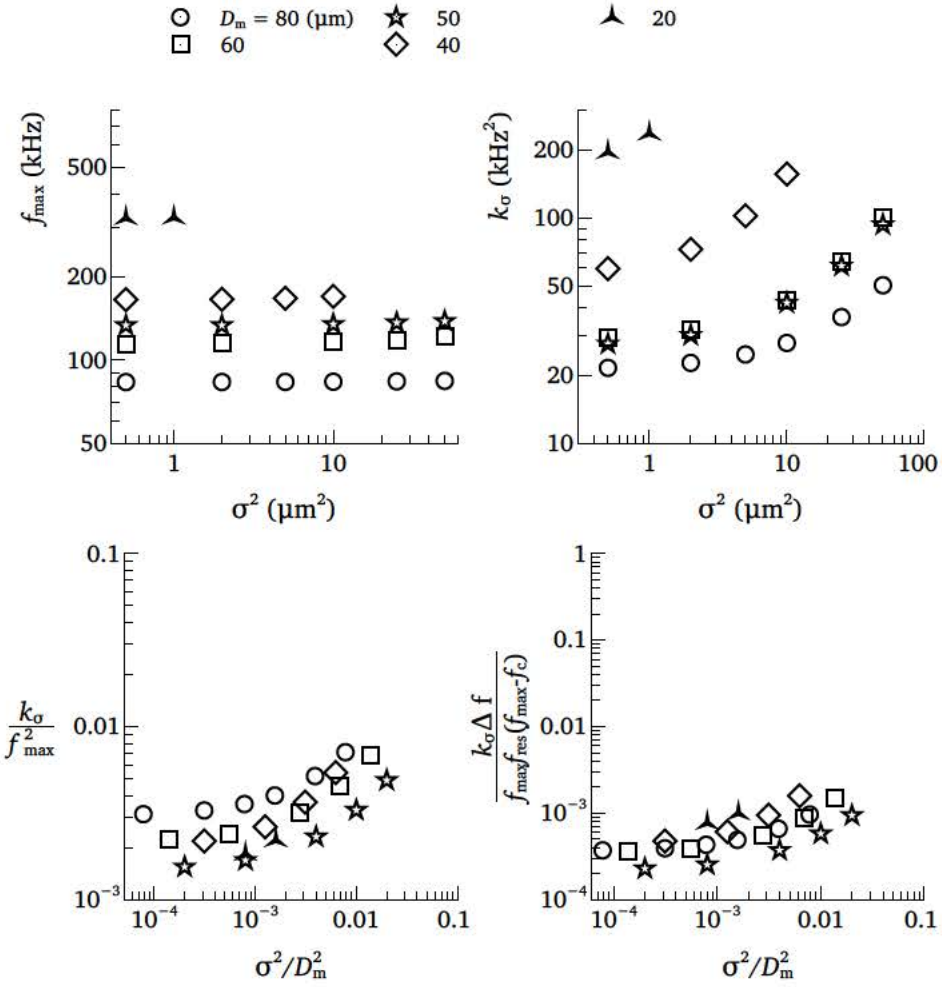

Figure 3.26: Case 2 (f_c = 500 kHz, L_p = 0.25 ms). Resonance frequency and width of the resonance peak as a function of the variance, for different mean sizes (top). Normalized curvature as a function of the normalized variance (bottom).

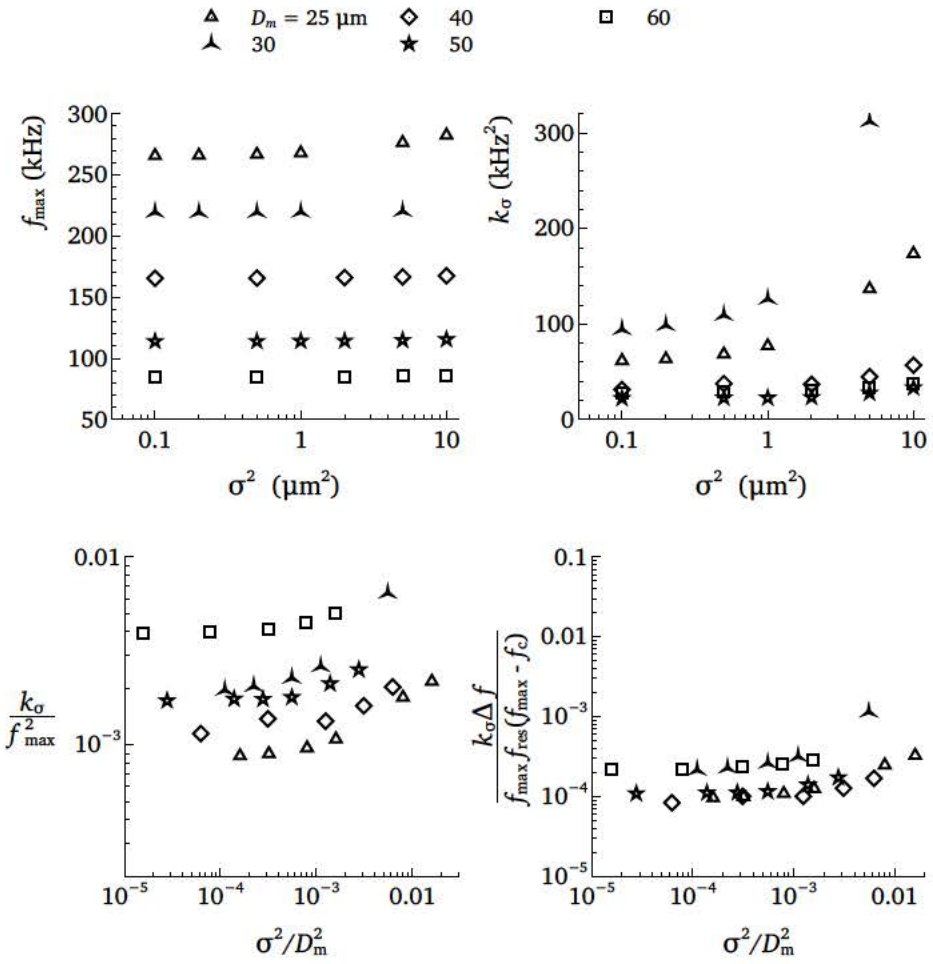

Figure 3.27: Case 3 ($f_c = 1$ MHz). Resonance frequency and width of the resonance peak as a function of the variance, for different mean sizes (top). Normalized curvature as a function of the normalized variance (bottom).

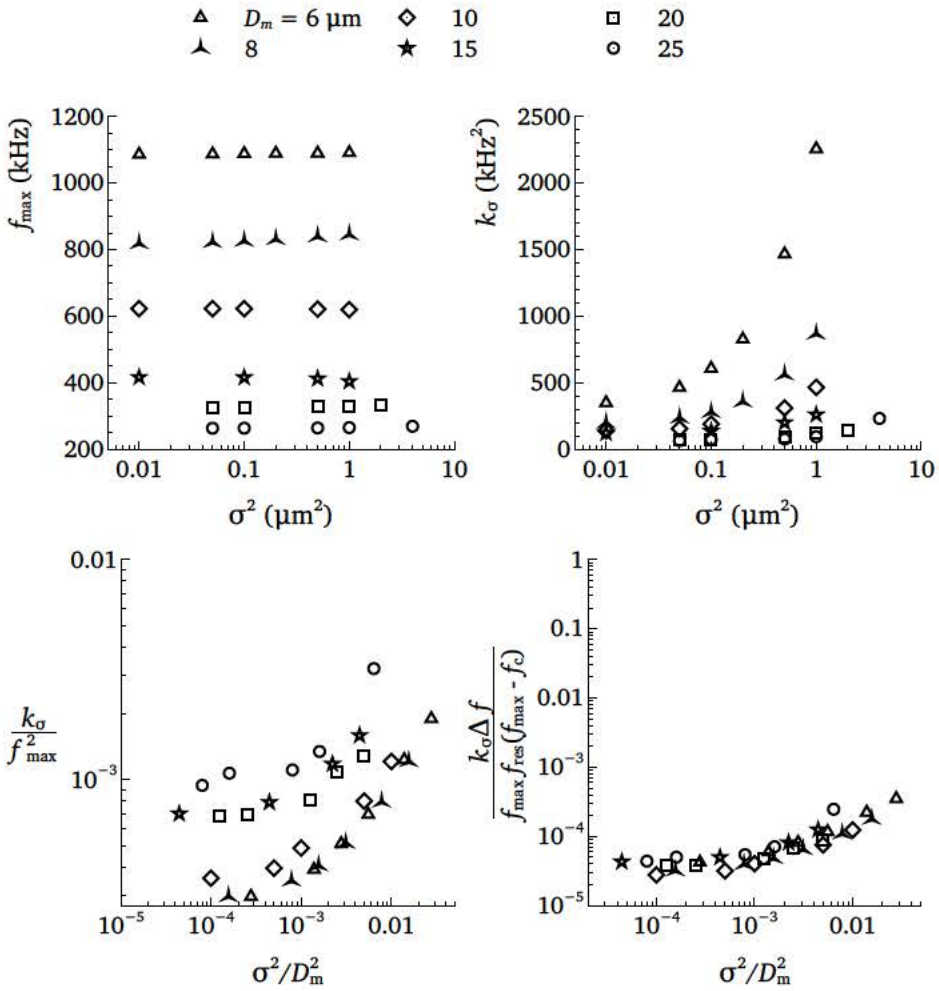

Figure 3.28: Case 4 ($f_c = 2$ MHz). Resonance frequency and width of the resonance peak as a function of the variance, for different mean sizes (top). Normalized curvature as a function of the normalized variance (bottom).

3.5 Analytical formulae for the acoustic spectra

In order to find a more inexpensive —from the computational point of view — method to study the acoustic spectrum of bubble clouds, we develop an analytic formulation for the pressure radiated by a cloud, based on the linear analysis of the equations defined in chapter 2. We can define the response of the bubble to a Dirac Delta excitation as

$$F(\omega;R_0) = \frac{1}{\left(\frac{\omega_0}{\omega}\right)^2 - 1 + i\frac{2\beta}{\omega}} \tag{3.4}$$

such that the response of a bubble cloud with a size probability distribution $f(R_0)$ is

$$I(\omega) = \int_0^\infty R_0 f(R_0) F(\omega;R_0) \mathrm{d}R_0. \tag{3.5}$$

In order to solve this integral analytically, we expand in Taylor series the function $R_0F(\omega;R_0)$ around the point R_m, which is the average size for the size distribution.

$$R_0F(\omega;R_0) \simeq R_mF(\omega;R_m) + (R_0 - R_m)\left|\frac{\mathrm{d}R_0F}{\mathrm{d}R_0}\right|_{R_m} + \frac{(R_0-R_m)^2}{2}\left|\frac{\mathrm{d}^2R_0F}{\mathrm{d}R_0^2}\right|_{R_m} \tag{3.6}$$

$$
\begin{aligned}
I(\omega) \simeq & \int_0^\infty R_m F(\omega;R_m) f(R_0)\mathrm{d}R_0 + \\
& + \int_0^\infty (R_0 - R_m)\left[R_m \left|\frac{\mathrm{d}F}{\mathrm{d}R_0}\right|_{R_m} + F(\omega;R_m)\right] f(R_0)\mathrm{d}R_0 + \\
& + \int_0^\infty \frac{(R_0-R_m)^2}{2}\left[R_m \left|\frac{\mathrm{d}^2F}{\mathrm{d}R_0^2}\right|_{R_m} + 2\left|\frac{\mathrm{d}F}{\mathrm{d}R_0}\right|_{R_m}\right] f(R_0)\mathrm{d}R_0 \\
& = R_m F(R_m) \overbrace{\int_0^\infty f(R_0)\mathrm{d}R_0}^{1} \\
& + \left[R_m \left|\frac{\mathrm{d}F}{\mathrm{d}R_0}\right|_{R_m} + F(R_m)\right] \underbrace{\left[\underbrace{\int_0^\infty R_0 f(R_0)\mathrm{d}R_0}_{R_m} - R_m \underbrace{\int_0^\infty f(R_0)\mathrm{d}R_0}_{1} \right]}_{0} \\
& + \left[\left|\frac{\mathrm{d}F}{\mathrm{d}R_0}\right|_{R_m} + \frac{R_m}{2}\left|\frac{\mathrm{d}^2F}{\mathrm{d}R_0^2}\right|_{R_m}\right] \underbrace{\int_0^\infty (R_0-R_m)^2 f(R_0)\mathrm{d}R_0}_{\sigma^2}
\end{aligned}
$$

$$
I(\omega) \simeq R_m F(R_m) + \sigma^2 \left|\frac{\mathrm{d}F}{\mathrm{d}R_0}\right|_{R_m} + \frac{\sigma^2 R_m}{2}\left|\frac{\mathrm{d}^2F}{\mathrm{d}R_0^2}\right|_{R_m} \tag{3.7}
$$

We compare the result obtained with equation (3.7) with the numerical integration of equation (3.5). In figure $I(\omega)$ is plotted as a function of $f = \omega/2\pi$, for two clouds with different distribution sizes. We see that for small variances, that is, almost monodisperse bubbles, both results are very similar. However, when we increase the variance of the size distribution, the approximation for $I(\omega)$ does not match well with the result obtained with equation (3.5), being the maximum peak much more pronounced.

To calculate the response of a bubble to a certain excitation function we should multiply $I(\omega)$ by the Fourier transform of the excitation signal. In the following figures we compare the solution obtained with the analytic approximation (3.7) with that provided by the numerical integration of equation (3.5). Both solutions are also compared to the numerical simulations.

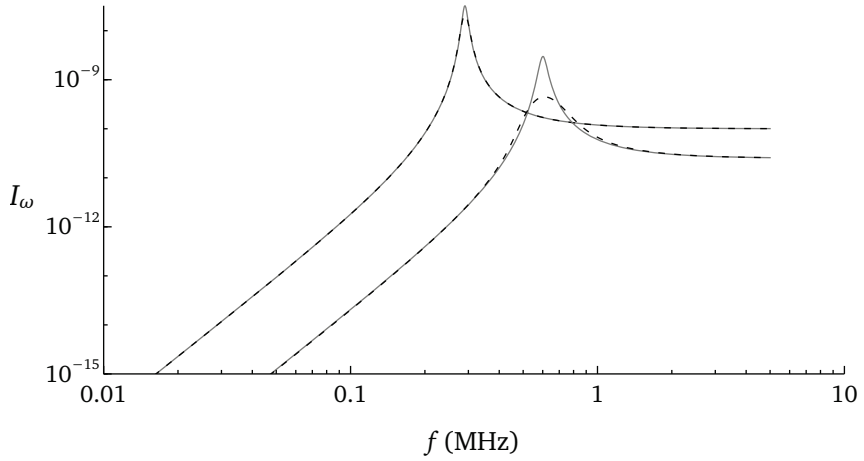

Figure 3.29: $I(\omega)$ computed numerically with equation (3.5) (dashed line) and calculated through the approximation (3.7) (solid line), for two clouds, one with mean size $R_m = 5\,\mu$m and $\sigma^2 = 1\,\mu\text{m}^2$ and the other one with $R_m = 10\,\mu$m and $\sigma^2 = 0.1\,\mu\text{m}^2$.

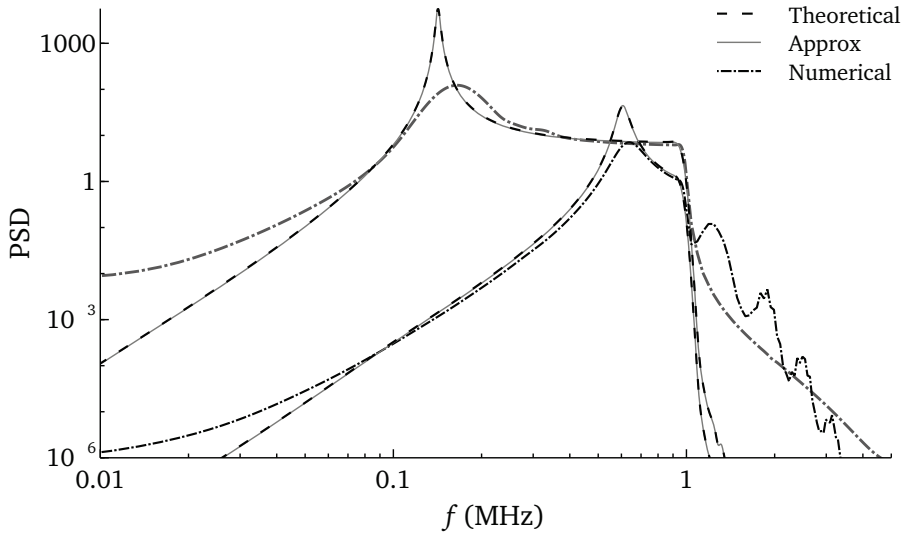

Figure 3.30: $D = 10\,\mu$m and 40. Monodisperse cloud

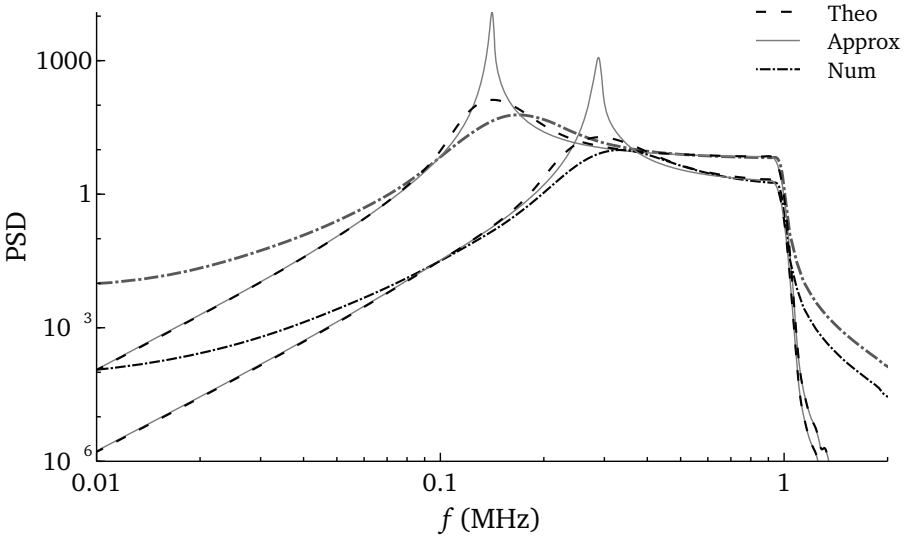

Figure 3.31: $D = 20\,\mu$m and 40, variances of 10 and 25. Great polydispersion

References

VAN DER MEER, SANDER 2007 Ultrasound contrast agents. resonances of coated bubbles. PhD thesis, Universiteit Twente.

PARRALES, M.A., FERNANDEZ, J.M., PEREZ-SABORID, M., KOPECHEK, J.A. & PORTER, T.M. 2014 Acoustic characterization of monodisperse lipid-coated microbubbles: Relationship between size and shell viscoelastic properties. *J. Acoust. Soc. Am.* **136** (3), 1077–1084.

PROSPERETTI, A. 1977 Thermal effects and damping mechanisms in the forced radial oscillations of gas bubbles in liquids. *J. Acoust. Soc. Am.* **61** (1), 17–27.

ZHENG, H., BARKER, A. & SHANDAS, R. 2006 Predicting backscatter characteristics from micron- and submicron-scale ultrasound contrast agents using a size-integration technique. *IEEE Trans. Ultrasonics, Ferroelectrics and Freq. Control* **53**, 639–644.

CHAPTER

FOUR

Acoustic spectrum of a monodisperse bubble cloud: experimental results

4.1 Introduction and goal

As we have seen, the resonance frequency of bubbles can be determined theoretically. The question now rises if we can also detect the acoustical response of the bubbles in real experimental conditions. There are several effects which will influence the experimental measurements, for example the electronic noise of the different devices, the noise in the excitation signal, the relative position between the bubbles and the hydrophone, the bubble density level, etc. In few words, the backscattered signal is weak.

The resonance frequency of bubbles depends strongly on their sizes, therefore a large polydispersity index in the bubble size distribution implies many different resonance frequencies. Consequently, the spectrum of the scattered pressure of a polydisperse bubble population has high energy in a wide range of frequencies, making it impossible to clearly distinguish a peak corresponding to the resonance frequency of the mean size. In contrast, a monodisperse population produces a spectrum with a clear peak corresponding to the resonance frequency of the bubbles. With this in mind, we decided to carry out experiments using a monodisperse population of bubbles. These sets of experiments were carried out at the facilities of the Fluid Mechanics Research Group of the Universidad de Sevilla (GIMFUS), where monodisperse coated microbubbles can be produced through microdevices operated in co-flow regime.

The goal of this chapter is to listen acoustically to the response of one bubble or a monodisperse group of bubbles to a short ultrasound pulse produced by a pulse generator, with a certain driving frequency.

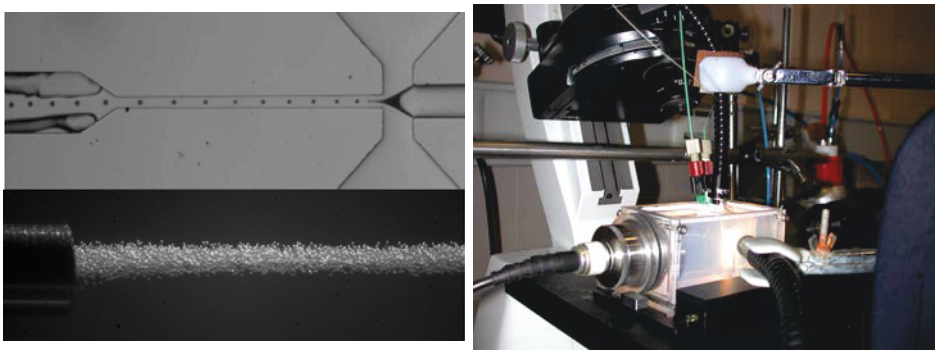

Figure 4.1: (upper-left) Picture of the bubbles generated in the micro-device, and (lower-left) the column of bubbles that is produced. (right) Picture of the experimental setup.

4.2 Experimental Setup

For the bubble generation we used a 2D flow-focusing microdevice operating in co-flow regime (see figure 4.1) with air as gas and a phospholipid solution as liquid. The microdevice was placed inside of a transparent acrylic container of dimensions 12 cm × 6 cm ×5 cm. This container has a porthole at one of its sides to couple the transducer probe that will transmit the acoustic wave. To assure the stability of the microbubbles going out of the microdevice to the container, the latter was filled with the same phospholipid solution. The small transparent container was placed on the inverted miscroscope (Nikon) that was used to record the bubble generation process. The sketch of the experimental setup is represented in figure 4.2. Since the production rate with the co-flow technique is very high, but only a few bubbles are desirable for this experiment, the production was stopped suddenly and just the last bubbles going out the device were insonated. To know the number of bubbles that were excited, a camera (Phantom) was placed to record the insonation focal point through which the bubbles pass.

A pulser/receiver (RITEC) able to generate a short pulse with a determined driving frequency was used to supply the electrical signal to a broadband focused transducer (Sonatest, central frequency of 1 MHz, focal distance of 50 mm). The acoustic signal emitted by the transducer is a sinusoidal signal. The same equipment is used to receive the wave backscattered by the bubbles that arrives a short time after the emission. This wave is visualized on an oscilloscope (Tektronic) and acquired with a National Instruments (NI) acquisition card at a sample rate of 10 MHz. The bubbles are recorded with a high speed camera at a frame rate of 60 fps. A sketch of the entire setup is represented in figure 4.3.

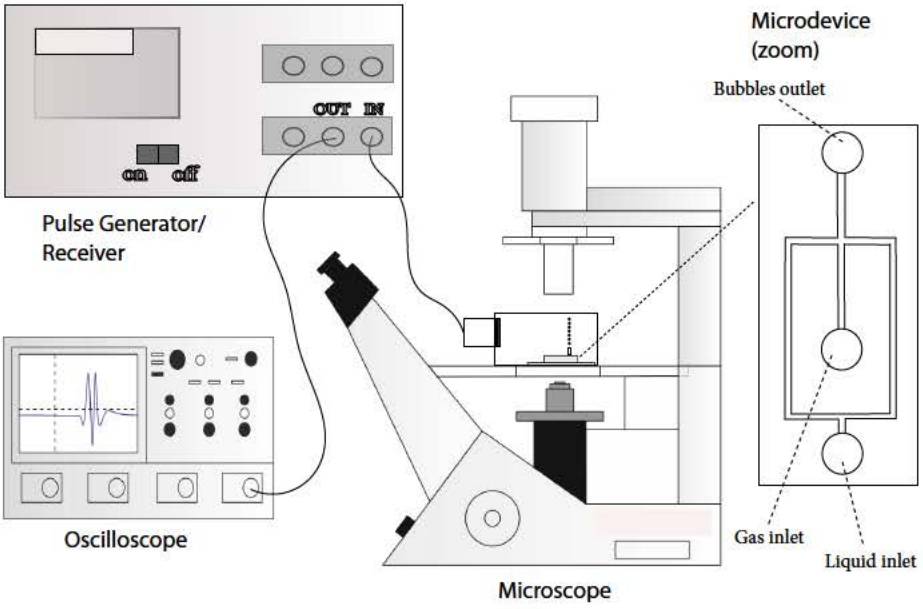

Figure 4.2: General sketch of the experimental setup. The container with the microdevice was placed on the inverted microscope to visualize the bubble generation. The signals that were emitted and received with the pulse generator were visualized on an oscilloscope. The received signal was acquired with an acquisition card (NI 6203) at a sample rate of 10 MHz.

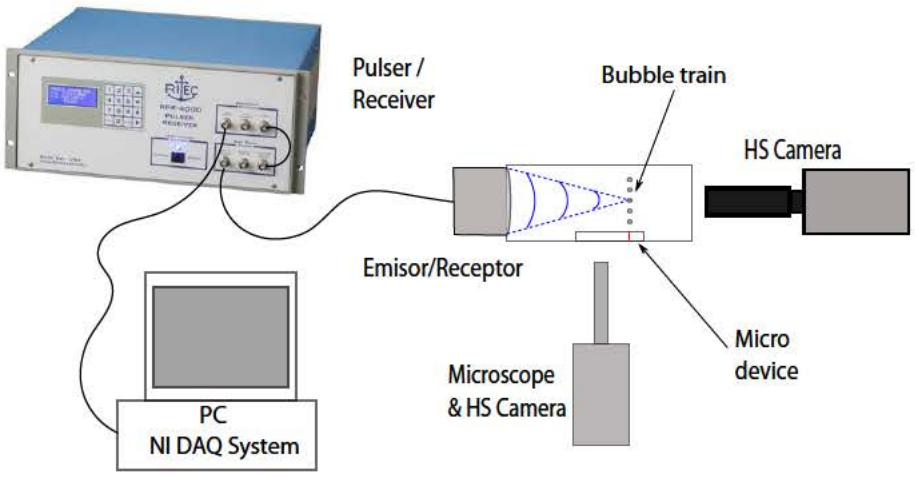

Figure 4.3: Sketch of the setup. The wave is produced by the pulser, and transmitted and received by the transducer. A high speed camera records the bubbles that are being excited.

4.3 Experimental Results

With the co-flow bubble generation technique that was employed, the size of the lipid-coated bubbles is controlled through the flow rate of the gas and that of the lipid solution, denoted by Q_g and Q_l respectively. The diameter of the bubbles is proportional to the power 5/12 of ratio of the two flow rates, such that $D_b \propto (Q_g/Q_l)^{5/12}$ (Castro-Hernandez *et al.*, 2011). With this technique bubbles as small as 5 microns in diameter can be produced, with a production rate as high as 10^5 bubbles/s. Due to the high production rate, a very thick column of bubbles is produced, which behaves acoustically as a rigid body—when the pressure wave collides with the bubble column, it is reflected in the opposite direction. There is no resonant backscattered signal in this case, but only geometrical backscatter coming from the bubble column. In order to have an acoustical response from the bubbles we should have a very diluted cloud. To achieve this we suddenly stop the flow of gas and liquid in order to stop the production of bubbles, and use just the last bubbles produced by the system. Nevertheless, by doing this, we are forcing the microdevice to work in a transient regime. Since the stability of the meniscus from which the bubbles are detached is crucial for the production of very small monodisperse bubbles, we cannot achieve such small bubbles in a transient regime. Therefore, to guarantee the stability of the bubble production, the minimum bubble size that we can generate is $30-40$ microns in diameter. The resonance frequency for a free air bubble of this size is $f_{\text{res}} \simeq 169-340$ kHz. We can estimate that the resonance frequency of bubbles with a lipid shell increases about 40 or 50 % with respect to that given by Minnaert (Van der Meer *et al.*, 2007; Parrales *et al.*, 2014), and therefore we expect resonance frequencies of the order $f_{\text{res}} \sim 250-350$ kHz.

We radiated the bubbles with different driving frequencies between 50 kHz and 300 kHz, close to the expected resonance frequency. Since the driving frequency that maximizes the power transmitted by the transducer is 1 MHz, we are not exciting the bubbles with strong amplitudes. In addition, the transducer does not respond well to such low frequencies: the emitted low-frequency sinosoidal pulse is disturbed by two spurious 1 MHz pulses. This can be seen, for example, in figure 4.4(a), where the emitted signal was measured indirectly by the geometrical backscatter from the dense bubble column that just reflects the signal.

For each selected driving frequency we acquire a signal in which there are no bubbles present, in order to have a reference signal to compare with the backscattered signal radiated by the bubbles. We compute the spectra of the signal without bubbles, of the signal backscattered by the bubbles, and of the difference between these two signals.

4.3.1 Driving frequency 50 kHz

The signal acquired without bubbles is very weak, and its spectrum does not present remarkable peaks at any frequency. On the contrary, when the bubble column is present (see figure 4.4(c)), the backscattered signal is strong and the peak at 1 Mhz in the frequency spectrum is very clear (figure 4.4(a) and (b)). When the bubble column disappears and only a few bubbles are present, the backscattered signal decreases, becoming similar to that without bubbles. At the same time, the amplitude of the peak at 1 Mhz decreases while another peak appears at a frequency of about 300 kHz. This peak is distinguished clearly in the frequency spectrum of the difference between the backscattered signal and the reference signal. According to the size of the produced bubbles a resonance frequency of about this value is expected. That might mean that this peak is due to the resonance of the oscillating bubbles. In figures 4.4 and 4.5 the backscattered signals and their spectra for four different instant of time are shown, as well as the image of the bubble cloud corresponding to that time.

4.3.2 Driving frequency 100 kHz

In this case, we can observe in the spectrum of the reference signal (without bubbles) a notable peak at approximately 300 kHz (see figures 4.6 and 4.7). This may imply two things: that this low frequency is due to some electrical effect or noise, or that some remaining isolated bubbles were still present when acquiring the signal and this frequency is due to the resonance of those bubbles. When exciting the thick bubble column, we also can see this peak at 300 kHz, although there is another peak with much higher amplitude at 1 Mhz (see figure 4.6(a), (b) and (c)). When the production of bubbles is stopped and we get a diluted cloud of bubbles, the peak at 1 Mhz disappears and the one at 300 kHz is more remarkable, as can be observed in figure 4.7.

4.3.3 Driving frequency 200 kHz

In this case, shown in figure 4.8, the excitation frequency is higher and the transducer provides a better reponse. The emitted signal, and therefore the signal backscattered by the thick column of bubbles, consists of just one pulse instead of the two pulses that were present in the previous experiments. The spectrum of this signal has a remarkable peak around a frequency of 1 Mhz, and another less clearly visible peak at a lower frequency of 300 kHz. In the spectrum of the reference signal—without bubbles—we see that there also exist a peak at 300 kHz. When the column of bubbles becomes more diluted, the amplitude of the peak at 1 Mhz decreases while the amplitude of the peak at 300 kHz increases. Again, as this peak is also found in the

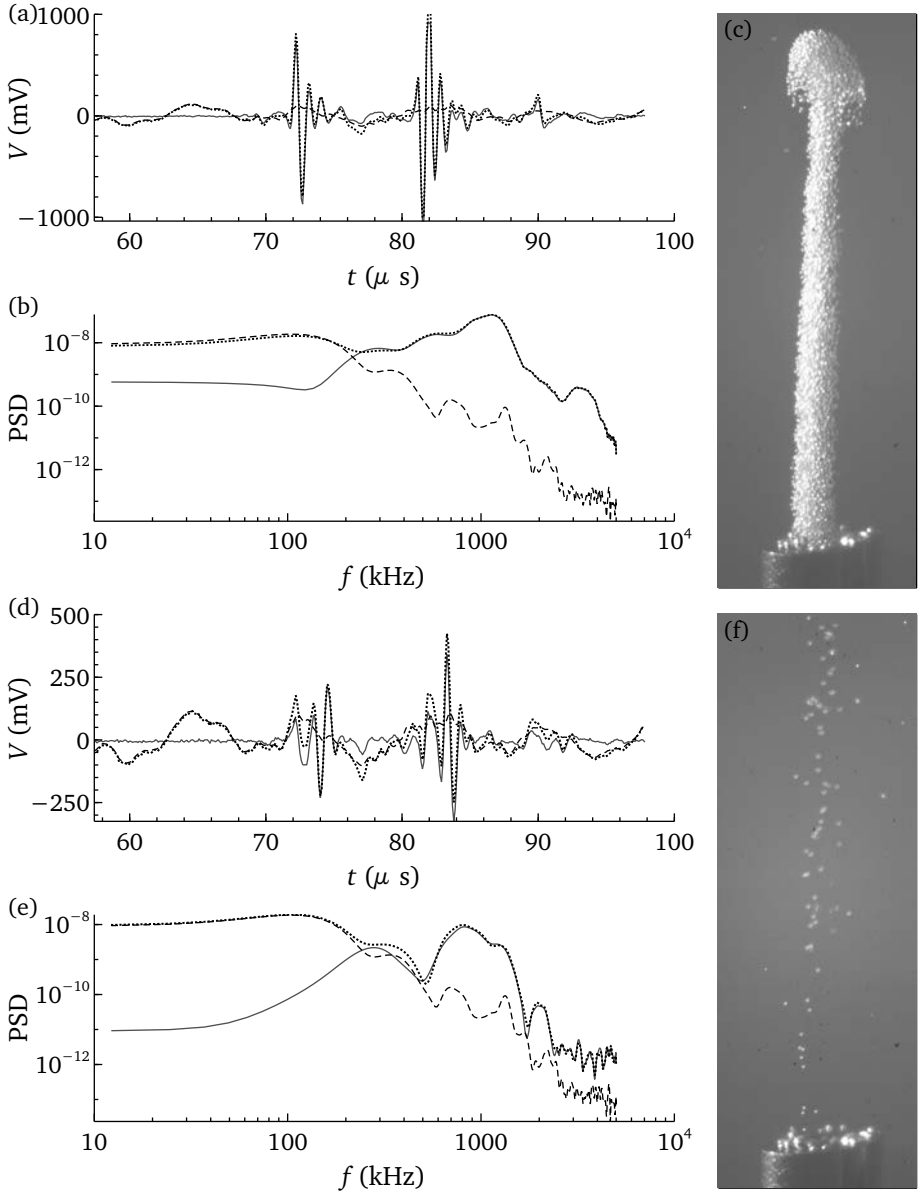

Figure 4.4: Driving frequency 50 kHz. In (a) and (d) the backscattered signals for two consecutive instants of time are plotted. The dashed line represents the signal without bubbles, the dotted line the signal scattered by the bubbles, and the difference between them is represented by the solid line. In (b) and (e) the frequency spectra of these signals is shown. The pictures (c) and (f) are the images captured at the two instants of time.

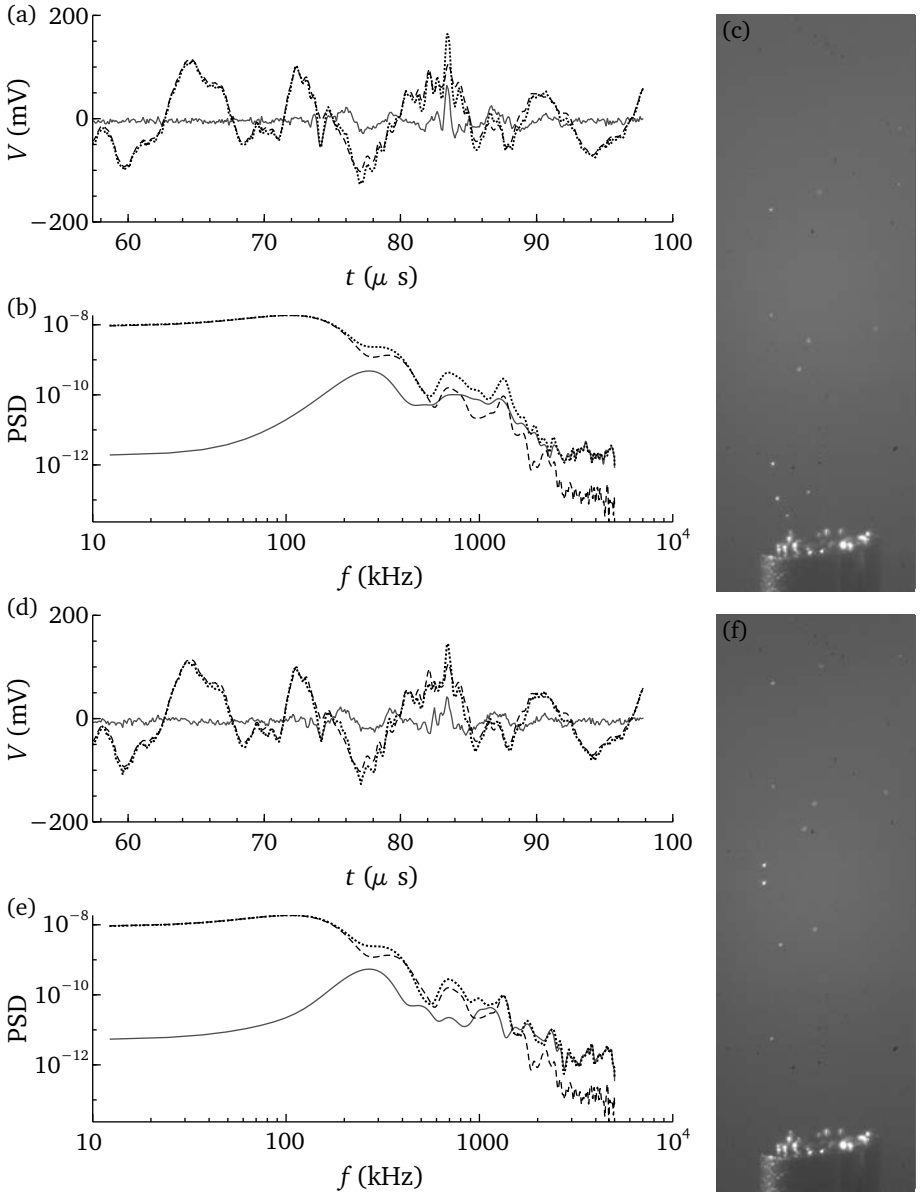

Figure 4.5: Continuation of figure 4.4, at two additional instants of time.

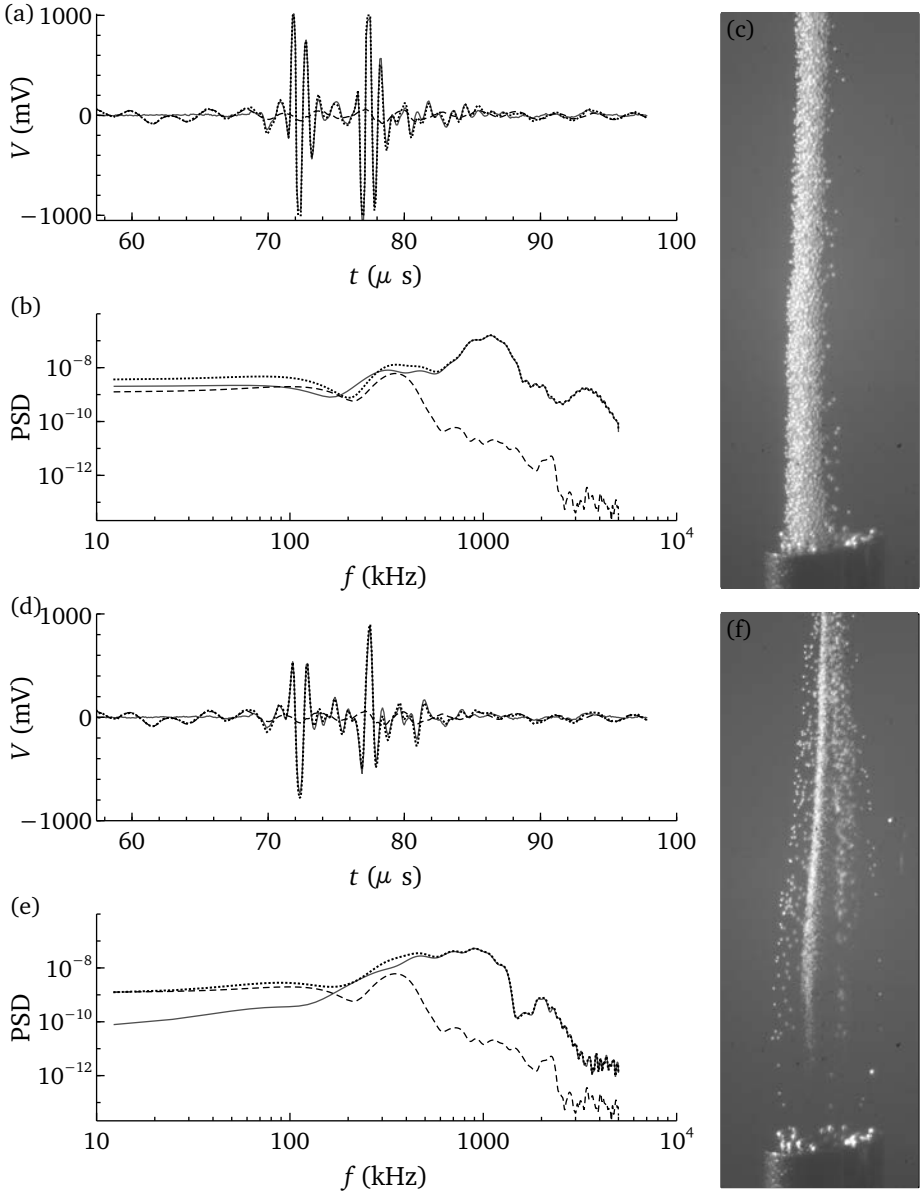

Figure 4.6: Driving frequency 100 kHz. In (a) and (d) the backscattered signal for two consecutive instants of time is plotted. The dashed line represents the signal without bubbles, the dotted line the signal scattered by the bubbles, and the difference between them is represented by the solid line. In (b) and (e) the frequency spectra of these signals is shown. The pictures (c) and (f) are the images captured at the two instants of time.

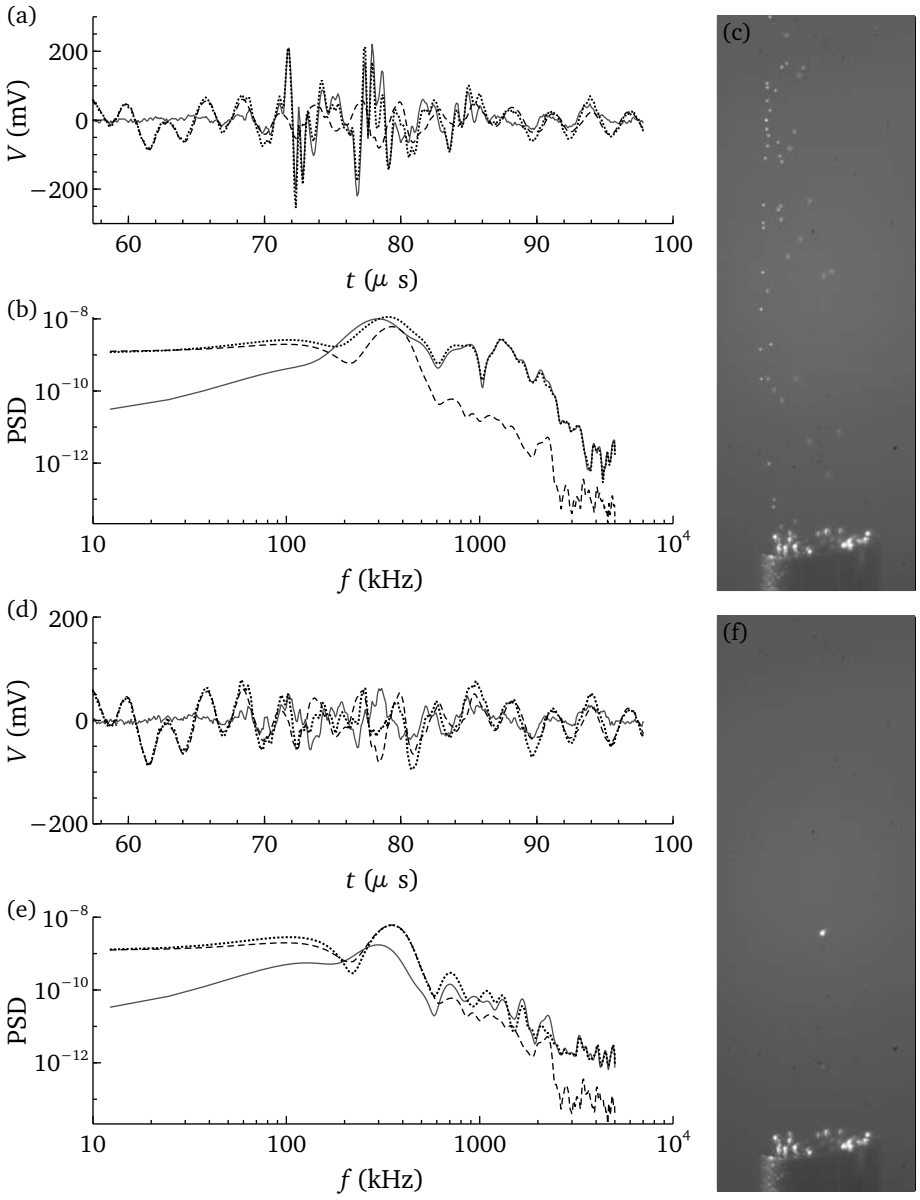

Figure 4.7: Continuation of figure 4.6, at two additional instants of time.

spectrum of the reference signal, we cannot conclude that it is exclusively due to the resonance of the bubbles.

4.3.4 Driving frequency 300 kHz

In figure 4.9 it can be observed that, like in the previous case, the transducer provides a better reponse, observable in the signal reflected by the thick column of bubbles containing just one pulse. The spectrum of this signal has a clearly distinguishable peak around a frequency of 1 Mhz, and another peak at a lower frequency of 300 kHz, which is also present in the spectrum of the reference signal. When the column of bubbles disappears, the amplitude of the peak at 1 Mhz decreases.

4.4 Discussion and conclusion

The expected resonance for coated bubbles with a size $D_m = 30$ μm is $f_{\text{res}} \simeq 300$ kHz. Effectively, in the experimentally obtained spectra shown before we can see a peak at approximately this frequency. Nevertheless, this peak also appears in some of the acoustic reference signals that were acquired when no bubbles were present. There is a possibility that diluted bubbles were present near the focal point when acquiring those reference signals. Indeed, the reference signal for $f_c = 50$ kHz was the first one that was acquired and its spectrum does not present a peak at 300 kHz. Another possible explanation for the 300 kHz peak is electronic noise caused by the multiple devices. Therefore, these experiments are not conclusive and more experiments should be performed. Furthermore, the transducer that was used is not suitable, since the maximum emitted amplitude lies at a frequency of $f = 1$ MHz and its response at low frequencies is weak and distorted. A broadband transducer able to produce a chirp in a range of frequencies close to the expected resonance frequency would fit better for the desired purpose. Indeed, Aldham *et al.* (2010) achieved to detect the resonance of large bubbles ($D \simeq 5$ mm) using a chirp signal that varied linearly in frequency between 1 and 1.5 kHz. Also Renaud *et al.* (2012) achieved to detect the resonance frequency of SonoVue® microbubbles, which have a diameter between 2 μm and 10 μm, using a frequency chirp varying between 0.5 and 5 MHz.

Finally, this technique of bubble generation produces too many bubbles for the desire purpose. Normally these bubbles are collected and diluted in water or another solution after production, in order to excite them acoustically. The main problem here is the stability of the bubbles. When they are collected, they can cluster and their size increases. Because of this, we are going to explore others techniques for bubble generation, as we will see in next chapter.

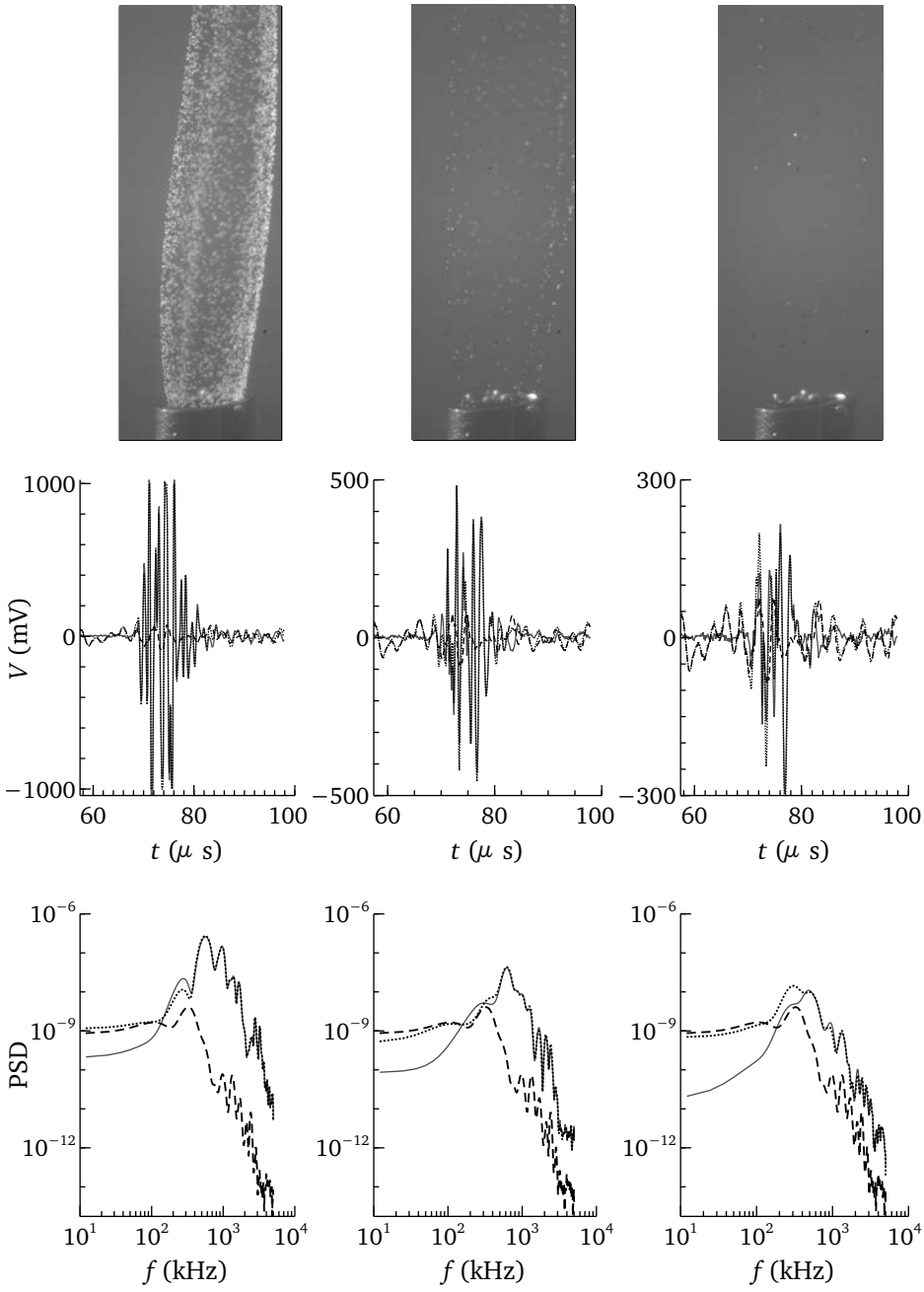

Figure 4.8: Driving frequency 200 kHz. (top row) The bubble column for three different instants of time; (middle row) the backscattered signal for the different times: the dashed line represents the signal without bubbles, the dotted line the signal scattered by the bubbles, and the difference between them is represented by the solid line; (bottom row) the frequency spectra corresponding to the backscattered signals.

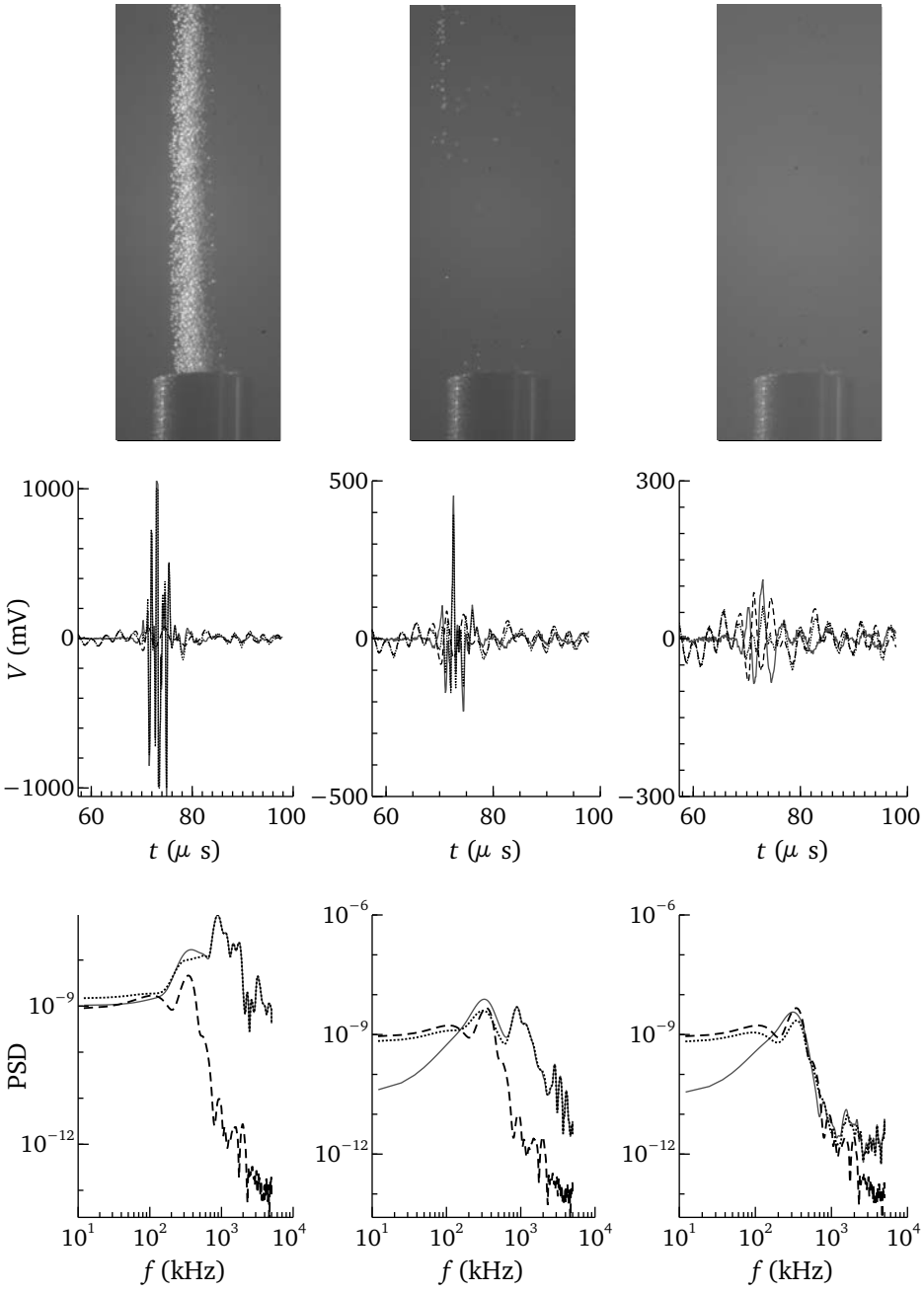

Figure 4.9: Driving frequency 300 kHz. (top row) The bubble column for three different instants of time; (middle row) the backscattered signal for the different times: the dashed line represents the signal without bubbles, the dotted line the signal scattered by the bubbles, and the difference between them is represented by the solid line; (bottom row) the frequency spectra corresponding to the backscattered signals.

References

ALDHAM, B., MANASSEH, R., ILLESINGHE, S., LIFFMAN, K., OOI, A. & SUTALO, I. D. 2010 Measurement of pressure on a surface using bubble acoustic resonances. *Meas. Sci. Technol.* **21**, 027002.

CASTRO-HERNANDEZ, E., VAN HOEVE, W., LOHSE, D. & GORDILLO.JM. 2011 Microbubble generation in a co-flow device operated in a new regime. *Lab Chip* **11**, 2023–29.

VAN DER MEER, S., DOLLET, B., VOORMOLEN, M.M., CHIN, C.T., BOUAKAZ, A., DE JONG, N., VERSLUIS, M. & LOHSE, D. 2007 Microbubble spectroscopy of ultrasound contrast agents. *J. Accoust. Soc. Am.* **121**, 648–656.

PARRALES, M.A., FERNANDEZ, J.M., PEREZ-SABORID, M., KOPECHEK, J.A. & PORTER, T.M. 2014 Acoustic characterization of monodisperse lipid-coated microbubbles: Relationship between size and shell viscoelastic properties. *J. Acoust. Soc. Am.* **136** (3), 1077–1084.

RENAUD, G., G., BOSCH J., VAN DER STEEN, A. F. W. & DE JONG, N. 2012 Chirp resonance spectroscopy of single lipid-coated microbubbles using an acoustical camera. *J. Acoust. Soc. Am. Ex Lett.* **132** (6), 470–475.

CHAPTER

FIVE

Generation of mini-clusters of microbubbles using water electrolysis

5.1 Introduction

In the last years, the interest in producing a single microbubble, or a mini-cluster, i.e. between two and ten bubbles, has increased significantly. Bubbles appear in many technological and industrial applications, in the fields of medicine, pharmacology, material science and chemical industry. In the medical field, for example, they are used as contrast agents in combination with ultrasound waves. They have also application in novel therapeutical techniques oriented to the elimination of thrombi or tumor ablation, since they can be selectively driven towards precise targets. These important applications disclose the importance of knowing the physical behavior of bubbles under the influence of different effects such as, for example, an ultrasound wave. It is known that bubble clouds behave differently than single bubbles, thus the importance of isolating them. In order to study these phenomena experimentally we must be able to generate singles bubbles of different sizes, in the range of several microns to a few hundred microns, in a controlled and easy way.

There exist several techniques for bubble generation. The most common technique to generate a single bubble is maybe the release of gas through an orifice or nozzle of small diameter. The size of the produced bubble depends strongly on the diameter of the injector (Longuet-Higgins & Prosperetti, 1991). If the bubbles are produced in a quiescent liquid, they will detach from the injector due to buoyancy forces when the bubble reaches a critical size (Oguz *et al.*, 1991). Therefore, achieving bubbles with a diameter of around 1 mm is relatively simple with this technique, but achieving smaller bubbles becomes more complicated. In order to generate micrometric bubbles by gas injection, a very small diameter of the nozzle is required, with the obstruction problems that this involves. For example, Ran & Katz (1991) reported the generation of a train of uniform bubbles with a size in the range of 90 to 400 microns using glass injectors with a diameter smaller than 10 microns.

Najafi *et al.* (2008) reported a novel technique consisting in using pressure pulses to inject the gas flow through micropipettes of different diameters into a quiescent liquid. They obtained bubbles with a uniform diameter between 200 and 600 microns, the smaller ones corresponding to the micropipette of smaller inner diameter (2 μm tip diameter). If the gas flow is injected into a moving liquid, the shear stresses help the detachment of the bubbles, achieving smaller bubbles for the same diameter of the needle. For example, Ohl (2001) generated single bubbles with radii between 300 μm and 3 mm, by injecting a short burst of gas into a liquid channel flow. The diameter of this channel was 4 mm.

To generate bubbles with sizes in the range of a few microns, we should use microdevices in which a gas stream is injected in a laminar liquid stream (Rodriguez-Rodriguez *et al.*, 2015). The existing configurations can be classified in three groups: gas-liquid coflow, flow-focusing and cross-flow configuration, the last one being the configuration which yields the smallest bubbles as well as the maximum bubbling frequency (Gordillo *et al.*, 2004; Castro-Hernandez *et al.*, 2011). The main advantage of these techniques is the capability of producing uniform microbubbles with an exact control of their size. Conversely, the production rate is high, making this technique unsuitable for generating a single bubble or a mini-cluster.

Acoustic forcing can be used to control the exit pressure in the gas supply line. For example, Shirota *et al.* (2008) used pairs of pulsed pressure waves, consisting of a compression to induce the formation of the bubble through an orifice, followed by a rarefraction to produce the neck pinch-off that leads to the detachment. The main advantage of this technique is the precise control of the bubble size. The bubble size however is limited by the diameter of the orifice. Indeed, the sizes reported by Shirota are millimetric instead of micrometric. Makuta *et al.* (2006) used an acoustic standing wave to induce the periodic formation and pinch-off of a cusp on the surface of a gas meniscus emerging from a needle, leading to a train of uniform micrometer-sized bubbles that flow away from the tip. In this way, microbubbles of uniform diameter from 4 to 15 μm were generated at a constant periodic rate. Nevertheless, the control of the amplitude of the pressure wave is not trivial, and the generation of bubbles results to be stable only for liquids with relatively high viscosity. Related to acoustics, sonication is used in medical applications to generate coated microbubbles in an easy and fast way (Zhang *et al.*, 2000; Zhao *et al.*, 2005). This procedure consists of inducing cavitation in a dissolution which contains the gas that will fill the bubble and the coating substance, normally lipids. This technique is widely used in the field of medicine due to its simplicity. The principal drawback here is the large polydispersity index in the size distribution and the large amount of bubbles.

More recently, laser techniques have been used to generate bubbles with controlled parameters. For example, Quinto-Su *et al.* (2008) generated cavitation bub-

bles using a high intensity laser. The main inconvenience here is that a complex and expensive system is required. Rodriguez-Rodriguez *et al.* (2014) also generated microbubbles by focusing a low-energy YaG laser pulse inside the bulk liquid with a convergent lens.

In conclusion, we can assert that there are many good techniques of bubble generation available nowadays, which produce uniform bubbles with a very precise control of the size distribution. Nonetheless, these techniques present certain shortcomings: some of them are difficult or expensive to develop and control, others are simply not appropriate for determined applications, either because the bubbling frequency is too high, or because the bubble size achieved is too large. Moreover, for some applications, such as the study of the displacement of a bubble in an acoustic field, bubbles are required to be released in a quiescent liquid far from any boundary. All these shortcomings motivate the present study, in which we consider the possibility of generating bubbles using water electrolysis.

The electrolysis of water is a good method for generating micrometric hydrogen bubbles. There are several published works studying this method of bubble generation. Lee *et al.* (2005) used micro-fabricated electrolytic micro-bubblers to generate hydrogen bubbles. They were able to achieve a size distribution with a low polidispersity index controlling the applied voltage and the dimensions of the micro-device. However, the production rate is too high and they did not report if only a few bubbles can be produced under certain conditions. Moreover, they used a flowing water channel to facilitate the detachment of the bubble from the electrode.

The method we propose consists of the generation of a few micron-sized bubbles using water electrolysis and electrical pulses. The lack of accuracy in controlling the bubble size is compensated by the easy, quick and inexpensive implementation of the method. We show that we can get an acceptable size distribution for the purpose we desire to study.

5.2 Experimental facility

The generation of hydrogen bubbles by water electrolysis is easy and cheap. We only need a power supply, water and two electrodes, namely, the cathode and the anode. The cathode is negatively charged and a reduction reaction takes places on it, producing hydrogen bubbles, meanwhile the anode is positively charged and suffers an oxidation reaction causing oxygen generation. When a continuous voltage is applied, many polydisperse bubbles are produced. Pulsed electrolysis can be used to regulate bubble size (Khosla *et al.*, 1991). To achieve the production of only a few bubbles, or even a short train of bubbles we use voltage pulses during which the intensity is on during a certain time, t_{on}, and then it is turned off during a time t_{off}. The relevant

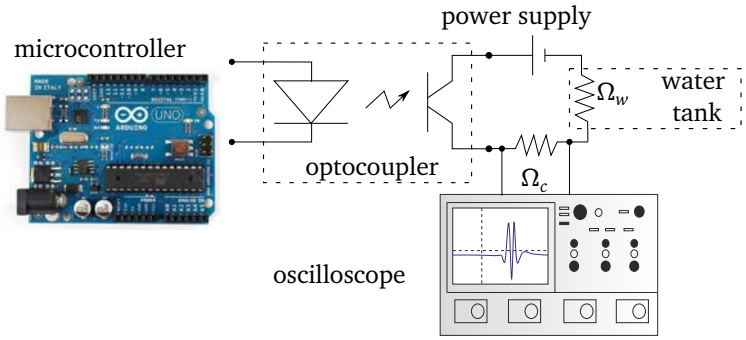

Figure 5.1: Scheme of the electrical circuitry used to generate the electrical pulses.

parameters here are t_{on}, t_{off}, the number of pulses N_p and the current intensity that passes through the electrodes, I_{c}. The goal is to determine how the variations of these parameters affect the number and size distribution of the produced microbubbles.

To generate electrical pulses we use an optocoupler. The circuitry is controlled using Arduino as a microcontroller, running its corresponding user-friendly open-source software. In order to know the current intensity in the circuitry, I_{c}, a known resistance $\Omega_{\text{c}} = 31$ kΩ is placed in line with the water resistance, Ω_w. The voltage V_c across Ω_c is measured and acquired with an oscilloscope. A sketch of the system is represented in figure 5.1.

Regarding the design of the electrodes, we are interested in the cathode having the least possible surface in contact with the water, to avoid the massive generation of bubbles. The surface of the anode, however, is not significant. The distance between cathode and anode is not very relevant either as long as we are measuring the intensity, as we did during the experiments. Nevertheless, we maintain the same distance in every experiment, with the cathode placed in the center of the tank and the anode in one of the corners. The cathode electrode consists of a 3 mm diameter copper rib with a length of 5 cm. This is covered with a plastic PVC cup, which has a hole of 1 mm in diameter at the top in order to get the water in contact with the metal. The entire electrode is isolated except by the hole in the cap, in order to make the electrolysis difficult so that only a few bubbles are generated. The anode electrode consists of a 3 mm diameter copper rib with a length of 20 cm, and its entire surface is conductor.

The bubble generation was recorded using a high speed camera (NAC MEMRECAM HX-3) with a high magnification lens (Navitar 12X). To illuminate, a cold light (Dedocool COOLT3) was placed in front of the camera to provide diffused backlighting. During the experiment, a video of the bubbles leaving the electrode was recorded with a frame rate of 100 fps and a shutter speed of 1/50000 s. The acquired images were post-processed with a custom-made software developed in Matlab in order to

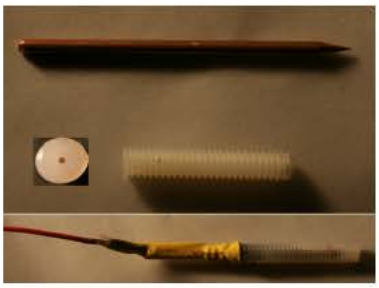

Figure 5.2: Picture of the electrode.

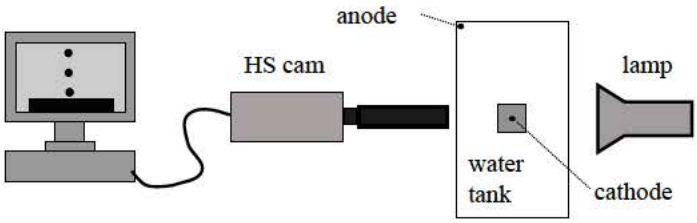

Figure 5.3: Sketch of the experimental facility. The high speed camera is connected to the computer to have real time visualization. A microscope video lens is used to have a good resolution of the bubble.

determine the bubble radius. Since the contour of the bubble is detected using a certain gray level threshold, for a certain bubble the maximum and minimum possible radii were determined selecting two different gray levels. The error was estimated to be about $5-10\%$ of the radius.

In order to measure the velocity with which the bubbles rise, a different experiment was done. The bubbles were recorded 1 cm above the electrode to make sure they had reached their terminal velocity. In addition the water tank was seeded with neutrally buoyant tracking microspheres in order to check that no flow existed in the tank and the only forces acting on the bubbles were buoyancy and drag.

5.3 Results

To prove that the generated bubbles can be considered isolated, i.e. that there are no collective effects, we measured the rising velocity U of different bubbles and compare it with that corresponding to a clean bubble and to a rigid sphere. In figure 5.4(a) we can see that the terminal velocity increases with the bubble size, as expected. In figure 5.4(b) the inverse of the Reynolds number based on the radius, $Re = UR/\nu$,

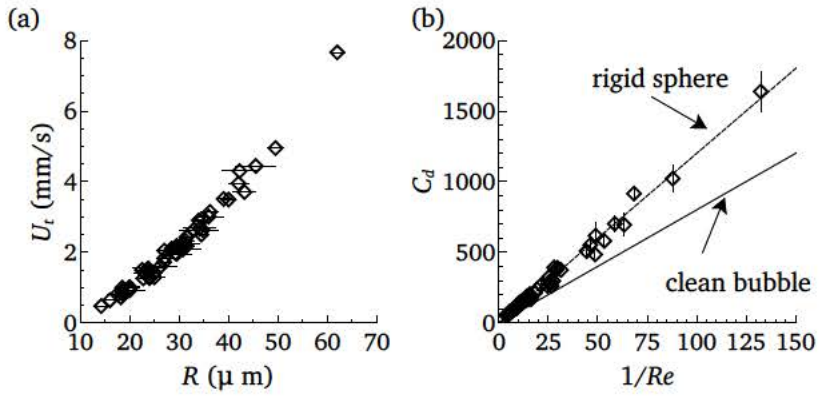

Figure 5.4: (a) Terminal velocity U_t as a function of the bubble radius R. (b) Drag coefficient C_d as a function of the inverse of the Reynolds number Re based on the radius of the bubble. The experimental values agree with the curve corresponding to a rigid sphere.

is represented versus the drag coefficient, $C_d = F_D/\frac{1}{2}\rho U^2 A_f$, where A_f is the cross-sectional area of the bubble, $A_f = \pi R^2$. Using Newton's second law we can calculate the drag force $F_D = B - W \simeq 8Rg/(3U^2)$, where B represents the buoyancy force and W is the weight, which can be neglected since the density of hydrogen is much lower than the density of water. For $Re < 1$, Stokes' law states that for a rigid sphere $F_D = 6\pi RU\mu$, so that $C_d = 12/Re$, with Re based on the radius of the sphere. For a clean bubble, $C_d = 8/Re$, with the Reynolds number based on the radius. Since the water is not perfectly clean (the electrolysis causes the degradation of the electrodes and pollutes the water), we cannot expect that the interface between the bubble and the water is purely clean. In fact, we checked that the terminal velocity corresponds to that for a rigid sphere, as can be seen in figure 5.4.

In order to generate only a few bubbles, we varied the characteristics of the pulses. We varied the on-time t_{on}, the off-time t_{off}, the current intensity I_c (measured through the voltage V_c), and the number of pulses N_p to find a relationship between these parameters and the bubble size distribution. We found that for shorter t_{on} and larger t_{off}, the bubbling rate was slower, producing a single bubble or a few of them with larger sizes. When t_{off} was decreased, the bubbling frequency increased and the mean size also decreased. Increasing I_c resulted in a higher quantity of bubbles with a smaller size. In general, the generation of a single bubble is difficult and not very repetitive, but it can be achieved for certain combinations of the parameters. In table 5.1 the electrical parameters that were used for the different experiments are summarized, as well as the statistical variables of the size distributions that were obtained: the mean bubble size R_m, the standard deviation SD, and the median of the distribution. The detailed results for the different experiments are plotted in

I_c (mA)	V_c (V)	N_p	t_{on} (ms)	t_{off} (ms)	R_m (μm)	SD	Median
0.61	19	5	60	30	26.03	8	25.15
0.32	10	3	50	50	19.97	6.9	16
0.29	9	5	25	25	13.35	5.9	11.5
0.19	6	4	60	40	21.1	10.3	20.5
0.42	13	2	20	20	16.6	8.3	13.75

Table 5.1: Different experimental conditions used to obtain mini-clusters of bubbles.

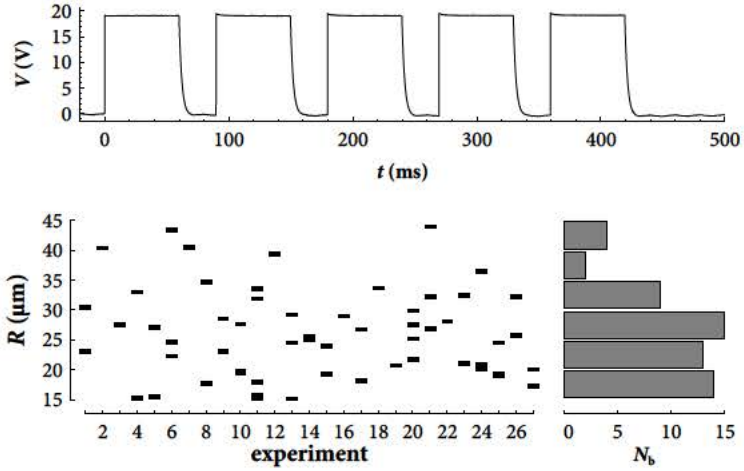

Figure 5.5: (top) The electrical pulse corresponding to $t_{on} = 60$ ms, $t_{off} = 30$ ms and $V_c = 19$ V; (bottom-left) the number of bubbles obtained in each experiment as well as their size; (bottom-right) the size histogram corresponding to all the experiments with this pulse.

figures 5.5 to 5.9.

5.4 Conclusion and applications

We remark here that this method of bubble generation is not as accurate as others mentioned, but is not our intention to improve the existing methods of bubble generation. The goal was to produce an isolated bubble or a mini-cluster of bubbles sufficiently separated one from other, and we succeeded in this goal. The obtained bubble sizes are not totally repetitive, but we have seen that some sizes prevail over others, depending on the pulse parameters. As we said before, the importance of producing isolated bubbles or mini-clusters of bubbles comes from the interest in studying their behavior. The technique we have developed permits, for example, to

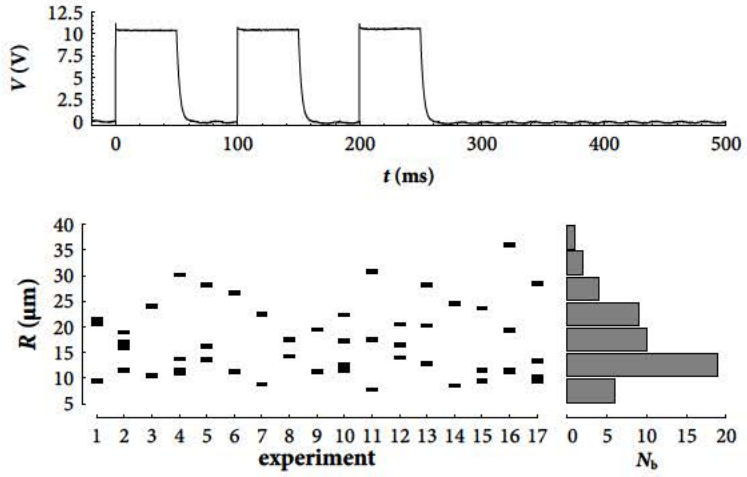

Figure 5.6: (top) The electrical pulse corresponding to $t_{on} = 50$ ms, $t_{off} = 50$ ms and $V_c = 10$ V; (bottom-left) the number of bubbles obtained in each experiment as well as their size; (bottom-right) the size histogram corresponding to all the experiments with this pulse.

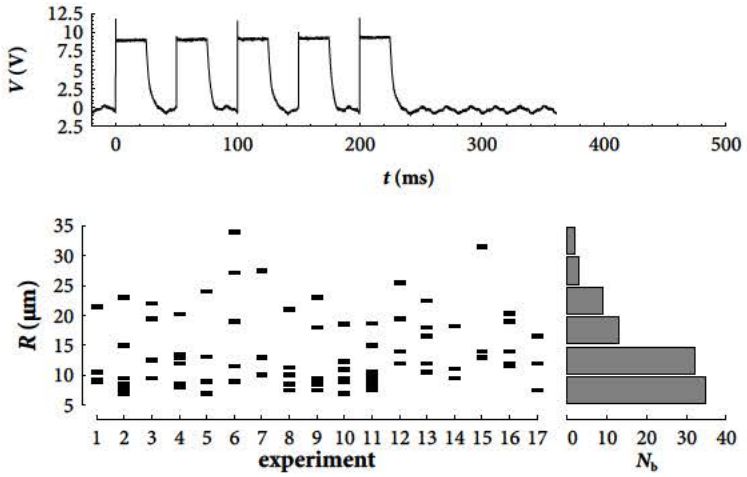

Figure 5.7: (top) The electrical pulse corresponding to $t_{on} = 25$ ms, $t_{off} = 25$ ms and $V_c = 9$ V; (bottom-left) the number of bubbles obtained in each experiment as well as their size; (bottom-right) the size histogram corresponding to all the experiments with this pulse.

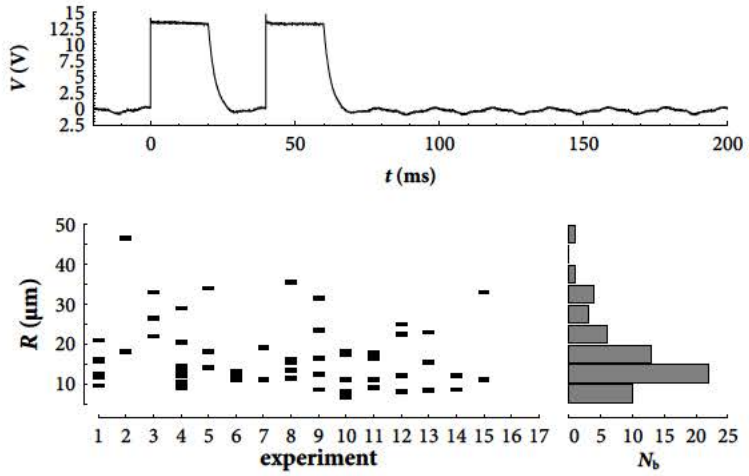

Figure 5.8: (top) The electrical pulse corresponding to $t_{on} = 20$ ms, $t_{off} = 20$ ms and $V_c = 13$ V; (bottom-left) the number of bubbles obtained in each experiment as well as their size; (bottom-right) the size histogram corresponding to all the experiments with this pulse.

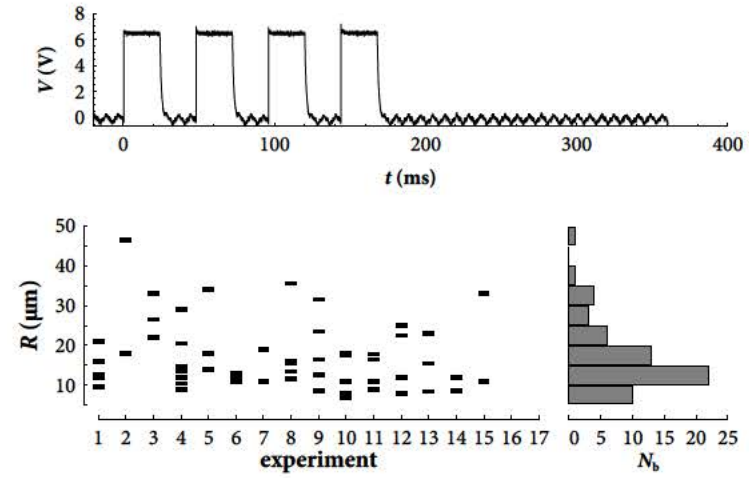

Figure 5.9: (top) The electrical pulse corresponding to $t_{on} = 60$ ms, $t_{off} = 40$ ms and $V_c = 6$ V; (bottom-left) the number of bubbles obtained in each experiment as well as their size; (bottom-right) the size histogram corresponding to all the experiments with this pulse.

study the interaction of a few bubbles, three or four, under the influence of an ultrasound field, or the behavior of a single bubble subjected to a standing wave. In our case, we are interested in the generation of bubbles to study the effect of the Bjerknes force on a single bubble subjected to a short travelling wave, as we will see in chapter 6.

References

CASTRO-HERNANDEZ, E., VAN HOEVE, W., LOHSE, D. & GORDILLO.JM. 2011 Microbubble generation in a co-flow device operated in a new regime. *Lab Chip* **11**, 2023–29.

GORDILLO, JM., CHENG, Z., MARQUEZ, M., GANAN-CALVO, AM. & WEITZ, DA. 2004 A new device for the generation of microbubbles. *Phys. Fluids* **16**, 2828–34.

KHOSLA, NK., VENKATACHALAM, S. & SOMASUNDARAN, P. 1991 Pulsed electrogeneration of bubbles for electroflotation. *J. Applied Electroch.* **21**, 986–990.

LEE, S., SUTOMO, W., LIU, C. & LOTH, E. 2005 Micro-fabricated electrolytic microbubblers. *I. J. Multiphase Flow* **31**, 706–722.

LONGUET-HIGGINS, H.N. & PROSPERETTI, A. 1991 The release of air bubbles from an underwater nozzle. *J. Fluid Mech.* **257**, 365–390.

MAKUTA, T., TAKEMURA, F., HIHARA, E., MATSUMO, Y. & SHOJI, M. 2006 Generation of micro gas bubbles of uniform diameter in an ultrasonic field. *J. Fluid Mech.* **548**, 113–131.

NAJAFI, AS., XU, Z. & MASLIYAH, J. 2008 Single micro-bubble generation by pressure pulse technique. *Chemical Engineering Science* **63**, 1779–1787.

OGUZ, MS., KERMAN, BR. & LUNDE, K. 1991 Dynamics of bubble growth and detachment from a needle. *J. Fluid Mech.* **230**, 111–145.

OHL, CD. 2001 Generator for single bubbles of controllable size. *Rev. Sci. Instrum.* **72** (1), 252–254.

QUINTO-SU, P.A., VENUGOPALAN, V. & OHL, C.D. 2008 Generation of laser-induced cavitation bubbles with a digital hologram. *Optics Express* **16** (23), 18964–9.

RAN, B. & KATZ, J. 1991 The response of microscopic bubbles to sudden changes in the ambient pressure. *J. Fluid Mech.* **224**, 91–115.

RODRIGUEZ-RODRIGUEZ, J. SEVILLA, A., MARTINEZ-BAZAN, C. & GORDILLO, J. M. 2015 Generation of microbubbles with applications to industry and medicine. *Annu. Rev. Fluid Mech.* **47**, 405–429.

RODRIGUEZ-RODRIGUEZ, J.R, CASADO, A. & FUSTER, D. 2014 Physics of beer tapping. *Phys, Rev. Let.* **113** (21), 214501.

SHIROTA, M., SANADA, T., SATO, A. & WATANABE, M. 2008 Formation of a submillimeter bubble from an orifice using pulsed acoustic pressure waves in gas phase. *Phys. Fluids* **20** (4), 043301.

ZHANG, D., GONG, XF., LIU, JH., SHAO, LZ., LI, XR. & ZHANG, QL. 2000 The experimental investigation of ultrasonic properties for a sonicated contrast agent and its application in biomedicine. *Ultrasound Med. and Bio.* **26** (2), 347–351.

ZHAO, YZ., LIANG, HD., MEI, XG. & HALLIWELL, M. 2005 Preparation, characterization and in vivo observation of phospholipid-based gas-filled microbubbles containing hirudin. *Ultrasound Med. and Bio.* **31** (9), 1237–1243.

CHAPTER

SIX

Experimental study of the translation of bubbles in a travelling acoustic wave due to primary Bjerknes force

6.1 Introduction

It is well known that gas bubbles suspended in an acoustically driven fluid undergo radial oscillations and also suffer steady (time-averaged) hydrodynamic forces that make them translate, interact with each other, and form clusters, among other effects. These forces are called acoustic radiation forces or Bjerknes forces and they can be classified in two types: primary Bjerknes forces and secondary Bjerknes forces. The former are experienced by single bubbles and cause them to travel along the direction of propagation of the acoustic wave. The secondary forces produce bubble-bubble interactions, making them attract or repel each other.

Mathematically, the primary Bjerknes force is calculated as the time average of the instantaneous radiation force exerted on a single bubble by the surrounding acoustically excited liquid, $F_B = -\langle \upsilon \nabla p_a \rangle$, where υ is the instantaneous volume of the bubble and ∇p_a is the pressure gradient due to the external excitation, evaluated at the position of the bubble. Accordingly, the sign of the Bjerknes force indicates the resultant direction of the bubble translation in an acoustic field. In a traveling wave field, the force moves the bubble away from the sound source. Assuming that the excitation is a planar wave in the horizontal direction with general frequency ω, and that the radial oscillations are sufficiently weak to consider a linear regime, this force can be written as (Leighton, 1994)

$$\mathbf{F}_B = \frac{2\pi P_A^2 k R_o}{\rho \omega^2} \frac{2\beta/\omega \mathbf{u}_z}{\left[(\omega_0/\omega)^2 - 1\right]^2 + (2\beta/\omega)^2}, \tag{6.1}$$

where ω_0 is the natural frequency of the bubble, and 2β is the sum of the viscous,

acoustic and thermal damping.

To determine the trajectory of a bubble, it is necessary to derive a time-averaged equation using Newton's Second Law, the expression for the primary Bjerknes force, the drag force and the so-called added-mass force. The latter is an additional inertia force that acts on a moving body in a fluid that is also set into motion, and can be written as $F_I = -\frac{1}{2}\rho \mathrm{d}(VU)/\mathrm{d}t$, where V is the volume of the bubble and U is the relative velocity of the bubble with respect to the liquid velocity.

The drag force for low Reynolds numbers (based on the translation velocity of the bubble) can be written as (Yang & Leal (1991))

$$F_D = -4\pi\mu RU - F_H, \tag{6.2}$$

where F_H is the so-called history force, analogous to the Basset-Boussinesq force on a sphere. According to Magnaudet & Legendre (1998), this history force is significant in strongly unsteady situations, as is the case of a bubble with time-variable radius. For a bubble with a small Reynolds number based on the velocity of the bubble, $Re = \rho UR/\mu$, and also a small ratio between the velocity of the bubble's wall and the velocity of the bubble, $\mathscr{U} = \dot{R}/U$, the history force is expressed (Magnaudet & Legendre, 1998) as

$$F_H = 8\pi\mu \int_0^t \exp\left[\int_\tau^t \frac{9\mu}{\rho_\infty R_1^2(t')}\mathrm{d}t'\right] \mathrm{erfc}\left[\sqrt{\int_\tau^t \frac{9\mu}{\rho_\infty R^2(t')}\mathrm{d}t'}\right] \frac{\mathrm{d}[R_1(\tau)U(\tau)]}{\mathrm{d}\tau}\mathrm{d}\tau. \tag{6.3}$$

The importance of the history force depends on the Stokes number, defined as $St = \omega_i \rho R_0^2/\mu$. For large Stokes numbers, the history force can be neglected. Nevertheless, in this case the Reynolds number also increases, and care should be taken since equation (6.2) is not valid for $Re > 1$. In the latter regime, the drag force is written as (Kang & Leal (1988))

$$F_D = -12\pi\mu R_0 U, \tag{6.4}$$

In order to derive the equation for the translation of the bubble, we use the expression given by Magnaudet & Legendre (1998) for the force exerted by the surrounding liquid on a bubble with a time-varying radius $R(t)$ that moves with a velocity $\mathbf{V}(t)$ inside a uniform flow field, $\mathbf{v}_\infty(t)$. Assuming that the Reynolds number based on the bubble's relative velocity, $R_0(v_\infty - V)/\nu \ll 1$ and that the one based

on the bubble's wall velocity also satisfies $R_0\dot{R}/\nu \ll 1$, then the force is given by:

$$\mathbf{F} = \frac{4}{3}\pi R^3\rho\frac{\mathrm{d}\mathbf{V}}{\mathrm{d}t} + \frac{2}{3}\pi\rho\left[\frac{\mathrm{d}}{\mathrm{d}t}R^3(\mathbf{v}_\infty - \mathbf{V}) + 2R^3\frac{\mathrm{d}}{\mathrm{d}t}(\mathbf{v}_\infty - \mathbf{V})\right] + 4\pi\mu R(\mathbf{v}_\infty - \mathbf{V}) + F_H \tag{6.5}$$

If the mass of the gas inside the bubble is neglected, Newtown's second law states that this force must be zero at all times. Rewriting equation (6.5) in order to express it through the relative velocity $\mathbf{U} = \mathbf{v}_\infty - \mathbf{V}$, instead of the bubble velocity, $\mathbf{V}$ the equation for the translation of the bubble yields

$$0 = \frac{4}{3}\pi\rho R^3\frac{\mathrm{d}\mathbf{v}_\infty}{\mathrm{d}t} + \frac{1}{2}\rho\left[\frac{4}{3}\pi\frac{\mathrm{d}}{\mathrm{d}t}\left(R^3\mathbf{U}\right)\right] + 4\pi\rho\,\nu R\mathbf{U} + F_H \tag{6.6}$$

where the first term is the inertia of the external fluid which can be related with the external acoustic field as $\frac{\mathrm{d}\mathbf{v}_\infty}{\mathrm{d}t} \simeq \frac{\partial\mathbf{v}_\infty}{\partial t} = -\frac{1}{\rho}\nabla p_a$, being equivalent to $-\upsilon\nabla p_a$, which is the instantaneous Bjerknes force. The second term refers to the added-mass force, the third is the drag force and the last term is the history force.

To simplify the equation for the translation of the bubble, we assume that the history force is negligible and that the bubble has reached a steady state, moving with terminal velocity U much larger than the velocity of the fluid u. Hence, the inertia force will be zero and the only forces acting on the bubble will be the Bjerknes force and the drag force modelled as (6.4), anticipating $Re > 1$. Under this condition we can calculate the dependency of the terminal velocity with the bubble size for a fixed pressure amplitude and driving frequency. For bubble sizes whose corresponding resonance frequency is much lower than the driving frequency, this dependency is linear, as can be observed in figure 6.1. The maximum observed corresponds to the resonance size for the driving frequency, which is $R_0 \simeq 6\mu$m. According to this linear and steady formulation, the Bjerknes force will be maximum for resonance bubbles, that is, bubbles excited at their resonance frequency.

The purpose of this study is to experimentally determine the displacement of the bubble as well as the evolution of the velocity in the direction of the sound wave, for different bubble sizes and for different parameters of insonation. Remarkably, there are not many experiments concerning primary Bjerknes force in travelling waves reported in the literature. Dayton *et al.* (2002) reported simulations and experiments of the Bjerknes force with contrast agents. Bubbles with radius $R_0 = 1.5\mu$m achieved velocities over 500 mm/s with a pressure amplitude of $P_A = 380$kPa and driving frequency $f_i = 2.25$MHz. Also Vos *et al.* (2007) reported experiments with contrast agents, using the measured displacement of the bubbles to determine the physical properties of the shell. The main inconvenience of working with encapsulated mi-

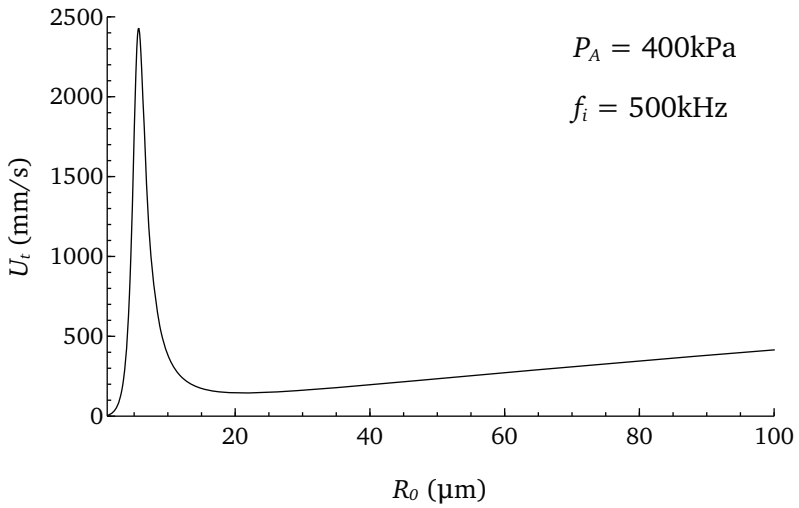

Figure 6.1: Terminal velocity for different bubbles sizes with fixed pressure amplitude and driving frequency. The velocity is maximum for the bubble size whose associated resonance is equal to the driving frequency. For larger bubbles with resonance frequencies much lower than the driving one, the relation between terminal velocity and size is linear.

crobubbles is that *a priori* it is difficult to know the properties of the shell. In this work we use hydrogen bubbles without coating, which have been produced as explained in chapter 5.

6.2 Experimental setup

The experiments were carried out in an acrylic tank of dimensions 22x29x51 cm filled with deionized water. 500 mg of potassium carbonate were added to make the water conductive and generate bubbles by electrolysis, as explained in chapter 5. The transducer was placed on one side of the tank, approximately midway between the two corners, and on the opposite side an absorbent material was fixed to the wall to avoid reflections of the acoustic wave. The cathode electrode was placed at a distance d_c from the transducer such that $d_c > N_F = D^2 f/4c_0$, where N_F is the near field distance, D is the diameter of the transducer, f is the driving frequency of the transducer and c_0 is the sound speed in water. Two different transducers (SONATEST Sound Solutions) were used with central driving frequencies of 0.5 MHz and 1 MHz, both of them unfocused, with a diameter $D = 2.54$ cm. The near field distances for the two transducers are $N_F \simeq 5.5$ cm and $N_F \simeq 11$ cm.

The bubbles were produced at the bottom of the tank using water electrolysis.

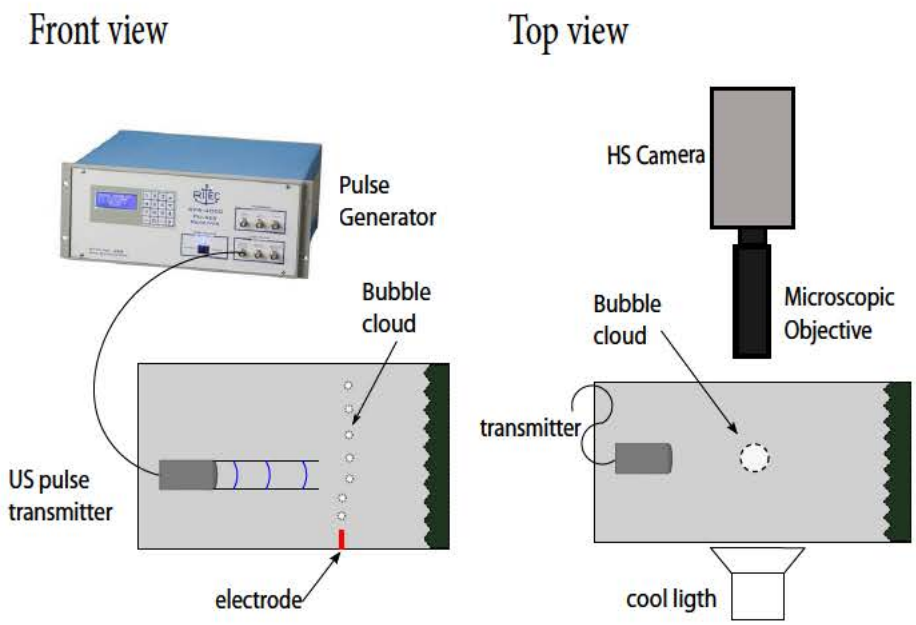

Figure 6.2: Sketch of the experimental setup to measure the bubble displacement caused by the Bjerknes force.

Buoyancy causes them to rise to the top. The bubbles were recorded with a high speed camera and microscopic objective. To capture the motion of bubbles accurately, the frame rate was set between 35000-40000 images per second, which is the maximum value we can set in order to have a compromise between temporal and spatial resolution. In figure 6.3 a frame of a experimental session can be observed with the bubble generator and the acoustic pulse schematized. We call direction x to the direction of the ultrasound pulse and direction y to the perpendicular direction to x. Bubbles move in y direction due to buoyancy, and in x direction due to the ultrasound pulse.

To generate the ultrasound wave, we used a pulser/receiver (RITEC) able to generate a sinusoidal-type wave with a determined number of cycles, a central driving frequency and a determined power. The wave is transmitted to the water through a broadband focused transducer (Sonatest, central frequency of 1MHz). We selected the driving frequency (0.5 or 1 MHz), the number of cycles (50 or 100) and the repetition rate (5 or 10 Hz). The duration of the pulse used is $T_p = 0.1$ ms for all the experiments done. The emitted pulse was measured with a needle hydrophone with a calibration $1mV/bar$. Before producing any bubbles, the hydrophone was placed directly in front of the transducer to record the maximum amplitude. Then the bub-

ble generator was placed underneath the hydrophone tip, and this was focused and captured with the camera. The hydrophone was removed and the production of bubbles was started. Bubbles that passed through the imaging window were recorded. Since the imaging window is smaller than the transducer and it is located at a height corresponding to the middle of the transducer, the bubble in the window has suffered previously other pulses.

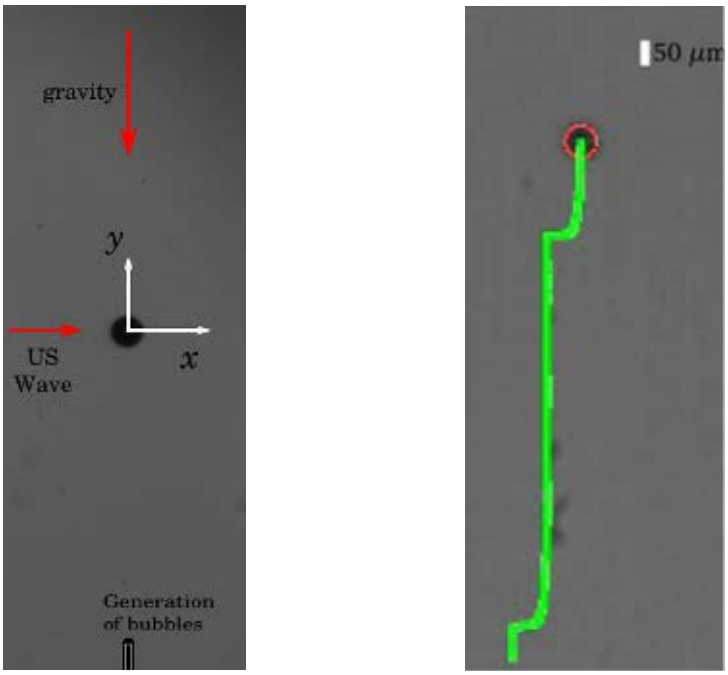

Figure 6.3: Frame of a microbubble (left) during an experimental session that shows a sketch of the acoustic pulse; and high-speed video sequence (right) which illustrates the trajectory (green line) of a bubble with radius $R \simeq 36$ rising in water by buoyancy and under the effect of a short acoustic pulse

6.3 Experimental Results

The trajectories of the bubbles have been analyzed through digital image processing of the high-speed videos. In figure 6.4 an example of the trajectory of a bubble, as well as the time evolution of the position (x, y) has been represented. Knowing the experimental trajectory, the velocities have been computed using finite differences. The terminal velocity in the vertical direction y can be calculated through the slope of the straight curve (t, y) represented in figure 6.4.

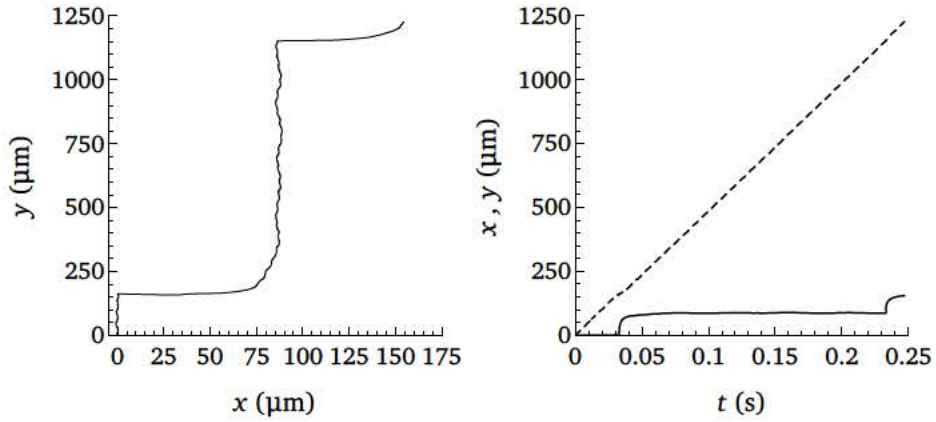

Figure 6.4: Trajectory of a bubble with $R_0 = 36.5\,\mu$m and time evolution of the position x (direction along the acoustic pulse) and y (perpendicular to x).

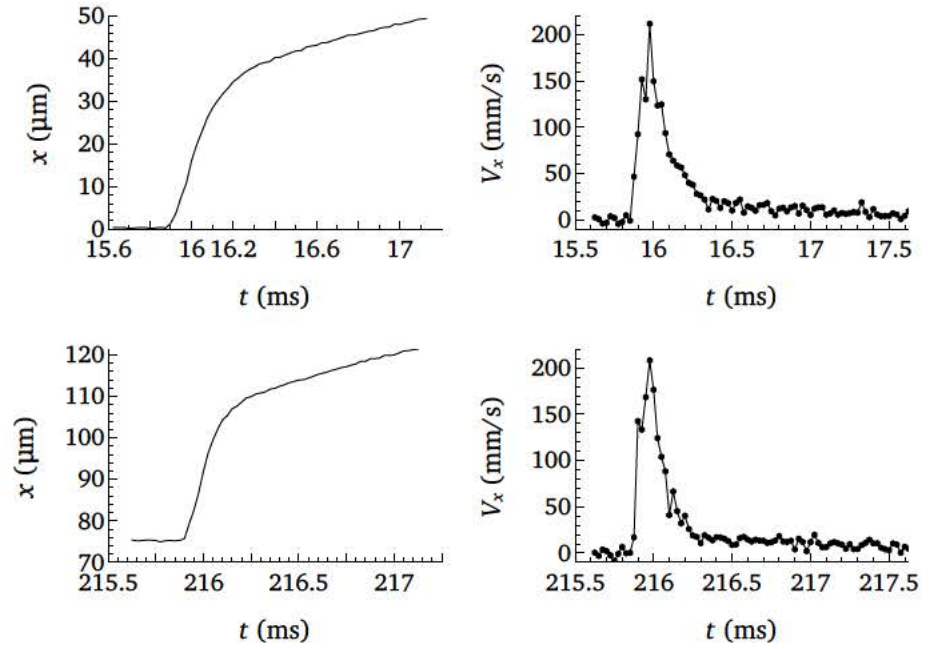

Figure 6.5: The two x trajectories during the two pulses can be observed (left), as well as the evolution of the velocity in direction x (right). The maximum velocities reached are $V_x = 212$ ans $V_x = 208$ mm/s for the first and the second pulse

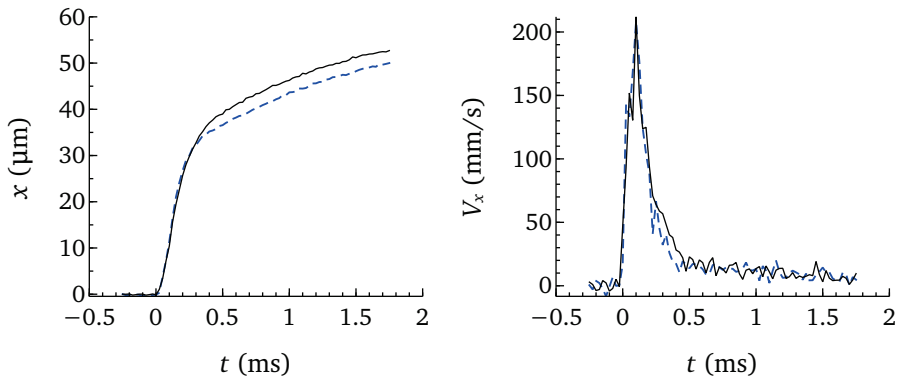

Figure 6.6: Trajectories and velocities represented in figure 6.5 superimposed in order to visualized the little difference between the two pulses

The goal is to determine the displacement produced in the bubble by the Bjerknes force, as well as the evolution of the velocity during the pulse. In figure 6.5 an example is shown of the trajectories and velocity experienced by a bubble with $R_0 = 36.5\,\mu$m in two consecutive pulses (with a repetition rate of 5Hz). Both the trajectory and the velocity are very similar for the two acoustic pulses, as can be checked in figure 6.6.

As seen in figure 6.1, a linear relation between maximum velocity reached and bubble size is expected for a fixed pressure amplitude and driving frequency. This means that a bubble with a certain size should reach the same velocity for pulses with the same irradiation conditions. This can be seen in figure 6.6. However, this does not happen in all experiments; indeed, in most of them we find a great dispersion in the results. A same bubble experiences different displacements and maximum velocities during consecutive pulses, as we can see in figure 6.7. In this case in particular, both the maximum velocity and the displacement decrease in each consecutive pulse. Also, the velocity in the direction x is not zero between pulses, but it has a negative value, as can be well appreciated in the trajectory plot. The reason for this is that the image is highly amplified (it has a magnification of 14) and a small inclination of the camera turns into a big inclination in the image.

The results shown in figure 6.7 correspond to a set of experiments in which different bubbles are excited with a pressure amplitude of $P_A \simeq 400$kPa (the measured signal can be seen in figure 6.8), a driving frequency of $f_i = 500$kHz and a repetition rate of $RR = 10Hz$. In figure 6.9 the consecutive maximum velocities experienced by all the bubbles is collected. To clarify, each experiment and therefore, each bubble is represented by a different marker. A great dispersion is observed, as we mentioned before.

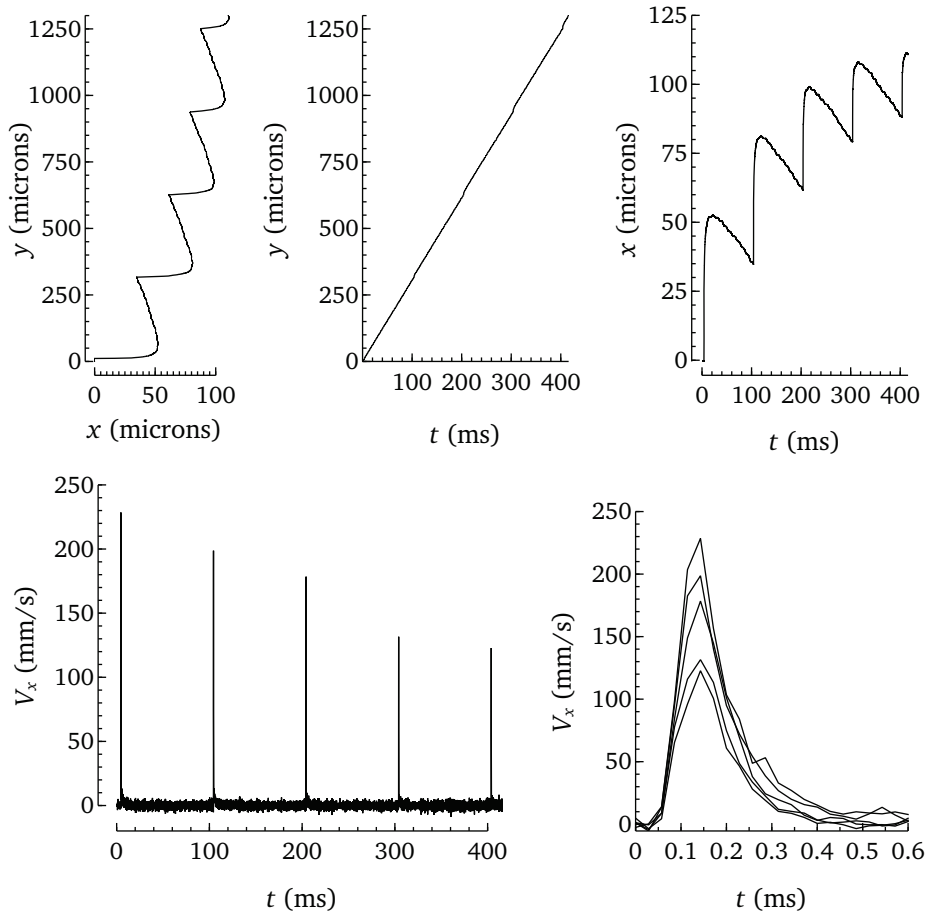

Figure 6.7: Top, trajectory and time evolution of the position (x, y) of a bubble with $R \simeq 40\,\mu$m. Bottom left, time evolution of the velocity in x direction, V_x. Bottom right, V_x during the pulses superposed in order to compare them. The maximum velocities achieved are 228.52, 198.68, 178.43, 131.55 and 122.74 mm/s

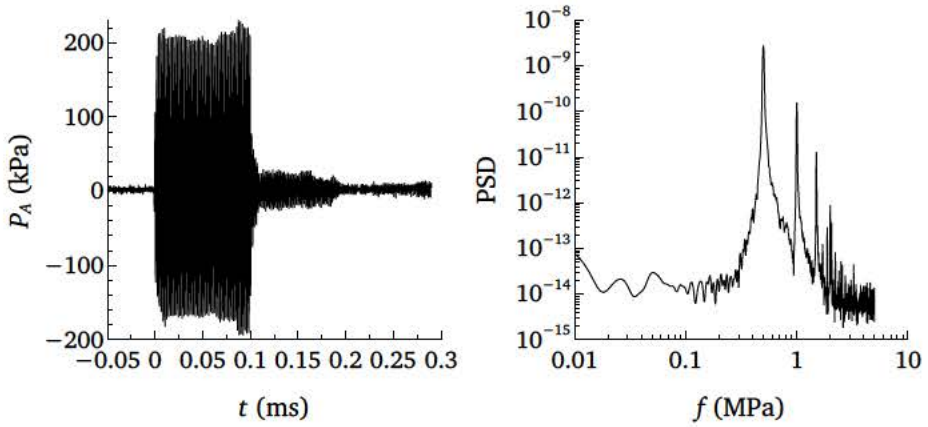

Figure 6.8: Experimental acoustic pulse measured with the hydrophone using an amplification of 20dB, which correspond to x10. This signal correspond to an amplitude of $P_A \simeq 400$kPa. The spectrum of the signal is also shown, where is clear that the driving frequency is $f_i = 500$kHz

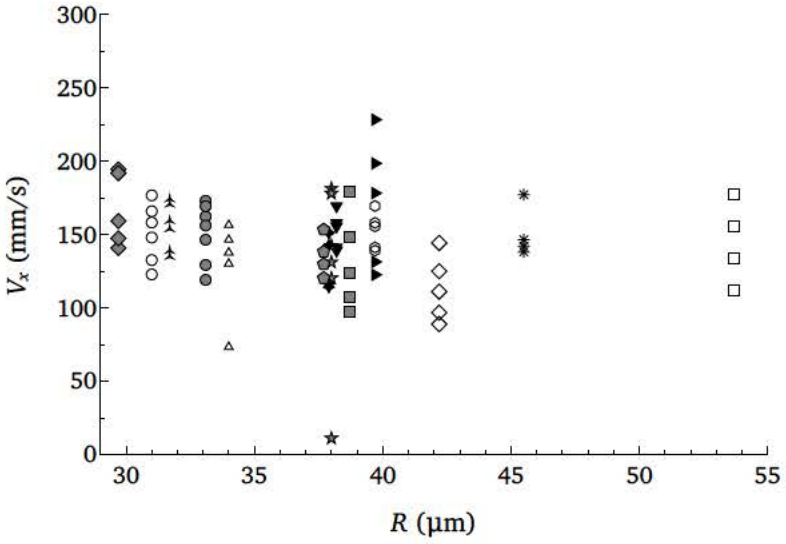

Figure 6.9: Maximum velocity reached during the pulse for bubbles with different radius, and for the same bubble for equal consecutive pulses.

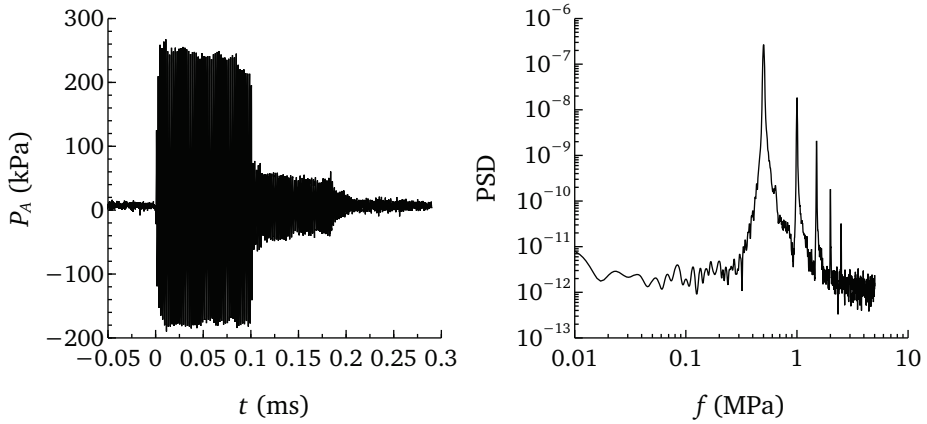

Figure 6.10: Experimental acoustic pulse measured with the hydrophone using an amplification of 40dB, which correspond to x100. This signal correspond to an amplitude of $P_A \simeq 400$kPa. The spectrum of the signal is also shown, where is clear that the driving frequency is $f_i = 500$kHz

We repeat the previous experiments using a lower repetition rate, $RR = 5$kHz, but maintaining same driving frequency and pressure amplitude. In this way, there are more time between consecutive pulses such that the residual oscillations of the bubble are damped. The acquired acoustic signal is very similar to the previous one, as can be seen in figure 6.10. Again, the dispersion of the results for the velocity is quite large (see figure 6.11).

6.4 Discussion of the results

The first notorious result is that the maximum velocities achieved by different bubbles are in general larger that the one expected. Through the numerical simulations carried out by Elena Igualada, which included the history force, we see that a bubble of $R_0 = 40\,\mu$m insonated with a continuous sinusoidal wave at a driving frequency of $f_c = 500$ kHz, reaches a velociy of $v_x \simeq= 100$ m/s when it is continuously insonated with a pressure amplitude of $P_A = 800$ kPa (see figure 6.12). However, according to our experimental measurements, the amplitude of the pressure is the half, and the velocities are even larger.

There is also a great dispersion in the values of the maximum velocities achieved by bubbles with equal sizes. Indeed, a same bubble behaves in a different way for consecutive pulses. This dispersion is also observed in the experiments reported by Dayton *et al.* (2002), although they display maximum displacement instead of

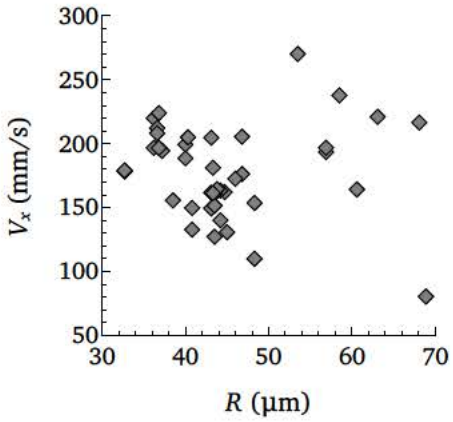

Figure 6.11: Maximum velocity reached during the pulse for bubbles with different radius, and for the same bubble for equal consecutive pulses.

maximum velocity. The figure 6.1 shows the terminal velocity that the bubble reaches in a steady state. However, the pressure tone burst we are applying to the bubble in our experiments is very short (0.1 ms), therefore the steady state has not been reached. Moreover, the bubble is continuously excited by consecutive pulses and we cannot assure that the initial conditions for the bubble, namely, radius at rest and radial velocity, are the same in each pulse. In theory, two consecutive pulses are sufficiently spaced in time (0.1 s or 0.2 s) so that the radial oscillation has been damped. Nevertheless, a residual velocity could exist.

In view of the experimental results, we are going to explore numerically the influence of the initial condition for the velocity of bubble's wall. To compute the translation and the velocity of the bubble, equation (6.6) must be integrated, together with the Keller-Miksis equation ((2.10), chapter 2) for the instantaneous radius R. As we already mentioned, equation (6.6) is valid if $Re \ll 1$ and $\sqcap Re \ll 1$. Regarding to the obtained experimental results, bubbles with $R_0 040\,\mu$ m moves with velocity $V_x = 100|\mathrm{m/s}$. Therefore $Re\emptyset \sim 1$ and $\mathscr{U}Re = R\dot{R}/\nu \sim R_0^2\omega a\dot{a}/\nu$, where a and $\dot{a}$ are the dimensionless radius and the dimensionless velocity of the bubble's wall, respectively. Clearly $a \sim 1$ but also $\dot{a} \sim 1$ during the duration of the acoustic pulse, obtaining $\mathscr{U}Re \gg 1$. Under these conditions, the equation we must integrate according to Magnaudet & Legendre (1998) is

$$0 = \frac{4}{3}\pi\rho R^3\frac{\mathrm{dv}_\infty}{\mathrm{d}t} + \frac{1}{2}\rho\left[\frac{4}{3}\pi\frac{\mathrm{d}}{\mathrm{d}t}\left(R^3\mathrm{U}\right)\right] + 12\pi\rho\nu R\mathrm{U} \tag{6.7}$$

Using the already defined dimensionless variables, $a = R/R_0$, $\tau = \omega t$, and the

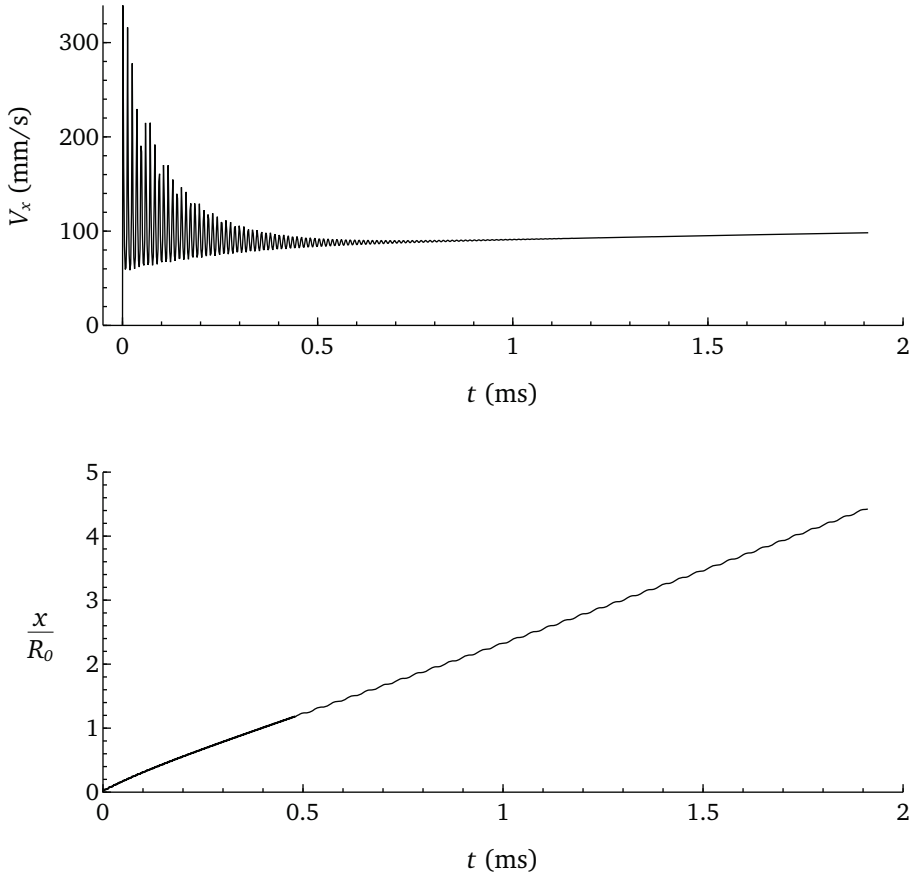

Figure 6.12: Temporal evolution of the horizontal velocity (top) and the displacement (bottom) reached by a bubble with $R_0 = 40\,\mu$m excited with a continuous sinusoidal wave with driving frequency $f_c = 500$ kHz and pressure amplitude $P_A = 800$ kPa. Results obtained through numerical simulations included history force.

new ones, $\tilde{\mathbf{V}} = \mathbf{V}/(R_0\omega)$ and $\tilde{\mathbf{v}_\infty} = \mathbf{v}_\infty/(R_0\omega)$ the system equation to solve yields

$$\ddot{a}\left[\frac{M}{Re} - a(\dot{a}M-1)\right] + \frac{3}{2}\dot{a}^2\left(1-\frac{M}{3}\dot{a}\right) = \Pi_0\left(\frac{1}{a^{3\gamma}}-1\right)$$
$$+ We^{-1}\left(\frac{1}{a^{3\gamma}}-\frac{1}{a}\right) - Re^{-1}\frac{\dot{a}}{a} - (1+M\dot{a})\,\epsilon f(\tau - M\tilde{x}) \tag{6.8a}$$
$$+ M\dot{a}\left[\Pi_0\left((1-3\gamma)\frac{1}{a^{3\gamma}}-1\right) + We^{-1}\left((1-3\gamma)\frac{1}{a^{3\gamma}}-\frac{1}{a}\right)\right]$$

$$\frac{1}{2}a^3\frac{\mathrm{d}\tilde{V}}{\mathrm{d}\tau} = \frac{3}{2}a^3\frac{\mathrm{d}\tilde{v}_\infty}{\mathrm{d}\tau} + \left(\frac{3}{2}a^2\dot{a} + \frac{9}{4}St^{-1}a\right)(\tilde{v}_\infty - \tilde{V}) \tag{6.8b}$$

$$\frac{\mathrm{d}\tilde{v}_\infty}{\mathrm{d}\tau} = \epsilon M f'(\tau - M\tilde{x}) \tag{6.8c}$$

$$\frac{\mathrm{d}\tilde{x}}{\mathrm{d}\tau} = \tilde{V} \tag{6.8d}$$

where the only new parameter appearing is the Stokes number $St = \omega R_0^2/(4\nu)$. Note that the dimensionless excitation in this case is $f(\tau - M\tilde{x})$, instead of $f(\tau - m\tilde{x})$. Since the bubble is moving along the x direction due to the radiation force, the center of the bubble is changing, and we have to take this fact into account.

Numerically, we can check that for an infinitely large pulse, the bubble will reach the same displacement and velocity independently of the initial conditions. However, for the first instants the bubble displacement is strongly influenced by the initial conditions. In figure 6.13, the translation achieved by the bubble has been plotted for different values of the radial velocity. We assume that the dimensionless wall velocity will be of the order of the dimensionless amplitude excitation, ϵ. The pressure amplitude is $P_A = 400$ kPa, the driving frequency is $f_c = 500$ kHz and the length of the pulse is $T_p = 0.1$ ms. Here, we can see that the displacement achieved by the bubble changes strongly if we vary the initial velocity of the radius of the bubble. Also, the change is more remarkable for smaller bubbles, since their resonance frequency is closer to the driving frequency used.

We can check also that the horizontal displacement of the bubble are larger for higher pressure amplitudes. In figure 6.14 the maximum displacement reached by a bubble of $R_0 = 40\mu$m for different initial conditions and for two different pressure amplitudes is plotted. Also we represent the temporal evolution of the displacement for the two amplitudes of pressure with two similar initial conditions.

In seen of these results, we can conclude that the bubble is suffering a chaotic behavior, possibly due to the chaotic oscillations that a bubble driven to an acoustic field can suffer. Lauterborn & Kurz (2010) report the study of these deterministically chaotic oscillations through dynamical system theory.

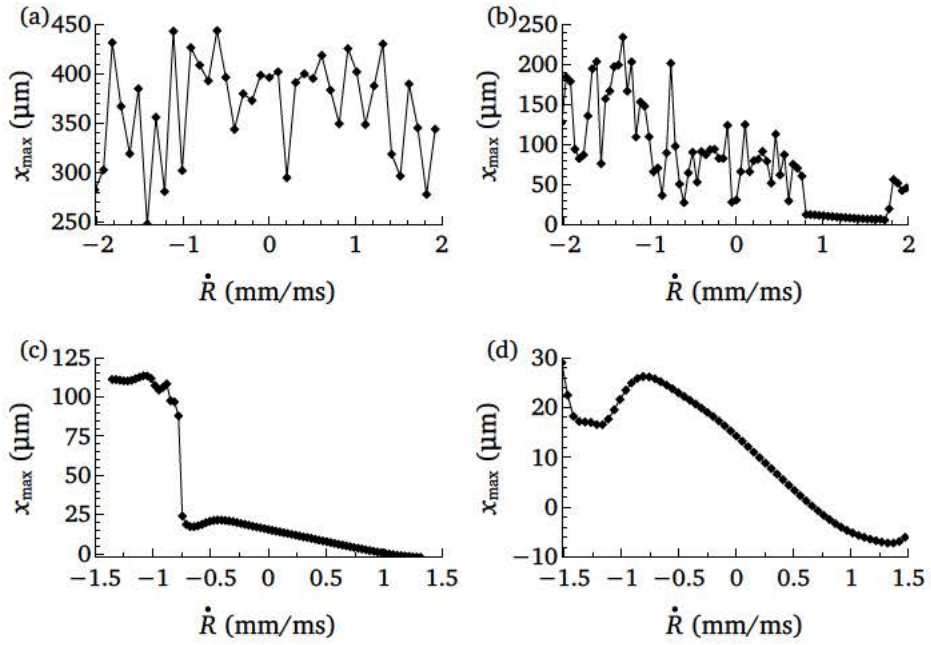

Figure 6.13: Numerical results for the maximum displacement achieved versus different values of the dimensionless radial velocity. (a) $R_0 = 10\,\mu$m, (b) $R_0 = 20\,\mu$m, (ac $R_0 = 30\,\mu$m, (d) $R_0 = 40\,\mu$m.

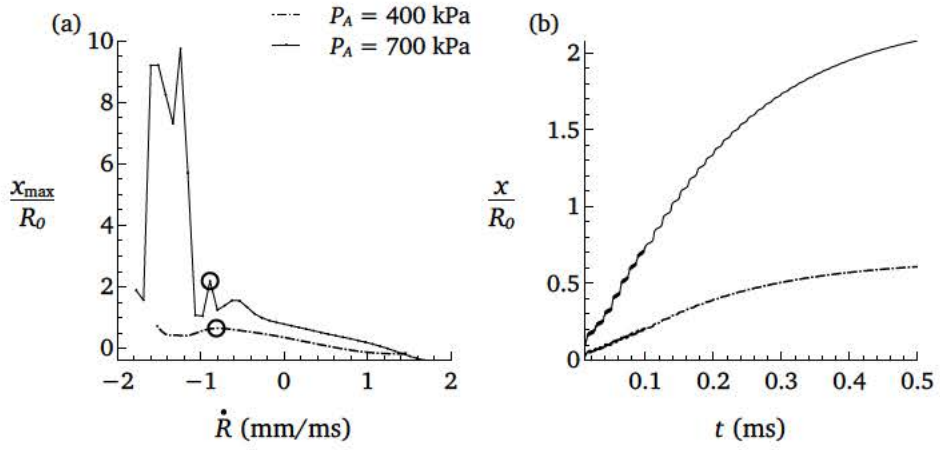

Figure 6.14: (a), maximum dimensionless displacement achieved by a bubble of $R_0 = 40\,\mu$m for pressure amplitude of 400 and 700kPa. (b), time evolution of the translation of the bubble for the conditions selected in (a) with circle markers.

References

DAYTON, P.A., ALLEN, J.S. & FERRARA, K.W. 2002 The magnitude of radiation force on ultrasound contrast agents. *J. Acoust. Soc. Am.* **112**, 2183–2192.

KANG, I.S. & LEAL, L.G. 1988 The drag coefficient for a spherical bubble in a uniform streaming flow. *Phys. Fluids* **31**, 233–237.

LAUTERBORN, W. & KURZ, T. 2010 Physics of bubble oscillations. *Rep. Prog. Phys.* **73**, 106501.

LEIGHTON, T.G. 1994 *The acoustic bubble*. Academic Press, London.

MAGNAUDET, J. & LEGENDRE, D. 1998 The viscous drag force on a spherical bubble with a time-dependant radius. *Phys. Fluids* **10**, 550–554.

VOS, H. J., GUIDI, F., BONI, E. & TORTOLI, P. 2007 Method for microbubble characterization using primary radiation force. *IEEE Trans. Ultrasonics, Ferr. and Freq. control* **54**, 1333–1345.

YANG, S. & LEAL, L.G. 1991 A note on memory-integral contributions to the force on an accelerating drop at low reynolds number. *Phys. Fluids A* **3**, 1923–1930.

CHAPTER

SEVEN

Conclusions and future work

We have formulated the problem for the radial motion of a bubble subjected to an ultrasound field, based on several previous works. We prove how thermal effects are very important in this problem and consequently cannot be neglected. In order to quantify the importance of the different parameters that appear in the problem, several numerical simulations have been carried out. We conclude that an ultrasound wave with a linear variable frequency—a chirp—is better in order to excite the resonance of bubbles. Of course, the resonance frequency of the bubbles that are excited must lie within the range of frequencies of the chirp. The length of the excitation is also important. In order to excite a cloud with a large polydispersity, the range of frequencies should be large. This makes that the length of the excitation, L_p should also be large enough such that the rate of the frequency increase, $k_f = \frac{f_{\max} - f_{\min}}{L_p}$, is small and all bubbles can be excited.

In addition, we have studied how the polydispersity affects the acoustic spectrum of a bubble cloud, in order to detect the resonance frequency. We have seen that the width of the resonance peak increases with the variance of the population, as well as its amplitude decreases becoming almost indistinguishable for clouds with a large polydispersity. The conclusion is that monodisperse bubbles produce a stronger response, and therefore, the resonance frequency is more notable in their spectra.

We have checked that the ambient pressure has an influence on the resonance frequency, which can be appreciated in the spectra. Nevertheless, there is a manifold of other factors that affect the resonance frequency as well, and their influence is not easy to quantify. This renders the accurate calculation of the ambient pressure through the measured resonance frequency very difficult. For example, in medicine, an accuracy of approximately 10 mmHg would be necessary for this technique to be useful. There are other fields however, where such a high precision is not necessary, for example in the oil extraction industry, where this technique could be applied to measure the pressure in oil deposits.

The experiments concerning the detection of the resonance frequency of a monodisperse bubble cloud did not lead to conclusive results. There have been several issues.

The production rate obtained using flow-focusing or co-flow techniques is too high to consider the resulting cloud to be diluted. As a consequence, the production of bubbles was stopped in order to analyze only the last bubbles remaining in the focal point. A HS camera was used to record this focal point and to know the number of bubbles forming the cloud. Since the generation was stopped suddenly, the number of bubbles cannot be chosen, being different in every experiment. Therefore, we could not compare the backscattered signal acquired in each session. Concerning to the acoustical parameters, the cloud was excited with a gaussian-type pulse with a low central frequency, 50 or 100 kHz. However, the frequency for which the transducer produces the maximum power was much higher, $f_c \simeq 1$ MHz. Indeed, a peak at that driving frequency is very remarkable in the spectra of the analyzed signals. Despite these issues, we can observe a peak located at the expected resonance frequency for coated bubbles. The problem is that this peak also appears in control signals in which there are no bubbles, at least *a priori*. Nevertheless, we cannot dismiss the fact that bubbles might exist out of the focal point due to the previous generation.

We found that a broadband transducer able to produce a chirp in frequency fits better for the desired purpose, that is, to detect the resonance frequency of bubbles. Using a function generator, one can supply a chirp signal to the transducer. The main problem here is that the generator cannot work also as receiver, being necessary to place a hydrophone in the setup. Also, the power supplied by the function generator must be amplified for the transducer to be able to emit an intense signal. A sketch of the set-up necessary for this experiment is represented in figure 7.1

We are convinced that this new setup would be better in order to experimentally detect the resonance frequency of the bubble, as Renaud *et al.* (2012) showed in their work. In order to solve the problem of the high production rate of microbubbles that the microdevice does have, we think of two possible solutions. The first one is to excite the bubbles inside the microdevice, once the bubble is detached from the meniscus. Since the material which the microdevice is made of is echogenic, we believe that the acoustical response will not be much affected by it. The second idea is to place the microdevice in perpendicular position and cut it off such that the generated bubble go out directly without accumulating in the collecting pool. Another suggestion is to trap a single bubble in a solid gel and excite this with an ultrasound pulse. If this gel is placed in a pressurized chamber, the variations of the acoustical response with the ambient pressure could be measured, and an experimental estimation of the variation in the resonance frequency of the bubble could be done, similarly to the experiments carried out by Aldham *et al.* (2010).

Alternatively, we have developed an easy, inexpensive and home-made technique for the production of a mini-cluster of bubbles, even an isolated bubble, in order to study some physical behaviors of these under the influence of ultrasound an field.

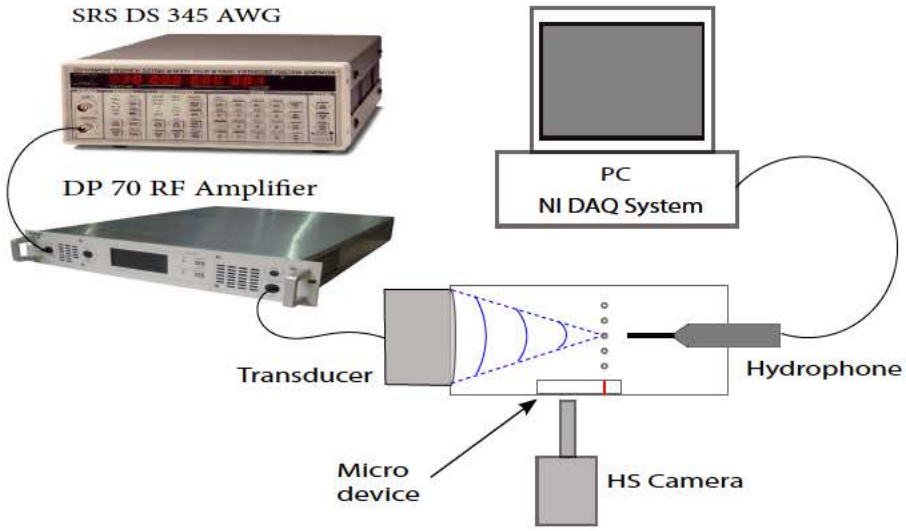

Figure 7.1: Setup of the experiment. The excitation pulse is produced by a function generator and the pressure radiated by the bubble cloud is listened using a hydrophone.

We demonstrate that, although the technique is not totally repetitive, bubbles of a few tens of microns in diameter are consistently generated.

We have studied experimentally the translational motion of a single bubble induced by the primary radiation or Bjerknes force, as well as the maximum velocity reached by the bubble. The expected result would be that for resonance sizes much bigger than the associated to the driving frequency, the maximum velocity increases with size. However, we find a great dispersion in the results. Indeed, for a same bubble experiencing consecutive pulses, the maximum velocities reached in each pulse are different, and consequently so are the achieved displacements. The same dispersion is shown in the experiments carried out by Dayton *et al.* (2002), although they make no comments about this. A plausible explanation is that the bubble is suffering shape instabilities that make it behave in different manners. But numerically we prove that even considering spherical symmetry, the behavior of the bubble is different when the initial conditions are changed even slightly. Effectively, the bubble has suffered several acoustic pulses, thus it may have residual oscillations once the new pulse excites it. The value of the velocity and acceleration of the bubble wall influences extremely the radiation force suffered by this, even displacing it in the opposite direction of the acoustic excitation, as we showed in chapter 6. Although there exist several works about the sign of the Bjerknes force and the unpredictable behavior of bubbles in standing waves, the chaotic behavior in travelling waves has not yet been reported in the literature, for the best of our knowledge.

Finally, we must remark that the results concerning the Bjerknes force are transient, since the pulse is too short for the bubbles to reach their terminal velocity. This transient effect is perfectly collected in the numerical simulations, thus the results can be perfectly compared. Nevertheless, in the simulations we check that the influence of the initial condition is negligible for long excitation times, achieving the bubble the same displacement. Therefore, it would be interested to study if the same dispersion is found experimentally when the pulse length is sufficiently long for the bubble to achieve the terminal velocity. This is not possible in our tank, since it is too short and a long excitation turns into a standing wave due to rebounds from the opposite wall. According to the simulations carried out by Elena Igualada, it is necessary that the pulse length takes at least 1 ms in order to reach the terminal velocity, under the conditions examined. Since we are using driving frequencies of 500 kHz or 1 MHz, we should have a pulse length of $N = 500$ or $N = 1000$ cycles in order to get a duration of 1 ms. The sound speed in water is $c_o \simeq 1500$ m/s, therefore the sound wave travels a distance of 1.5 m in that time. This means that we need to build a tank with a length of 2 m to avoid the rebounds. This would definitely be an interesting proposal for future work.

References

ALDHAM, B., MANASSEH, R., ILLESINGHE, S., LIFFMAN, K., OOI, A. & SUTALO, I. D. 2010 Measurement of pressure on a surface using bubble acoustic resonances. *Meas. Sci. Technol.* **21**, 027002.

DAYTON, P.A., ALLEN, J.S. & FERRARA, K.W. 2002 The magnitude of radiation force on ultrasound contrast agents. *J. Acoust. Soc. Am.* **112**, 2183–2192.

RENAUD, G., G., BOSCH J., VAN DER STEEN, A. F. W. & DE JONG, N. 2012 Chirp resonance spectroscopy of single lipid-coated microbubbles using an acoustical camera. *J. Acoust. Soc. Am. Ex Lett.* **132** (6), 470–475.

Alphabetical list of references

ABRAMOWITZ, M. & STEGUN, I. A. 1970 *Handbook of Mathematical Functions*. Dover Publications Inc., New York.

ADAM, D., SAPUNAR, M. & BURLA, E. 2005 On the relationship between encapsulated ultrasound contrast agent and pressure. *Ultrasound Med. Biol.* **31**, 673–686.

ALDHAM, B., MANASSEH, R., ILLESINGHE, S., LIFFMAN, K., OOI, A. & SUTALO, I. D. 2010 Measurement of pressure on a surface using bubble acoustic resonances. *Meas. Sci. Technol.* **21**, 027002.

ANDERSEN, K.S. & JENSEN, J.A. 2009 Ambient pressure sensitivity of microbubbles investigated through a parameter study. *J. Acoust. Soc. Am.* **126** (6), 3350–3358.

ANDERSEN, K.S. & JENSEN, J.A. 2010 Impact of acoustic pressure on ambient pressure estimation using ultrasound contrast agent. *Ultrasonics* **50**, 294–299.

ARIANI, M., FISHBEIN, M.C., CHAE, J.S., SADEGHI, H., MICHAEL, T., DUBIN, S.B. & SIEGEL, A. 1991 Dissolution of peripheral arterial thrombi by ultrasound. *Circulation* **84** (4), 1680–1688.

BJERKNES, V. F. K. 1906 *Fields of Force*. Columbia University Press, New York.

BOUAKAZ, A., FRINKING, P. JA., DE JONG, N. & BOM, N. 1999 Noninvasive measurement of the hydrostatic pressure in a fluid-filled cavity based on the disappearance time of the micrometer-sized free gas bubbles. *Ultrasound Med. Biol.* **25**, 1407–1415.

BRENNEN, C. E. 2002 Fission of collapsing cavitation bubbles. *J. Fluid Mech.* **472**, 153–166.

CALVISI, M. L., LINDAU, O., BLAKE, J. R. & SZERI, A. J. 2007 Shape stability and violent collapse in acoustic travelling waves. *Physics of Fluids* **19**, 047101.

CASTRO-HERNANDEZ, E., VAN HOEVE, W., LOHSE, D. & GORDILLO.JM. 2011 Microbubble generation in a co-flow device operated in a new regime. *Lab Chip* **11**, 2023–29.

CHIN, C. T. & BURNS, P. N. 2000 Predicting the acoustic response of a microbubble population for contrast imaging in medical ultrasound. *Ultrasound Med. Biol.* **26**, 1293–1300.

COMMANDER, K.W. & PROSPERETTI, A. 1989 Linear pressure waves in bubbly liquids: Comparison between theory and experiments. *J. Acoust. Soc. Am.* **85** (2), 732–746.

D'AGOSTINO, L. & BRENNEN, C. E. 1988*a* Acoustical absorption and scattering cross sections of spherical bubble clouds. *J. Acoust. Soc. Am.* **84** (6), 2126–2134.

D'AGOSTINO, L. & BRENNEN, C. E. 1988*b* Linearized dynamics of spherical bubble clouds. *J. Fluid Mech.* **199**, 155–176.

DAYTON, P.A., ALLEN, J.S. & FERRARA, K.W. 2002 The magnitude of radiation force on ultrasound contrast agents. *J. Acoust. Soc. Am.* **112**, 2183–2192.

DOINIKOV, A. 2002 Translational motion of a spherical bubble in an acoustic standing wave of high intensity. *Physics of Fluids* **14** (4), 1420–1425.

DOLLET, B., VAN DER MEER, S., GARBIN, V., DE JONG, N., LOHSE, D. & VERSLUIS, M. 2008 Nonspherical oscillations of ultrasound contrast agent microbubbles. *Ultrasound in Med. & Biol.* **34** (9), 1465–1473.

FAIRBANK, W. K. & SCULLY, M. O. 1977 A new noninvasive technique for cardiac pressure measurement: resonance scattering of ultrasounds for bubbles. *IEEE Trans. Biomed. Eng.* **24**, 107–110.

FLYNN, H. G. 1975 Cavitation dynamics i. a mathematical formulation. *J. Acoust. Soc. Am.* **57** (6), 1379–1396.

GANOR, Y., ADAM, D. & KIMMEL, E. 2005 Time and pressure dependence of acoustic signals radiated from microbubbles. *Ultrasound Med. Biol.* **31**, 1367–1374.

GARBIN, V., DOLLET, B., OVERVELDE, M., COJOC, D., DI FABRIZIO, E., VAN WIJNGAARDEN, L., PROSPERETTI, A., DE JONG, N., LOHSE, D. & VERSLUIS, M. 2009 History force on coated microbubbles propelled by ultrasound. *Physics of Fluids* **21**, 092003.

GILMORE, F.R. 1952 The collapse and growth of a spherical bubble in a viscous compressible liquid. *California Imtitute of Techdogy Hydrodynumica Laboratory, Rep* **26-4**.

GORDILLO, JM., CHENG, Z., MARQUEZ, M., GANAN-CALVO, AM. & WEITZ, DA. 2004 A new device for the generation of microbubbles. *Phys. Fluids* **16**, 2828–34.

GRAMIAK, R. & SHAH, P. M. 1968 Echocardiography of the aortic root. *Invest. Radiol.* **3**, 356–388.

HALLDORSDOTTIR, V.G., DAVE, J.K., LEODORE, L.M., EISENBREY, J.R., PARK, S., HALL, A.L., THOMENIUS, K. & FORSBERG, F. 2011 Subharmonic contrast microbubble signals for noninvasive pressure estimation under static and dynamic flow conditions. *Ultras. Imag.* **33**, 153–164.

HERRING, C. 1941 Theory of the pulsations of the gas bubble produced by an underwater explosion. *OSRD Rep.* **236**.

DE JONG, N., TEN CATE, F.J., VLETTER, W.B. & J.T.C.R., ROELANDT 1993 Quantification of transpulmonary echoconstrast effects. *Ultrasound Med. Biol.* **19**, 179–188.

KANG, I.S. & LEAL, L.G. 1988 The drag coefficient for a spherical bubble in a uniform streaming flow. *Phys. Fluids* **31**, 233–237.

KELLER, J. B. & MIKSIS, M. 1980 Bubble oscillations of large amplitude. *J. Acoust. Soc. Am.* **68** (2), 628–633.

KHISMATULLIN, D. B. & NADIM, A. 2002 Radial oscillations of encapsulated microbubbles in viscoelastic liquids. *Physics of Fluids* **14**, 3534–3556.

KHOSLA, NK., VENKATACHALAM, S. & SOMASUNDARAN, P. 1991 Pulsed electrogeneration of bubbles for electroflotation. *J. Applied Electroch.* **21**, 986–990.

LANDAU, L. & LIFSHITZ, E. 1959 *Fluid Mechanics*. Adison-Wesley, Reading, MA.

LAUTERBORN, W. & KURZ, T. 2010 Physics of bubble oscillations. *Rep. Prog. Phys.* **73**, 106501.

LEE, S., SUTOMO, W., LIU, C. & LOTH, E. 2005 Micro-fabricated electrolytic microbubblers. *I. J. Multiphase Flow* **31**, 706–722.

LEIGHTON, T.G. 1994 *The acoustic bubble*. Academic Press, London.

LEIGHTON, T. G. 1987 An experimental study of the sound emitted from gas bubbles in a liquid. *Eur. J. Phys.* **8** (2), 98 – 104.

LEIGHTON, T. G., WALTON, A.J. & M.J.W., PICKWORTH 1990 Primary bjerknes forces. *Eur. J. Phys.* **11**, 47 – 50.

LONGUET-HIGGINS, H.N. & PROSPERETTI, A. 1991 The release of air bubbles from an underwater nozzle. *J. Fluid Mech.* **257**, 365–390.

LUCAS, TM. & HARNETT, CK. 2011 Control of electrolysis-generated microbubbles for sensor surface passivation. *App. Physics L.* **98**, 011915.

MAGNAUDET, J. & LEGENDRE, D. 1998 The viscous drag force on a spherical bubble with a time-dependant radius. *Phys. Fluids* **10**, 550–554.

MAKUTA, T., TAKEMURA, F., HIHARA, E., MATSUMO, Y. & SHOJI, M. 2006 Generation of micro gas bubbles of uniform diameter in an ultrasonic field. *J. Fluid Mech.* **548**, 113–131.

MARMOTTANT, P., VAN DER MEER, S., EMMER, M., VERSLUIS, M., DE JONG, N., HILGENFELDT, S. & LOHSE, D. 2005 A model for large amplitude oscillations of coated bubbles accounting for buckling and rupture. *J. Acoust. Soc. Am.* **118** (6), 3499–3505.

VAN DER MEER, SANDER 2007 Ultrasound contrast agents. resonances of coated bubbles. PhD thesis, Universiteit Twente.

VAN DER MEER, S., DOLLET, B., VOORMOLEN, M.M., CHIN, C.T., BOUAKAZ, A., DE JONG, N., VERSLUIS, M. & LOHSE, D. 2007 Microbubble spectroscopy of ultrasound contrast agents. *J. Accoust. Soc. Am.* **121**, 648–656.

MINNAERT, M. 1933 On musical air bubbles and the sounds of running water. *Phil. Mag.* **26** (104), 235–248.

NAJAFI, AS., XU, Z. & MASLIYAH, J. 2008 Single micro-bubble generation by pressure pulse technique. *Chemical Engineering Science* **63**, 1779–1787.

OGUZ, MS., KERMAN, BR. & LUNDE, K. 1991 Dynamics of bubble growth and detachment from a needle. *J. Fluid Mech.* **230**, 111–145.

OHL, CD. 2001 Generator for single bubbles of controllable size. *Rev. Sci. Instrum.* **72** (1), 252–254.

OMTA, R. 1987 Oscillations of a cloud of bubbles of small and not so small amplitude. *J. Acoust. Soc. Am.* **82** (3), 1018–1033.

PARRALES, MIGUEL 2013 Propagación y dispersión de ondas acústicas a través de nubes de microburbujas. PhD thesis, Universidad de Sevilla.

PARRALES, M.A., FERNANDEZ, J.M., PEREZ-SABORID, M., KOPECHEK, J.A. & PORTER, T.M. 2014 Acoustic characterization of monodisperse lipid-coated microbubbles: Relationship between size and shell viscoelastic properties. *J. Acoust. Soc. Am.* **136** (3), 1077–1084.

PLESSET, MS. & PROSPERETTI, A. 1977 Bubble dynamics and cavitation. *Annu. Rev. Fluid Mech.* **9**, 145–185.

PLESSET, M. S. 1949 The dynamics of cavitation bubbles. *J. Appl. Mech.* **16**, 277–282.

PLESSET, M. S. 1954 On the stability of fluid flows with spherical symmetry. *J. Appl. Phys.* **25**, 96–98.

POSTEMA, M., BOUAKAZ, A. & DE JONG, N. 2004 Noninvasive microbubble-based pressure measurements: a simulation study. *Ultrasonics* **42**, 759–762.

PROSPERETTI, A. 1977 Thermal effects and damping mechanisms in the forced radial oscillations of gas bubbles in liquids. *J. Acoust. Soc. Am.* **61** (1), 17–27.

PROSPERETTI, A. & LEZZI, A. 1986 Bubble dynamics in a compressible liquid. part 1. first-order theory. *J. Fluid Mech.* **168**, 457–478.

QUINTO-SU, P.A., VENUGOPALAN, V. & OHL, C.D. 2008 Generation of laser-induced cavitation bubbles with a digital hologram. *Optics Express* **16** (23), 18964–9.

RAN, B. & KATZ, J. 1991 The response of microscopic bubbles to sudden changes in the ambient pressure. *J. Fluid Mech.* **224**, 91–115.

RAN, B. & KATZ.J 1991 The response of microscopic bubbles to sudden changes in the ambient pressure. *J. Fluid Mech.* **224**, 91–115.

RAYLEIGH, LORD 1917 On the pressure developed in a liquid during the collapse of a spherical cavity. *Phil. Mag.* **34** (200), 94–98.

RENAUD, G., G., BOSCH J., VAN DER STEEN, A. F. W. & DE JONG, N. 2012 Chirp resonance spectroscopy of single lipid-coated microbubbles using an acoustical camera. *J. Acoust. Soc. Am. Ex Lett.* **132** (6), 470–475.

ROBERTS, G. O. 1975 A new method to cure thrombi by ultrasonic cavitation. pp. 273–5. Ultrasonics International 1975, J. Ultrasonics.

RODRIGUEZ-RODRIGUEZ, J. SEVILLA, A., MARTINEZ-BAZAN, C. & GORDILLO, J. M. 2015 Generation of microbubbles with applications to industry and medicine. *Annu. Rev. Fluid Mech.* **47**, 405–429.

RODRIGUEZ-RODRIGUEZ, J.R, CASADO, A. & FUSTER, D. 2014 Physics of beer tapping. *Phys, Rev. Let.* **113** (21), 214501.

SHI, W.T., FORSBERG, F., RAICHLEN, J.S., NEEDLEMAN, L. & GOLDBERG, B.B. 1999 Pressure dependence of subharmonic signals from contrast microbubbles. *Ultrasound Med. Biol.* **25**, 275–283.

SHI, W. T., GAO, S., FRANCOIS, V., POWERS, J. E., DRVOL, L., JUNG, K.W., XIE, F., LOF, J., EVERBACH, E.C. & PORTER, T. R. 2010 Investigation of effectiveness of microbubble stable cavitation in thrombolysis. pp. 330–3. IEEE International Ultrasonics Symposium Proceedings, IEEE, Piscataway, NJ, USA.

SHIROTA, M., SANADA, T., SATO, A. & WATANABE, M. 2008 Formation of a submillimeter bubble from an orifice using pulsed acoustic pressure waves in gas phase. *Phys. Fluids* **20** (4), 043301.

SIJL, J., VOS, H. J., DE JONG, N., LOHSE, D. & VERSLUIS, M. 2011 Combined optical and acoustical detection of single microbubble dynamics. *J. Acoust. Soc. Am.* **130** (5), 3271–3281.

STRICKER, L., PROSPERETTI, A. & LOHSE, D. 2011 Validation of an approximate model for the thermal behavior in acoustically driven bubbles. *J. Acoust. Soc. Am.* **130** (5), 3243–3251.

SUTTON, J. T., HAWORTH, K.J., PYNE-GEITHMAN, G. & HOLLAND, C.K. 2013 Ultrasound-mediated drug delivery for cardiovascular disease. *Expert opinion in drug delivery* **10** (5), 573–592.

TRILLING, L. 1952 The collapse and rebound of a gas bubble. *J. Appl. Phys.* **23**, 14–17.

TRUBESTEIN, G. G. 1976 Thrombolysis by ultrasound. *Clinical science and molecular medicine* **51**, 697–698.

TSUGE, H., OGAWA, T. & OHMASA, R. 2008 Microbubble formation by electrolysis using a new mixing equipment with low frequency vibratory fins. *J. Chem. Eng, Japan* **41** (7), 557–561.

VOS, H. J., GUIDI, F., BONI, E. & TORTOLI, P. 2007 Method for microbubble characterization using primary radiation force. *IEEE Trans. Ultrasonics, Ferr. and Freq. control* **54**, 1333–1345.

VAN WIJNGAARDEN, L. 1968 On equations of motion for mixtures of liquid and gas bubbles. *J. Fluid Mech.* **33**, 465–474.

YANG, S. & LEAL, L.G. 1991 A note on memory-integral contributions to the force on an accelerating drop at low reynolds number. *Phys. Fluids A* **3**, 1923–1930.

YASUI, K., TOWATA, A., TUZIUTI, T., KOZUKA, T. & KATO, K. 2011 Effect of static pressure on acoustic energy radiated by cavitation bubbles in viscous liquids under ultrasound. *J. Acoust. Soc. Am.* **130** (5), 3233–3241.

YOSHIDA, K., FUJIKAWA, T. & WATANABE, Y. 2011 Experimental investigation on reversal of secondary bjerknes force between two bubbles in ultrasonic standing waves. *J. Acoust. Soc. Am.* **130** (1), 135–144.

ZERAVCIC, Z., LOHSE, D. & VAN SAARLOOS, W. 2011 Collective oscillations in bubble clouds. *J. Fluid Mech.* **680**, 114–149.

ZHA, Z., WANG, J., QU, E., ZHANG, S., JIN, Y., WANG, S. & DAI, Z. 2013 Polypyrrole hollow microspheres as echogenic photothermal agent for ultrasound imaging guided tumor ablation. *Scientific Reports* **3**, 2360.

ZHANG, D., GONG, XF., LIU, JH., SHAO, LZ., LI, XR. & ZHANG, QL. 2000 The experimental investigation of ultrasonic properties for a sonicated contrast agent and its application in biomedicine. *Ultrasound Med. and Bio.* **26** (2), 347–351.

ZHAO, YZ., LIANG, HD., MEI, XG. & HALLIWELL, M. 2005 Preparation, characterization and in vivo observation of phospholipid-based gas-filled microbubbles containing hirudin. *Ultrasound Med. and Bio.* **31** (9), 1237–1243.

ZHENG, H., BARKER, A. & SHANDAS, R. 2006 Predicting backscatter characteristics from micron- and submicron-scale ultrasound contrast agents using a size-integration technique. *IEEE Trans. Ultrasonics, Ferroelectrics and Freq. Control* **53**, 639–644.